

## From diffuse gas to dense molecular cloud cores

Javier Ballesteros-Paredes · Philippe  
André, · Patrick Hennebelle, · Ralf  
S. Klessen, · Shu-ichiro Inutsuka, ·  
J. M. Diederik Kruijssen, · Mélanie Chevance, ·  
Fumitaka Nakamura, · Angela Adamo ·  
Enrique Vazquez-Semadeni

Received: 2020-01-31 / Accepted: 2020-05-17

**Abstract** Molecular clouds are a fundamental ingredient of galaxies: they are the channels that transform the diffuse gas into stars. The detailed process of how they

---

Javier Ballesteros-Paredes

Instituto de Radioastronomía y Astrofísica, UNAM, Campus Morelia, Antigua Carretera a Patzcuaro 8701.  
58090 Morelia, Michoacan, Mexico. E-mail: j.ballesteros@irya.unam.mx

Philippe André

Laboratoire d'Astrophysique (AIM), CEA/DRF, CNRS, Université Paris-Saclay, Université Paris Diderot,  
Sorbonne Paris Cité, 91191 Gif-sur-Yvette, France

Patrick Hennebelle

AIM, CEA, CNRS, Université Paris-Saclay, Université Paris Diderot, Sorbonne Paris Cité, 91191, Gif-  
sur-Yvette, France

Ralf S. Klessen

Universität Heidelberg, Zentrum für Astronomie, Institut für Theoretische Astrophysik, Albert-Ueberle-  
Str. 2, 69120 Heidelberg, Germany, Department of Physics, Nagoya University, Furo-cho, Chikusa-ku,  
Nagoya, Aichi 464-8602, Japan

J. M. Diederik Kruijssen

Astronomisches Rechen-Institut, Zentrum für Astronomie der Universität Heidelberg, Mönchhofstraße 12-  
14, 69120 Heidelberg, Germany,

Mélanie Chevance

Astronomisches Rechen-Institut, Zentrum für Astronomie der Universität Heidelberg, Mönchhofstraße 12-  
14, 69120 Heidelberg, Germany

Fumitaka Nakamura

National Astronomical Observatory of Japan, 2-21-1 Osawa, Mitaka, Tokyo 181-8588, Japan  
Department of Astronomy, The University of Tokyo, Hongo, Tokyo 113-0033, Japan  
The Graduate University for Advanced Studies (SOKENDAI), 2-21-1 Osawa, Mitaka, Tokyo 181-0015,  
Japan

Angela Adamo

Department of Astronomy, Oskar Klein Centre, Stockholm University, AlbaNova University Centre, SE-  
106 91 Stockholm, Sweden

Enrique Vázquez-Semadeni

Instituto de Radioastronomía y Astrofísica, UNAM, Campus Morelia, Antigua Carretera a Patzcuaro 8701.  
58090 Morelia, Michoacan, Mexico.

do it is not completely understood. We review the current knowledge of molecular clouds and their substructure from scales  $\sim 1$  kpc down to the filament and core scale. We first review the mechanisms of cloud formation from the warm diffuse interstellar medium down to the cold and dense molecular clouds, the process of molecule formation and the role of the thermal and gravitational instabilities. We also discuss the main physical mechanisms through which clouds gather their mass, and note that all of them may have a role at various stages of the process. In order to understand the dynamics of clouds we then give a critical review of the widely used virial theorem, and its relation to the measurable properties of molecular clouds. Since these properties are the tools we have for understanding the dynamical state of clouds, we critically analyse them. We finally discuss the ubiquitous filamentary structure of molecular clouds and its connection to prestellar cores and star formation.

**Keywords** ISM: kinematics and dynamics · Stars: formation · ISM: magnetic fields · ISM: clouds

## 1 Introduction

Since molecular clouds (MCs) are the sites where stars are born, the study of star formation necessarily passes through an understanding on the formation, dynamics, structure and evolution of molecular clouds. They are called molecular because they match the physical conditions for molecule formation: they are the densest, darkest and coldest regions of the interstellar medium.

MCs have temperatures  $\sim 10$ – $20$  K, and span a range of sizes between  $\sim 1$  and  $\sim 200$  pc (e.g., Miville-Deschênes et al., 2017). Inside them, smaller and denser structures are found at every level of the hierarchy, down to the resolution limit of the telescopes, a fact that has been interpreted as a fractal nature of MCs (Scalo, 1990; Falgarone et al., 1991, 2009). They are typically catalogued by size and mass (see e.g., Stahler and Palla, 2005) as: (i) giant molecular clouds (GMCs), the biggest clouds, with masses above  $10^5 M_\odot$ , and sizes  $\gtrsim 30$  pc, and up to  $100$ – $200$  pc, (ii) MCs, with masses of several  $10^2$  to some  $10^4 M_\odot$  and sizes of about  $10$ – $20$  pc, (iii) clumps, with masses between several  $10$ – $10^2 M_\odot$  and sizes between few and some pc, and (IV) cores, with masses below few  $10 M_\odot$  and sizes of  $0.1$  pc or less (Blitz, 1993; Heyer and Dame, 2015). They are nested in a hierarchical structure: while MCs and GMCs are embedded in a warmer ( $T \sim 8000$  K) atomic medium, clumps are nested inside MCs, and cores within the clumps. They exhibit a highly filamentary structure, and the hierarchy is such that smaller, denser structures always occupy a very small fraction of their parent structures' volume.

Although our understanding of MCs is continuously improving, still many questions remain open. Among them are the detailed process by which they are formed, what defines their inner structure, the role of filaments and cores in their evolution, the role of the different physical processes (turbulence, magnetic fields, galactic dynamics, etc.) in their dynamics, the meaning of the scaling relations between their mass or their internal velocity dispersion and their size. In the present paper we summarize the current state of our knowledge about MCs.

## 1.1 Connection between galactic scales and MC scales

The arrival of facilities capable of carrying out spectroscopy of the molecular and ionised interstellar medium (e.g. ALMA, MUSE) has not only brought about a revolution in terms of resolving large samples of Galactic MCs into protostellar cores, but has made a similar step change in terms of resolving large numbers of external galaxies into MCs and HII regions (e.g. Kreckel et al., 2018; Sun et al., 2018; Utomo et al., 2018). The resulting spatial dynamic range unlocks the interface between MC scales and those of the host galaxy, which in turn enables studies of:

1. how MC properties change as a function of their large-scale environment (e.g. Sun et al., 2018, 2020; Schruba et al., 2019),
2. how MCs are affected by galactic dynamics (e.g. Meidt et al., 2013, 2018, 2019; Jeffreson and Kruijssen, 2018),
3. how MCs combine to constitute the galaxy-scale star formation relation between the gas mass (surface density) and the star formation rate (surface density) (e.g. Kennicutt and Evans, 2012; Kruijssen et al., 2018),
4. how stellar feedback from the young stellar populations born in MCs affects the chemistry and energetics of the host galaxy (e.g. Kreckel et al., 2019; McLeod et al., 2019b),
5. how the evolutionary lifecycle of MCs that connects all of the above stages depends on the galactic environment (e.g. Chevance et al., 2020a).

The latter of these questions warrants a separate discussion and is treated more extensively in Section 1.2 below, and in Chevance et al. (2020b). We now first briefly summarise the (environmental dependence of) instantaneous statistical properties of MCs and how they constitute the star-forming properties of galaxies.

Firstly, observations show and theory predicts that MC properties depend on the galactic environment. This specifically concerns their surface and volume densities (e.g. Sun et al., 2018), turbulent pressure and velocity dispersion (e.g. Heyer et al., 2009; Field et al., 2011; Shetty et al., 2012; Kruijssen and Longmore, 2013), and virial parameter (e.g. Sun et al., 2018; Schruba et al., 2019), as well as their characteristic and maximum mass scales (e.g. Hughes et al., 2013; Reina-Campos and Kruijssen, 2017). Observations show and models predict that these quantities are also correlated: MC densities, velocity dispersions, masses, star formation rate, and cluster formation efficiency typically increase with the gas pressure in the galactic midplane (e.g. Vazquez-Semadeni, 1994; Krumholz and McKee, 2005; Elmegreen, 2008; Padoan and Nordlund, 2011; Kruijssen, 2012; Adamo et al., 2015).

In part, the environmental dependence of MC properties reflects a dependence on galactic dynamics. MCs initially condense out of the lower-density interstellar medium (ISM), from which they inherit turbulent and shear-driven motion (e.g. Meidt et al., 2018, 2019; Kruijssen et al., 2019a). Galactic dynamics can both stabilise clouds (e.g. Meidt et al., 2013) or compress them and induce star formation (e.g. Jeffreson and Kruijssen, 2018). The external gravitational potential and the ambient medium can lead to enhanced velocity dispersions and ‘apparent’ virial parameters, i.e. ones calculated without accounting for the gravitational force of the stars (e.g. Schruba et al., 2019; Sun et al., 2020).

Somewhat surprisingly, the resulting star formation efficiency per free-fall time seems relatively constant, at  $\epsilon_{\text{ff}} \sim 0.01$  (e.g. Barnes et al., 2017; Leroy et al., 2017; Utomo et al., 2018; Krumholz et al., 2019), in rough agreement with theoretical predictions (e.g. Federrath and Klessen, 2012, although see Schrupa et al. 2019 for important areas where observations and theory differ) and the galactic-scale efficiency per dynamical time (e.g. Elmegreen, 1987, 1993, 1997; Silk, 1997; Kennicutt, 1998). Observations of individual MCs in the solar neighbourhood suggest that their instantaneous star formation rate is situated above the expectation from the galactic-scale ‘star formation relation’ (e.g. Heiderman et al., 2010; Lada et al., 2010; Gutermuth et al., 2011) between the molecular gas mass surface density ( $\Sigma$ ) and the star formation rate surface density ( $\Sigma_{\text{SFR}}$ ), which is observed to have a power law form of  $\Sigma_{\text{SFR}} \propto \Sigma^N$  with  $N = 1 - 1.5$  (e.g. Kennicutt, 1998; Bigiel et al., 2008; Kennicutt and Evans, 2012; Leroy et al., 2013). However, this difference likely results from the fact that MC studies:

1. select single clouds that must contain both molecular gas tracers and star formation tracers, thereby restricting them to a specific evolutionary phase and biasing their position relative to the star formation relation (e.g. Schrupa et al., 2010; Kruijssen et al., 2018);
2. focus on the star-forming, inner regions of MCs, that achieve higher local star formation efficiencies than the lower-density outskirts of the clouds (e.g. Dobbs et al., 2014; Longmore et al., 2014).

Combining these biases with the fact that the MC lifecycle is highly dynamic and the instantaneous star formation efficiency is a strong function of an MC’s evolutionary stage (see Section 1.2 and e.g. Kruijssen et al., 2019b; Grudić et al., 2019; Chevance et al., 2020a), it is clear that the galactic-scale star formation relation can only arise after averaging over all evolutionary stages of MCs (Feldmann et al., 2011; Kruijssen and Longmore, 2014). While this explains the large scatter of the relation on sub-kpc scales (e.g. Bigiel et al., 2008; Leroy et al., 2013), it raises the question to what extent the galactic-scale star formation relation is purely statistical in nature and trivially arises from applying the central limit theorem to unresolved MC populations (as suggested by Lada et al., 2013). In other words, does the dynamic range in  $\Sigma$  and  $\Sigma_{\text{SFR}}$  of the galactic-scale star formation relation simply arise from adding up many individual MCs, without any underlying change in the physics of MC evolution and star formation, or do the properties of MCs change across this spectrum of galactic-scale densities? Can the galactic-scale star formation relation teach us anything at all about the MC-scale physics of star formation? The fact that MC properties are strongly environmentally dependent and change continuously over the full range of large-scale gas surface densities of the host galaxy (see above) suggests that the galactic-scale star formation relation is at least partially physical in nature, rather than being a trivial result of statistical averaging. To provide a definitive answer to this question, cloud-scale observations of the molecular ISM are necessary, which is now within reach. Irrespectively of the physics or statistics that set the galactic-scale star formation relation, it is clear that the scatter around this relation is a valuable probe of the MC lifecycle.

Finally, the stellar feedback from the young stellar populations born in MCs drives mass, energy, momentum, and metal enrichment into the surrounding ISM. Recent studies of ionised emission lines show that early feedback mechanisms dominate the dispersal of MCs (e.g. Lopez et al., 2011, 2014; Chevance et al., 2016, 2020a; Kim et al., 2018; Kruijssen et al., 2019b; McLeod et al., 2019a,b). Supernovae detonating in the resulting, cleared environments may contribute to driving galactic winds on spatial scales larger than the disc scale height (e.g. Walch and Naab, 2015). The chemical enrichment from the young stars drives inhomogeneity on spatial scales similar to the gas disc scale height (e.g. Kreckel et al., 2019). It remains an important open question on which timescales these inhomogeneities dissolve by mixing.

We now turn to a brief discussion of the lifecycle of MCs, synthesising the processes discussed above and placing them on an evolutionary timeline. For a more detailed discussion on this topic, we refer to Chevance et al. (2020b, this volume)

## 1.2 Lifecycle of MCs

Characterising the cloud lifecycle in galaxies is critical to understand the physical processes of star formation and feedback. However, measuring timescales has historically been notoriously difficult in astrophysics and the question of the molecular cloud lifetime has been highly debated, both from theoretical and observational points of view. In the Milky Way, the lack of observed post-T Tauri stars (with ages  $\sim 10$  Myr) associated to molecular clouds (Briceno et al., 1997; Hartmann et al., 2001) has suggested that molecular clouds are transient structures and disperse quickly after star formation. The fact that most molecular clouds in the Solar Neighbourhood are associated with young stars of ages less than 3 Myr (Ballesteros-Paredes et al., 1999a) is also in favour of short-lived GMCs. Supporting this idea, Elmegreen (2000) suggests that star formation occurs on a crossing time, based on the determination of cluster ages in the Large Magellanic Cloud (LMC).

Extragalactically, measuring the lifetimes of molecular clouds has been even more challenging. A variety of indirect methods has been developed, relying for example on the presence of inter-arm molecular clouds (e.g. Scoville and Hersch, 1979; Scoville and Wilson, 2004; Koda et al., 2009), on the classification of clouds based on their star formation activity (e.g. Engargiola et al., 2003; Blitz et al., 2007; Kawamura et al., 2009; Miura et al., 2012; Corbelli et al., 2017), or on the evolution of clouds along orbital streamlines (e.g. Kruijssen et al., 2015; Meidt et al., 2015; Henshaw et al., 2016; Barnes et al., 2017; Jeffreson et al., 2018). Due to differences in the experiment setups and subjective definitions of cloud categories, it remained unclear what part of the large range of values estimated by these different methods (from more than 100 Myr down to about 1 Myr) resulted from actual environmental dependence of the cloud lifetime, and what this could tell us about the physical processes regulating star formation and feedback in galaxies.

The new statistical approach developed by Kruijssen and Longmore (2014) and Kruijssen et al. (2018) now enables the characterisation of the evolutionary timeline between cloud formation and evolution, star formation and feedback in a systematic way, applicable to a large range of galaxies. This method has been applied to a sample

of galaxies in or near the Local Group (e.g. NGC300, Kruijssen et al. 2019b, M33, Hygate et al. 2019; the Large Magellanic Cloud, Ward et al. 2019) as well as outside of the Local Group (Chevance et al., 2020a, for a sample of nine galaxies). These new measurements, which can be extended to the large galaxies surveys at high spatial resolution observed with ALMA (e.g. with the PHANGS collaboration, Leroy et al. in prep.), now make it possible to quantitatively determine what parameters (such as ISM pressure, galactic dynamic, disc structure) govern cloud lifetime in galaxies. Chevance et al. (2020a) shows that there exist two regimes in galactic molecular gas surface density, where GMC lifetime is regulated by galactic dynamical processes at high ( $\geq 8 M_{\odot} \text{ pc}^2$ ) gas surface density (as in Jeffreson and Kruijssen, 2018), while at low ( $\geq 8 M_{\odot} \text{ pc}^2$ ) gas surface density, GMCs decouple from galactic dynamics and their lifetime is governed by local processes, so that they typically live for a free-fall time or a crossing time.

The characterisation of the lifecycle of molecular clouds, which can be seen as the building blocks of galaxies (Kruijssen et al., 2019b), is further developed in Chevance et al. (2020b, this volume). Measuring the duration of the successive phases of star formation, from cloud assembly, to cloud collapse and cloud destruction by feedback, as a function of the environment (e.g. galactic structure, rotation curve, ISM pressure, stellar density, metallicity) provides strong constraints on the physical mechanisms playing a role in these processes, and how they vary throughout galaxy evolution.

## 2 The formation of molecular clouds

One of the most fundamental questions regarding the understanding of the interstellar medium is to understand how molecular clouds form. Indeed, most of the volume in the Milky Way is filled by atomic gas which is several times more diffuse than the molecular gas. How the interstellar gas becomes denser and molecular? Here the various steps thought to be involved in the process are described.

As we discuss in (Girichidis et al., 2020, this volume), the total mass of the Galactic ISM is about  $10^{10} M_{\odot}$ . Most of the volume is occupied by ionized gas, which can extend high above and below the disk midplane. It accounts for about 25% of the mass. The rest of the mass is split roughly evenly between the atomic and the molecular phases of the ISM (Ferrière, 2001). The atomic component also has a large volume filling factor and extends to large scaleheights in particular in the outer parts of the Milky Way (Kalberla and Kerp, 2009).

Our discussion here focuses on the dense molecular component of the ISM, which forms by converting atomic hydrogen into  $\text{H}_2$ . We can compute the properties of this component by combining data from CO observations, which trace clouds with high concentrations of both  $\text{H}_2$  and CO, with measurements of  $\text{C}^+$ , which trace so-called “CO-dark  $\text{H}_2$  gas”, i.e. clouds with high  $\text{H}_2$  fractions but little CO (see e.g. Pineda et al., 2013). On global scales, the distribution of molecular gas shows a peak within the central few hundred parsec of the Galaxy, a region known as the Central Molecular Zone (CMZ, see e.g. Molinari et al., 2011). It then falls off sharply between 0.5 and 3 kpc, possibly owing to the influence of the Milky Way’s central stellar bar, before peaking again at a Galactocentric radius of around 4–6 kpc in a structure

known as the Molecular Ring. Outside of the Molecular Ring, the surface density of molecular gas declines exponentially, but it can still be traced out to distances of at least 12–13 kpc (Heyer et al., 1998). Its vertical scaleheight is very small ( $\sim 50$  pc) and so essentially all molecular gas is closely confined to a dense layer close to the disk midplane, occupying about 1–2% of the total ISM volume. We note that only about 5% of the molecular gas mass in the Milky Way is associated with the known molecular cloud complexes (Roman-Duval et al., 2016), by far the largest fraction follows a more diffuse and extended distribution (for a complete decomposition of the CO emission in the Galactic midplane, see Miville-Deschênes et al., 2017).

## 2.1 Three phase model of the ISM and H<sub>2</sub> formation

A very simple model of the phase structure of the ISM was suggested by Field et al. (1969). If one assumes that the atomic gas in the ISM is in thermal equilibrium, then there are two thermally stable solutions: a cold dense phase that is generally called cold neutral medium (CNM), and a warm, diffuse phase termed warm neutral medium (WNM). Gas at intermediate temperatures is thermally unstable. It will either cool down and get denser until it joins the CNM, or heat up and becomes more tenuous until it joins the WNM (see the discussion below in Section 2.2). This two-phase model was extended by McKee and Ostriker (1977), who realised that the momentum and energy input from supernovae would create large, ionized bubbles filled with very hot gas. At temperatures around  $10^6$  K this gas would cool very slowly compared to the other timescales relevant to the system, and so this component would constitute a third phase known as the hot ionized medium (HIM).

The chemically most straight-forward path to form H<sub>2</sub> in the ISM is via the radiative association of two hydrogen atoms:  $\text{H} + \text{H} \rightarrow \text{H}_2$ . However, the rate coefficients are extremely small, and similar applied to gas phase reactions involving the H<sup>-</sup> and H<sup>+</sup> radicals. These reactions are only relevant in the early universe in very low metallicity gas (see, e.g. Klessen and Glover, 2016). In the solar neighborhood and essentially in a present-day galaxies, almost all H<sub>2</sub> molecules form on dust (for a comprehensive overview, see Tielens, 2010; Draine, 2011). The association reactions between adsorbed hydrogen atoms occur readily on grain surfaces, and the rate at which H<sub>2</sub> forms is only limited by the rate at which H atoms are adsorbed onto the surface. As we discuss in (Girichidis et al., 2020), the rate for typical Milky Way conditions is

$$\left( \frac{R_{\text{H}_2}}{\text{cm}^3 \text{ s}^{-1}} \right) \sim 3 \times 10^{-17} \left( \frac{n_{\text{H}}}{\text{cm}^{-3}} \right) \quad (1)$$

where  $n$  is the total number density of gas particles and  $n_{\text{H}}$  is the number density of atomic hydrogen. For purely atomic hydrogen gas, both quantities are identical if we neglect contributions from helium and possibly metals.

While H<sub>2</sub> is easily formed on dust, it is also readily destroyed again when exposed to the interstellar radiation field. When molecular hydrogen is photodissociated, the H<sub>2</sub> molecule first absorbs a UV photon with energy  $E > 11.2$  eV and ends up in an excited electronic state. It then undergoes a radiative transition back to the electronic ground state, ending up either into a bound ro-vibrational level, in which case the

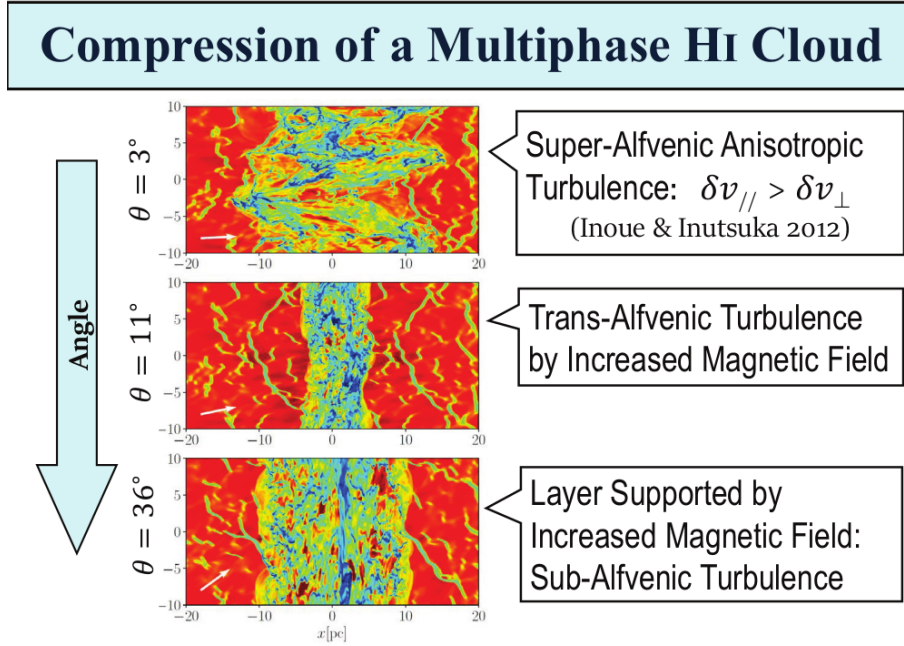


**Fig. 1** The result of compression of multiphase HI clouds by shock waves (Iwasaki et al., 2018). The column density is shown (red stands for WNM while Blue-green represents CNM). The relative angle ( $\theta$ ) between the shock wave propagation direction and the mean magnetic field is 3 degrees (upper panel), 11 degrees (middle panel) and 36 degrees (lower panel), respectively.

molecule survives, or into the vibrational continuum, in which case it dissociates. Because  $\text{H}_2$  photodissociation is line-based, rather than continuum-based, the rate at which this process occurs is highly sensitive to self-shielding (Draine and Bertoldi, 1996). Depending on the strength of the interstellar radiation field (expressed in terms of Habing units  $G_0$ , see Habing 1968) this becomes important when the total column density  $N$  exceeds a value of

$$\left(\frac{N}{\text{cm}^{-2}}\right) = 10^{20} G_0 \left(\frac{n}{\text{cm}^{-3}}\right)^{-1}. \quad (2)$$

Note that also dust extinction contributes to reducing the  $\text{H}_2$  photodissociation rate, however, it typically requires higher column densities than  $\text{H}_2$  self-shielding, and so it plays only a minor role under normal ISM conditions, (see Girichidis et al., 2020, this volume).

## 2.2 The role of thermal instability

The first step on the way toward getting dense molecular gas is certainly the transition from the warm neutral medium (with densities of about  $1 \text{ cm}^{-3}$  and temperature



$\simeq 8000$  K) into the cold neutral medium (roughly 100 times denser and 100 times cooler). The physics of thermal instability (Field, 1965) is discussed in Girichidis et al. (2020, this volume) Here we simply recalled the basic aspects. Thermal instability is due to the atomic cooling of the ISM (most important coolant being H, O and C II, see Wolfire et al., 2003) and more precisely to the fact that in a range of density, typically between a few and a few tens of particles per  $\text{cm}^{-3}$ , the cooling function has a relatively low dependence on the temperature. Therefore since the cooling is proportional to the square of the density (because it arises through the radiative deexcitation of the coolant which has been excited through collisions) while the heating is simply proportional to the density, an instability occurs. The consequence is that at equilibrium, gas in standard ISM conditions, cannot exist at intermediate densities, say between 1 and 20-30  $\text{cm}^{-3}$ . The gas is said to be thermally unstable. This means that when the WNM enters in the thermally unstable domain it starts contracting until it reaches the second branch of equilibrium, i.e. the CNM. This represents a contraction by a factor of about 100.

Numerical simulations have been used to study the non-linear development of thermal instability triggered either by shocks propagating in the WNM (Koyama and Inutsuka, 2000, 2002; Inoue and Inutsuka, 2012) or by a converging flow of WNM (Hennebelle and Pérault, 1999; Audit and Hennebelle, 2005, 2010; Heitsch et al., 2006; Vázquez-Semadeni et al., 2006). The effect of turbulent driving in the Fourier space, which corresponds to complex flows entailing all sort of compressive events (Seifried et al., 2011) has also been considered. From all these studies it has been deduced that (i) when sufficiently pushed out of equilibrium WNM breaks-up into a multi-phase medium composed of clumps of CNM surrounded by the WNM which confines them ; (ii) the CNM clumps present statistics which resemble the ones inferred for the CO clumps ; (iii) thermally unstable gas does exist and represents several percents of the gas. Its existence is due to the turbulence (e.g. Gazol et al., 2001); (iv) the various phases are interwoven; (v) the cold phase has supersonic motions and presents a velocity dispersion equal to a fraction of the WNM sound speed. Indeed the medium presents characteristics of a two phase flows as well as of a turbulent one.

Simulations including the magnetic field have also been performed. Although magnetic fields definitely modify the fluid dynamics, the above conclusions remain qualitatively similar. There is however an aspect where it possibly makes a significant difference. An important question is whether the clouds of CNM which constitutes the progenitor of molecular clouds are created by a single compression event from WNM or whether they are more gradually created from cold dense HI clouds. Inoue and Inutsuka (2008), Inoue and Inutsuka (2009), Heitsch et al. (2009b) and Körtgen and Banerjee (2015) have concluded that forming magnetized CNM tends to be difficult because magnetic field has a stabilizing influence. Inoue and Inutsuka (2012) have investigated the scenario in which a dense cloud form after a series of compression and a more detailed analyses has been carried out by Iwasaki et al. (2018). Figure 1 displays results for compression induced by shock waves propagating within magnetized multiphase HI clouds. The relative angle ( $\theta$ ) between the shock velocity and the mean magnetic field is 3 degrees (upper panel), 11 degrees (middle panel), 36 degrees (lower panel), respectively. With a small angle a substantial amount of dense gas formed. But for larger angles and above a certain critical value, the propagation

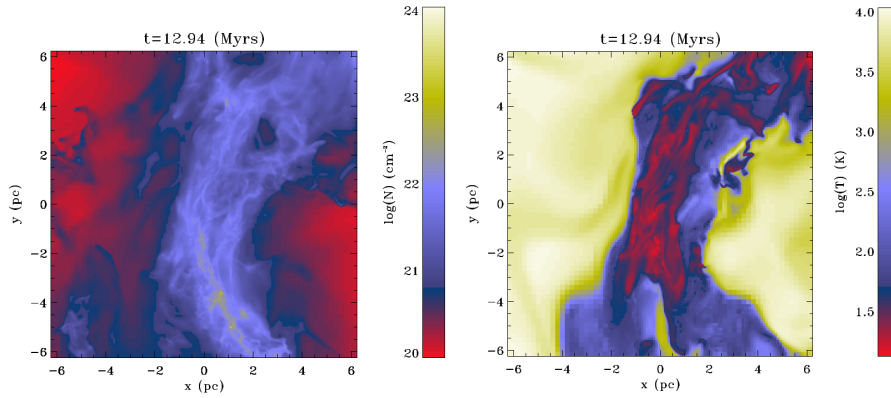


**Fig. 2** Cut of the temperature (*right*) and column density (*left*), of a simulation snapshot of molecular cloud formation (Hennebelle et al., 2008).

of shock wave becomes very inefficient in producing dense gas. Obviously the value of this critical angle depends on the flow velocity and of the magnetic intensity. In reality, there is a distribution of angles between the magnetic and the velocity fields. Detailed studies from larger scale simulations revealed that magnetic and velocity fields tend to be aligned (e.g. Iffrig and Hennebelle, 2017), which would imply that aligned configurations are more frequent than it was randomly determined.

### 2.3 The role of gravity

In the second step, gravity has been considered and the gas condensation has been further described (Vázquez-Semadeni et al., 2007; Heitsch et al., 2008; Hennebelle et al., 2008; Banerjee et al., 2009).

Figure 2 portrays a snapshot for a numerical simulation of a colliding flow (from Hennebelle et al., 2008) which has led to the formation of a molecular cloud. As described in the previous section, the dense gas has formed from the diffuse gas as well as from the denser structure of the multi-phase medium. Due to gravity, few regions undergo gravitational collapse. Interestingly, in few locations the temperature abruptly jumps from about  $10^4$  to 10 K. Thus the cloud depicted in Fig. 2 can be truly qualified as being a multi-phase molecular cloud. In a sense, it is a denser counterpart of the classical WNM/CNM where CNM has been replaced by denser gas.

In simulations including gravity, the clumps present many characteristics with the observed CO clumps as for instance their density, velocity dispersion and mass spectrum (e.g. Banerjee et al., 2009; Heitsch et al., 2009a).

It has been found that initially, that is to say soon after the dense gas have been assembled, the overall structure of the cloud remains largely unchanged compared to the case without gravity. One of the most important difference is obviously that in the self-gravitating case the PDF of the gas density extends towards much larger values. However, in MCs with conditions appropriate for the solar neighbourhood,

the bulk of the mass remains at a density on the order of  $n_{\text{H}} = 100 - 10^3 \text{ cm}^{-3}$ , even at late times, when collapse has already occurred in few places.

The velocity dispersion in particular is already high from the very beginning of the cloud lifetime and is likely the result of an accretion-driven process as emphasised by Klessen and Hennebelle (2010). This turbulence which is inherited from the dynamical building of the cloud is likely maintained by several processes including continuous accretion onto the cloud (Klessen and Hennebelle, 2010), the development of various instabilities such as the Kelvin-Helmholtz instability for instance (Heitsch et al., 2008), gravitational collapse of the densest cloud parts and later when stars have started to form by the feedback processes such as HII regions (Gritschneider et al., 2009) and jets (Federrath, 2015; Offner and Liu, 2018). In addition, as collapse proceeds, the kinetic energy of clouds tends to follow the gravitational energy (Vázquez-Semadeni et al., 2007). Thus, it is likely that a non-negligible contribution to the velocity dispersion comes from gravity itself, since the ensemble of observed MCs tend to organize along the virial/free fall collapse lines, with slightly overvirial values (Ballesteros-Paredes et al., 2011a, see also §4.5).

The H I streams collision mechanism depicted above is a general mechanism that should work regardless of the detailed mechanism that gave origin to the streams. The main proposed mechanisms for producing such H I streams are (see §2.5): (i) stellar feedback, as e.g., the expansion of H II regions or SNe explosions), (ii) the passage of a spiral arm, (iii) a large-scale gravitational instability, and (iv) cloud-cloud collisions. Depending on the origin and length of the streams, the resulting cloud can have more or less mass. For instance, it can be expected that, while bubbles due to stellar activity can produce  $10^4 M_{\odot}$ , spiral arms or gravitational instability can produce clouds with masses up to  $10^5 - 10^6 M_{\odot}$ .

An additional factor limiting the formation of the clouds is the relative orientation between the magnetic and the velocity fields. Numerical simulations have shown that the diffuse colliding streams have to move nearly parallel to the magnetic field in order to allow the formation of the molecular clouds in reasonably short timescales (10–20 Myr) (e.g., Heitsch et al., 2009b; Inutsuka et al., 2015). It should be noticed, however, that either the magnetic and the velocity fields in disk galaxies are, at first approximation, circular. Thus, one can conclude that large-scale galactic dynamics do play a role in the formation of molecular clouds.

## 2.4 The formation and role of molecules

The next step has been the modelling of the UV-driven chemistry which has been introduced either directly during the simulation (e.g. Glover and Mac Low, 2007; Glover and Clark, 2012b; Inoue and Inutsuka, 2012) or, at a more sophisticated level, as a post-treatment of the WNM colliding flow simulations (e.g. Levrier et al., 2012). This allows a proper treatment of the combined influence of density and UV-shielding upon chemistry and of the cooling function. The results provide a confirmation that the gas temperature is reasonably well computed in the magneto-hydrodynamical (MHD) simulations.

One important question which has been addressed by these simulations is the formation timescale of molecular hydrogen. For a long time, this has remained a mystery because the  $H_2$  formation is long: the  $H_2$  formation rates on grains are of the order of  $t_{\text{form}} \sim nR$ , where  $n$  is the density of the atomic hydrogen, and  $R$ , the rate coefficient, has typical values of the order of  $3 \times 10^{17} \text{ cm}^3 \text{ s}^{-1}$  (Jura, 1975). Then, the typical  $H_2$  formation timescales are given by

$$\left( \frac{t_{\text{form}}}{\text{yr}} \right) = 10^6 \left( \frac{n}{10^3 \text{ cm}^{-3}} \right) \quad (3)$$

From their simulations, Glover and Mac Low (2007) concluded that  $H_2$  forms at relatively large densities, therefore in a relatively short timescale, in dense clumps induced by turbulence. As these clumps are transient they eventually mix back with the more diffuse gas and therefore enriches it in molecular gas. This result has been confirmed by Valdivia et al. (2016). However, since multi-phase ISM is considered in their simulations, when  $H_2$  spreads from dense clumps to the surrounding medium, as this latter is composed of warm gas, a fraction of warm (500-1000 K) molecular gas develops and this may have consequences to form some chemical species (e.g.  $\text{CH}^+$  see Valdivia et al. (2017)).

Glover and Clark (2012a) have investigated the formation of the CO molecules in turbulent simulations using different methods. They find (see also Shetty et al., 2011; Gong et al., 2018) that all methods tend to produce similar amount of CO molecules in the dense gas and in good agreement with observations. It is worth stressing that so far all the adopted models failed to reproduce (by almost a factor of 10) the observed CO abundances in regions poorly shielded from the UV-field (Shetty et al., 2011; Levrier et al., 2012).

Generally speaking, it has been found (e.g. Glover and Clark, 2012b) that not unexpectedly, the gas dynamics is not sensitive to the details of the chemistry models.

## 2.5 Dynamical mechanisms for gathering mass

In addition to the thermal instability, which enables the gas to efficiently transit from a diffuse, warm phase into dense, cold clouds, different mechanisms have been proposed for collecting the mass. Ultimately, it is likely that all those mechanisms play a role in the formation of MCs and MC complexes. Some of these are, agglomeration (or coagulation), converging flows, the passage of spiral arms, cloud-cloud collisions, shock-wave passage, and large-scale instabilities. It should be recognized, however, that all cases are, in practice, converging flows, and the differences between them are, on one hand, the physical origin of the inflows, their length, their geometry, and their initial density.

Each one of the mechanisms producing MCs may also be related to the total mass that they can gather, which will be given by

$$M = \Delta t \oint_S \rho u_i \hat{n}_i dS, \quad (4)$$

where  $\rho$  is the density of the diffuse interstellar medium,  $u_i$  is the component of the velocity of the fluid in the direction  $\hat{n}_i$  perpendicular to the surface  $S$ , and  $\Delta t$  the time interval that the process lasts.

## 2.6 Agglomeration of smaller clouds

One of the earliest models of cloud formation was the so-called ‘‘agglomeration’’ or ‘‘coagulation’’ model. The idea started with Oort (1954), who proposed that HII regions produced by OB stars in MCs can produce a rocket effect on their parent clouds, ejecting them ballistically through the interstellar medium. Such motions could counteract the loss of kinetic energy produced by further shocks between clouds. This idea was taken later by Field and Saslaw (1965), who made a model for the evolution of the mass spectrum of MCs, assuming ballistic clouds with a typical velocity dispersion. In their model, small clouds could have inelastic shocks, allowing the construction of larger clouds. With simple assumptions about the cross sections of MCs, and their velocity dispersion, the authors could explain the observed shallow slopes of the MC mass spectrum, with  $\gamma \sim 0.5$  in eq. ([12], see §4.1). Similar results were found by Taff and Savedoff (1973) and Hausman (1982). This model was revisited later by Kwan (1979), who estimated the ages of clouds constructed in this way. He found a typical timescale of  $2 \times 10^8$  years to construct GMCs.

Blitz and Shu (1980) dismissed the coagulation models, arguing that there were substantial observational evidence to say that GMCs cannot live for more than some times  $10^7$  years. Among other reasons, they argued that: (i) Since the abundance of molecular gas had been overestimated, so should be the ages of GMCs, and (ii) if GMCs were long-lived, they should also be observed in the inter-arm region, forming OB stars there. However, OB stars appear to be highly correlated to the arms.

Some years later, Kwan and Valdes (1983), Tomisaka (1984) and Kwan and Valdes (1987) made actual numerical simulations of the evolution and coalescence of clouds in a galactic disk with a spiral potential and gravity between clouds. Although GMC formation in this model is accelerated by the spiral arms and by the mutual attraction between clouds, still timescales larger than  $10^8$  years were required to construct GMCs. However, with a similar model, Tomisaka (1984) found timescales of the order of  $4 \times 10^7$  yr, opening up the possibility that GMCs were constructed by coagulation, and addressing the criticisms raised by Blitz and Shu (1980).

Those models were due in part to the advent of more complex numerical simulations of the ISM, in which clouds were self-consistently treated as part of the fluid (e.g., Vazquez-Semadeni et al., 1995; Passot et al., 1995), rather than as discrete, ballistic objects. The possibility of cloud coagulation, however, has been recently renewed with state of the art numerical simulations of multiphase media in galactic disks (Dobbs, 2008; Tasker and Tan, 2009; Dobbs et al., 2015) which small clouds coalesce to form larger cloud complexes as consequence of the converging flows in spiral arms.

Although it is likely that actual agglomeration occurs to some degree, there are two observational constraints on this possibility: on one hand, all observed molecular clouds have a highly filamentary structure down to the resolution limit (e.g.,

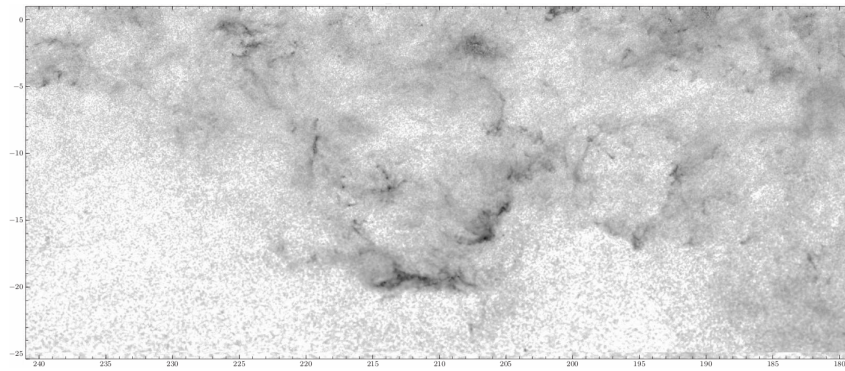


**Fig. 3** Extinction map towards the Orion molecular complex. Regardless the fact that different features are located at different distances, it is clear that the ISM is full of bubbles at different scales, with MCs located preferentially tracing segments of circles (figure adapted from Rowles and Froebrich, 2009).

Falgarone et al., 1991; André et al., 2014). In contrast, the small clouds coalescing in the quoted simulations lack inner structure, exhibiting roundish shapes on scales of 10–100 pc, indicating that those clouds are numerically under resolved. Additionally, the large majority of clouds in the Solar Neighborhood exhibits signs of star formation (Ballesteros-Paredes and Hartmann, 2007; Kainulainen et al., 2009), with ages typically of 1–3 Myr, and with no stars much older than 5 Myr. This suggests that the star formation events in small clouds are able to rapidly disperse their parent clouds (e.g. Agertz et al., 2013; Dale et al., 2014; Hopkins et al., 2018; Kruijssen et al., 2019b), limiting the possibility of coalescence. Thus, although the coalescence of smaller clouds into larger ones may occur to some extent, this process is probably overemphasized in the quoted simulations due to resolution effects, as well as to the lack of stellar feedback.

## 2.7 Converging flows

Local compressions like the passage of HII region or SN shells can produce supersonic compressions in the diffuse gas that nonlinearly trigger the formation of cold, dense atomic gas by thermal instability. If enough column density is achieved in the cold atomic gas, molecules can begin to form and a molecular cloud begins to appear in the deepest regions of the cold atomic cloud (Franco and Cox, 1986; Hartmann et al., 2001; Bergin et al., 2004; Clark et al., 2012). There is plenty of observational evidence that local MCs are at what would be the edges of bubbles and shells in the ISM (see Fig. 3, and, e.g., Heiles, 1979, 1984; Tenorio-Tagle and Bodenheimer, 1988, and references therein).

Numerical simulations of a piece of the interstellar medium including a variety of physical processes such as shear, rotation, magnetic fields, diffuse and stellar heating, cooling, and self-gravity (Vazquez-Semadeni et al., 1995; Passot et al., 1995), showed that clouds could be understood as turbulent density fluctuations, i.e., as density enhancements resulting from local turbulent compressions in the diffuse ISM

(Hennebelle and Pérault, 1999; Ballesteros-Paredes et al., 1999b). Furthermore, filamentary molecular clouds, with  $M \lesssim \text{several} \times 10^4 M_{\odot}$ , a few pc wide by  $\sim 20 - 40$  pc long, and densities  $n > 100 \text{ cm}^{-3}$ , could be produced in few megayears (Ballesteros-Paredes et al., 1999a), once enough material has been accumulated from the diffuse medium along distances of  $\sim 100$  pc (Hartmann et al., 2001). Note, however, that the clouds evolve for significantly longer timescales,  $\gtrsim 10$  Myr, in the cold atomic phase, with the transition to a mainly molecular composition occurring shortly before or nearly simultaneously with the onset of star formation (Franco and Cox, 1986; Hartmann et al., 2001; Bergin et al., 2004; Clark et al., 2012; Vázquez-Semadeni et al., 2018).

One of the achievements of the numerical simulations is that they were able to explain the synchronization of star formation over long distances, as a consequence of the large-scale streams collecting mass along the cross section of the collision, producing simultaneous star formation in apparently disconnected regions. Furthermore, once the stars form, the stellar feedback can disperse the cloud in a few more megayears. As a result, the timescales of MCs, from the time in which the CO appears, to their dispersal time, is around  $\sim 10$  Myrs, consistent with observations of stellar clusters (Leisawitz et al., 1989) and of the spatial association of the stars with the gas (Kruijssen et al., 2019b). This could explain the post-T Tauri problem, a 20-year observational puzzle, namely that no stars older than 5 Myrs are found associated to molecular gas (Herbig, 1978). Thus, by rapidly assembling the molecular component of the cloud, rapidly and coherently forming the stars, and rapidly dispersing the clouds, the post-T Tauri puzzle was solved.

The converging-flow mechanism has been successful in explaining the formation of several features observed in nearby ( $\lesssim 1$  kpc from the Sun) clouds, such as the ages and age histories of stars and clusters in nearby clouds (Zamora-Avilés et al., 2012; Hartmann et al., 2012; Vázquez-Semadeni et al., 2017), the core-to-core velocity dispersion in clouds (Heitsch et al., 2009a), the near-virial and over-virial distribution of clouds (Camacho et al., 2016; Ballesteros-Paredes et al., 2018), the column density probability distribution functions of clouds (Ballesteros-Paredes et al., 2011b), the position-velocity distribution of gas and stars (Kuznetsova et al., 2015, 2018), etc.

## 2.8 Large-scale gravitational instability of the Galactic disk

It is not clear how much of the mass in the Milky Way is in large molecular complexes, or scattered into small clouds. While it is true that all the cloud mass spectra  $dN/d\log M$  of CO clouds reported in the literature have power-laws shallower than  $-1$ , implying thus that most of the mass is in large complexes (see §4.1), it has to be recognised that such studies are seriously skewed by distance: there is no data for clouds smaller than  $\sim 10$  pc farther than  $\sim 3$  kpc from us (e.g., Miville-Deschênes et al., 2017, see the discussion in §4.1). Thus, it is clear that we are missing all the small clumps that are far away due to either resolution and/or sensitivity (Miville-Deschênes et al., 2017), as well as by superposition along the line of sight (Ballesteros-Paredes et al., 2019). In fact, Koda et al. (2016) estimated that approximately half of the molecular gas can be in smaller clouds in the interarm regions,

rather than organized in large complexes in the spiral arms. However, it is unclear to what extent this result is affected by the fact that non-circular motions play a key role in the difficulty of reconstructing the spiral structure of the Milky Way (Blitz and Shu, 1980; Gómez, 2006).

In any event, large complexes, with masses  $\gtrsim 10^6 M_\odot$  clearly do exist, and are observed in external galaxies too (see, e.g., Dobbs et al., 2014, and references therein) along the spiral arms. For these, it is necessary to have large-scale convergence of flows, as required by the continuity equation, and thus it is difficult to construct such complexes only *via* local turbulent streams or random agglomeration. For those complexes, the main mechanism driving the converging flows is likely to be a large-scale gravitational instability of rotating disks. This occurs when a thin disk of column density  $\Sigma$  and sound speed  $c_{\text{eff}}$  has a Toomre parameter

$$Q \equiv \frac{\kappa c_{\text{eff}}}{\pi G \Sigma} \lesssim 1 - 2 \quad (5)$$

(Goldreich and Lynden-Bell, 1965), where  $\kappa$  is the epicyclic frequency in the disk. The precise value of  $Q$  for which a disk can become gravitationally unstable depends on whether the disk is isothermal, magnetized, its thickness, etc., but typically these values are around  $Q \sim 1 - 2$  (Kim and Ostriker, 2001, 2002; Kim et al., 2003; Li et al., 2005; Kim and Ostriker, 2007). Numerical simulations have shown that GMC complexes with masses above  $10^5 - 10^6 M_\odot$  can be built up by gravitational instability in rotating disks (Shetty and Ostriker, 2008; Dobbs et al., 2011a; Tasker and Tan, 2009). In addition, it is likely that this mechanism is responsible for the agglomeration of smaller clouds in the vicinity of such complexes. However, we note that if the timescale for assembly of clouds exceeds the timescale on which stellar feedback from new-born stars disperses the gas, so the cloud agglomeration process is halted and the mass spectrum of MC complexes is truncated at the high-mass end (e.g., Reina-Campos and Kruijssen, 2017).

### 3 The virial theorem and energy budget of MCs.

#### 3.1 The virial theorem

A fundamental tool in the study of MCs has been the virial theorem (VT), basically, because it allows us to use the observable quantities, column density, line profiles and sizes, in order to estimate the dynamical state of clouds in terms of their gravitational, thermal, kinetic, and magnetic energies.

In its scalar version, the VT is obtained from the momentum equation, by dotting it by the position vector, and integrating over a volume of interest, typically, a cloud. Thus, the VT is a measure of the work done by the external forces on the medium and the resulting kinematic effects on the cloud. In the Lagrangian form, it is expressed as

$$\frac{1}{2} \frac{d^2 I}{dt^2} - 2E_{\text{kin}} = 2E_{\text{int}} - 2\tau_{\text{int}} + E_{\text{mag}} + \tau_{\text{mag}} + W \quad (6)$$



where  $I = \int_V \rho r^2 dV$  is the moment of inertia of the cloud  $E_{\text{kin}} = 1/2 \int_V \rho u^2 dV$  is the kinetic energy of the cloud  $E_{\text{int}} = 3/2 \int_V P dV$  is the internal energy,  $\tau_{\text{int}} = -1/2 \oint_S x_i P \hat{n}_i dS$  is the pressure surface term,  $E_{\text{mag}} = 1/8\pi \int_V B^2 dV$  is the magnetic energy,  $\tau_{\text{mag}} = 1/4\pi \oint_S x_i B_i B_j \hat{n}_j dS$  is the magnetic stress at the surface of the cloud,  $W = \int_V x_i \rho \partial\phi/\partial x_i dV$  is the gravitational term, which frequently is approximated as the gravitational energy of a homogeneous sphere,  $E_g = -3GM/5R$ , and where  $\phi$  is the gravitational potential. In the previous equation,  $\rho$ ,  $u_i$ ,  $B_i$ ,  $P$ , and  $\hat{n}$  are respectively the density, the  $i^{\text{th}}$  component of the velocity  $u$ , the  $i^{\text{th}}$  component of the magnetic field  $B$ , the pressure, and a unitary vector perpendicular to the surface  $S$  that surrounds the volume  $V$ , over which the integrals are performed. In the notation above, the Einstein convention is assumed, where repeated indexes are summed.

The measurements that are available through observations are the line profiles and/or the integrated emission, in a given solid angle. From there, the physical quantities that are available through observations are the column density, the area of the cloud, from which one can compute the total mass, and the line widths, from which one can in turn estimate the RMS value of the velocity field, and depending on the line, the magnetic field intensity, and the size of the cloud, which ideally should be computed as an independent measurement of the area, in order to properly understand the scaling properties of clouds, as well as their fractal properties. From these quantities, and making assumptions on the geometry of the cloud and its mass distribution, estimates of the energies involved in eq. (6) can be obtained. Finally, this allows an estimation of the physical state, and possibly of the evolutionary state, of MCs.

There are several assumptions that are frequently made when computing the energies of the VT, and that are not necessarily true in MCs, and thus, they should be discussed (see Ballesteros-Paredes, 2006, for details). These are:

1. “The role of nonthermal motions within a cloud is to provide support against collapse.” This is only true if the motions are truly random turbulent motions, microscopic, and driven by an energy source different from gravity. On the other hand, it should be stressed that, a collapsing cloud will have a kinetic energy of the order of the gravitational energy, very close to the virial value, although by no means this implies that the cloud is been supported. In reality, by just computing the kinetic energy, we cannot have tools to distinguish between a collapsing and an expanding cloud.
2. It is also frequently assumed that the surface terms in the VT are negligible compared to the volumetric ones. While some times it is recognised that the pressure at the boundary of the clouds could be important, it is less widely recognised that the kinetic pressure, or the magnetic tension at the surface of the cloud could play a role. Both terms could contribute to distorting the cloud, especially in a highly dynamic environment.
3. “The gravitational term of a cloud can be approximated by the gravitational energy of a homogeneous sphere.” That is, that,

$$W = \int_V \rho x_i \frac{\partial\Phi}{\partial x_i} dV \simeq -\frac{3}{5} \frac{GM^2}{R} = E_{\text{grav}}. \quad (7)$$

However, it should be noted that the gravitational potential is that generated by the entire mass distribution, and not just that interior to the cloud. Therefore, it

should be stressed, on the one hand, that tidal terms can be important either for the energetic balance of GMCs in the disk (Ballesteros-Paredes et al., 2009a,b; Meidt et al., 2018), as well as in the Central Molecular Zone, where the effective gravitational potential due to rotation and shear can play an important role. On the other hand, on small scales, it has been recognised that protostars still in the process of accretion can gravitationally compete for the available material (Bonnell and Bate, 2006; Maschberger et al., 2014; Ballesteros-Paredes et al., 2015; Lee and Hennebelle, 2018; Hennebelle et al., 2019, see also Lee et al. 2020, this volume), and that the actual gravitational energy computed from the standard recipe (right part of eq. [7]) can be modified even by a factor up to 10 when considering the actual structure of a stellar cluster (left part of eq (7), see e.g., Cottaar et al., 2012; Ballesteros-Paredes et al., 2018) from the standard recipe. Conversely, neglecting the actual gravitational potential can result in substantially wrong estimates of the total gravitational content of the clouds (Ballesteros-Paredes et al., 2018).

4. “The sign of the second-time derivative of the moment of inertia determines whether the cloud is contracting ( $\ddot{I} < 0$ ), expanding ( $\ddot{I} > 0$ ), or static ( $\ddot{I} = 0$ ).” However, one can easily find counterexamples in each case (see Ballesteros-Paredes, 2006).
5. “Molecular clouds are near virial equilibrium, and the Larson (1981) relations are the evidence of that.” Although still it is commonly found in the literature that clouds follow the Larson (1981) relations, and thus, that they are in virial equilibrium, it has become clear that, in reality, they exhibit a wide range of virial parameters (Bertoldi and McKee, 1992; Kauffmann et al., 2013; Leroy et al., 2015). We will discuss this point in §4.

Even though a variety of numerical simulations of (a) galactic disks (e.g., Dobbs, 2008; Tasker and Tan, 2009), (b) parts of the disk (e.g., de Avillez and Breitschwerdt, 2005; Shetty and Ostriker, 2008; Ibáñez-Mejía et al., 2016; Seifried et al., 2018), or (c) closed boxes (e.g., Federrath et al., 2010; Padoan et al., 2016; Kim et al., 2018, just to quote a few references), show a highly dynamical picture of MCs, almost no work in the literature evaluates the second time derivative of the moment of inertia, which presumably, should be relevant. The difficulty resides, in part, in the fact that this term is highly noisy, due to its second-derivative character. Early 1 kpc<sup>2</sup> 2D simulations of the galactic disk with cooling, stellar and diffuse heating, magnetic field, Galactic shear and rotation by Ballesteros-Paredes and Vázquez-Semadeni (1997) based on the simulations of Passot et al. (1995) have computed this term. These authors found that, indeed, the time derivative terms in the Eulerian virial theorem<sup>1</sup> are dominant, by one or two orders of magnitude, over the remaining energies. There is, however, substantial scatter in these results, likely due to the difficulty of comparing time derivatives to integrated quantities. However, even with such a large scatter, the picture in the ISM is clear: it seems unlikely that MCs obey  $\ddot{I} = 0$ .

In addition, it should be noted that in eq. (6) we have written the kinetic energy term,  $E_{\text{kin}}$  on the left hand side of the equation, because this term derives directly

<sup>1</sup>It should be noticed that the Eulerian virial theorem involves two additional terms, related to the distribution of mass inside the fixed volume, and the flux of momentum between the volume and its environment (see Parker, 1979; McKee and Zweibel, 1992).

from the time derivative term in the momentum equation, and so it is part of the kinematic response of the cloud to the work exerted by the forces, rather than an additional energy source of work. That is, the work exerted by the forces causes two types of kinematic responses in the cloud: a change in its internal mass distribution, as measured by its moment of inertia, and kinetic energy that can consist of either an internal velocity dispersion or a bulk motion of the cloud. Strictly speaking, the virial version of equilibrium or force balance should therefore be written as  $\dot{I}/2 - 2E_{\text{kin}} = 0$ , while the equality  $E_g + 2E_{\text{kin}} = 0$ , rather than equilibrium, implies that the kinetic energy is being driven by gravity.

### 3.2 Reconstructing the energy budget of MCs

All the caveats mentioned above should not stop us from computing the various work terms due to the different forces, and derived quantities, in order to approximately estimate the dynamical state of MCs. For instance, the fact that assuming  $\dot{I} = 0$  is incorrect in an evolving cloud should not stop us from obtaining at least an order-of-magnitude estimate of the different energies of clouds. In fact, there are several key concepts that can be derived from the VT, and that allow us to understand better the state of the clouds. In particular, approximations to the Jeans length

$$\lambda_J \sim \left( \frac{\pi c_s^2}{G \rho} \right)^{1/2} \quad (8)$$

(where  $c_s$  is the isothermal sound speed, and  $G$  is the constant of gravity), and the Jeans mass,  $M_J \sim \rho \lambda_J^3$ , can be obtained from equating the gravitational and thermal energies, and making assumptions on the geometry. Also, the ‘‘virial parameter’’, defined by Bertoldi and McKee (1992),

$$\alpha_{\text{vir}} = \frac{5\sigma_v^2 R}{GM} \simeq \frac{2E_{\text{kin}}}{E_g}, \quad (9)$$

where  $\sigma_{v,1d}$  is the non-thermal, 1D velocity dispersion, can give insights on whether a cloud could be collapsing or not, although only in order of magnitude due to different uncertainties (Kauffmann et al., 2013; Pan et al., 2016; Ballesteros-Paredes et al., 2018, see §4.6). Similarly, it can be noticed easily that the gravitational energy

$$E_{\text{grav}} \sim -\frac{3}{5} \frac{GM^2}{R} \quad (10)$$

and the magnetic energy,

$$E_{\text{mag}} \sim \frac{1}{8\pi} B^2 R^3 \propto \frac{\Phi_{\text{mag}}^2}{R} \quad (11)$$

(where  $\Phi_{\text{mag}} = \pi R^2 B$  is the magnetic flux) have the same dependency with size, since in ideal MHD the magnetic field is anchored to the gas such that the magnetic flux  $\Phi_{\text{mag}}$  remains constant. Thus, the magnetic and the gravitational energies scale with size in the same way, implying that if a cloud has more gravitational energy

(in absolute value), the magnetic field cannot prevent collapse, and if it is smaller, collapse will never occur.

In summary, evaluating the energies of MCs can provide insights on what the dynamics of MCs is. There are still some observational biases that have to be taken into account. We will further discuss these issues in §4.

#### 4 Cloud statistics and scaling relations

Statistical analyses of MC properties have been widely used in the literature to understand the dynamical, kinematic, structural and evolutive properties of MCs. These can be considered under two basic approaches: either analysing a single cloud, with different tracers and/or at different column densities, such that one can determine what is the internal structure of a single object, or analysing an ensemble of clouds (or cores within a cloud, with either one or more tracers; see e.g., Goodman et al., 1998). The most relevant properties of MCs, which we will discuss in what follows, are the mass spectrum of GMCs and/or cores, the column density probability distribution, the scaling relations between the mass, the velocity dispersion and the column density, and their size, the virial parameter, the magnetic field, and the fractal nature.

##### 4.1 The mass spectrum of MCs and their cores.

The mass spectrum of the clouds—i.e., the distribution of the masses of MCs and their substructures (clumps and cores)—is one of the fundamental properties of the clouds that requires a theoretical foundation. As a consequence, estimates of the mass spectra of GMCs have been reported, first from surveys of CO clouds, and later from dust continuum emission (and a few others in dust extinction). The resulting mass distributions show that there is no characteristic mass for MCs, but that they rather follow, typically, a power-law with a negative exponent,

$$\frac{dN}{d \log M} \propto M^{-\gamma} \quad (12)$$

The estimates of  $\gamma$  for large clouds (MCs and GMCs) based on CO observations give values between 0.2 and 0.9 (Sanders et al., 1985; Solomon et al., 1987; Williams et al., 1994; Heyer and Terebey, 1998; Heyer et al., 2001). The corresponding estimates for dense, compact, prestellar cores based on continuum emission give values of  $\gamma$  between 1 and 2, (Motte et al., 1998; Testi and Sargent, 1998; Johnstone et al., 2000, 2001; Motte et al., 2001; Beuther and Schilke, 2004; Mookerjee et al., 2004; Reid and Wilson, 2005, 2006a,b; Stanke et al., 2006; Alves et al., 2007; Könyves et al., 2015; Ohashi et al., 2016; Cheng et al., 2018, see also §8.3.3). This evidence strongly suggests that compact, self-gravitating cores have a mass distribution closer to the Salpeter (1955) stellar initial mass function (IMF), for which an exponent of  $-1.35$  has been taken as a standard value.

There are, however, a few works that do not quite match the picture of small cores with an IMF-like distribution, and large clouds with flat mass spectra. In the

first group, using CO data, values of  $\gamma \sim 0.7 - 0.8$  have been found for small-scale structures rather than for MCs and GMCs (Stutzki and Guesten, 1990; Heithausen et al., 1998; Kramer et al., 1998). In the second group, Rosolowsky et al. (2010) show Salpeter-like values of  $\gamma$  for large clouds seen in dust emission. These studies suggest instead that the actual value of the power-law of the mass spectra of clumps and cores could be biased due to the technique used. Among the possible causes playing a role are opacity effects, CO depletion in dense cores, and the clump identification procedure. Also, it should be noticed that the study by Rosolowsky et al. (2010) is based on interferometric observations, possibly filtering out large scales that could affect the slope of the mass distribution.

One more caveat should be mentioned: all the mass spectra derived from continuum emission quoted above, with the exception of Rosolowsky et al. (2010), exhibit a small ( $\lesssim$  one order of magnitude) dynamical range in mass over which a Salpeter-like slope can be fitted. In fact, looking carefully at the mass distributions of these studies (see, e.g., Motte et al., 2001; Reid and Wilson, 2005, 2006a; Stanke et al., 2006; Alves et al., 2007; Román-Zúñiga et al., 2010), rather than a single power-law, one can see that lognormal-type shapes can be fitted too, as pointed out by Ballesteros-Paredes et al. (2006) and Könyves et al. (2015).

Finally, it should be mentioned that, using ALMA observations, the star forming region W43-MM1 exhibits a top-heavy core mass function (Motte et al., 2018).

Although this study does not distinguish between prestellar and protostellar cores, and results could be quite sensitive to the assumed temperature, possibly modifying the slope of the mass spectra, the inferred slope of  $-0.96$  by Motte et al. (2018) is consistent with a value of  $-1$ , predicted by some models of gravity-driven formation of dense cores (see Vázquez-Semadeni et al., 2019a, and references therein).

With the various caveats mentioned above, it is clear that the relationship between the mass distribution of prestellar cores and the IMF remains an open problem. Further high-resolution observations as well as detailed high-resolution numerical simulations, with carefully controlled comparison schemes, are required.

## 4.2 Volume- and column-density probability distribution functions of MCs

The probability distribution function (PDF) of a variable is a one-point statistics that measures the relative fraction of volume (or mass) of a fluid that is in a given range of values of the variable under consideration. These functions are often computed as the histograms of the volume and column density fields. The fundamental hypothesis behind studies of the probability distribution function of the volume- and column-density fields ( $\text{PDF}_V$  and  $\text{PDF}_N$ , respectively) is that these are sensitive to the physical processes operating in the interstellar medium (e.g., Vázquez-Semadeni, 1994; Passot and Vázquez-Semadeni, 1998; Federrath et al., 2008; Kainulainen et al., 2009; Tassis et al., 2010; Kainulainen et al., 2011; Kritsuk et al., 2011; Ballesteros-Paredes et al., 2011b). However, the problem is degenerated, since different physical conditions can produce similar shapes of the PDF (e.g., Vázquez-Semadeni and García, 2001; Tassis et al., 2010; Pan et al., 2019).

It is well known that the density field of the galactic interstellar medium in general, and of molecular clouds in particular, is filled up by a low-density substrate, in which denser structures are embedded and occupy only a very small fraction of the volume, i.e., density enhancements have small filling factors, as can be inferred from the rapidly decreasing  $\text{PDF}_N$ s of MCs (e.g., Kainulainen et al., 2009).

Although different tracers have a characteristic density at which the emission is produced, it is not possible to estimate, in an unambiguous way, the  $\text{PDF}_\rho$  of a MC. This is because the length of a MC along the line of sight is always an unknown, and thus, so it is the exact fraction of the volume occupied by the gas that is producing the emission. However, the  $\text{PDF}_N$  is easily calculated by computing the total mass in each line of sight. In general terms, unless a particular arrangement of mass occurs, the  $\text{PDF}_N$  of the interstellar medium in general, and of the MCs in particular, is also a rapidly decreasing function.

First reported by Vázquez-Semadeni (1994), it is generally accepted that the  $\text{PDF}_\rho$  of an isothermal, supersonic, turbulent gas is lognormal (although departures of the lognormality may occur, depending on the nature of the turbulent field, see Pan et al., 2019, and references therein). The reason is the following: an isothermal shock of Mach number  $\mathcal{M}$  produces a density enhancement  $\delta\rho$  over the mean density  $\rho$  proportional to  $\mathcal{M}^2$ , i.e.,  $\delta\rho/\rho \propto \mathcal{M}^2$ . Then, in an isothermal turbulent fluid with characteristic Mach number  $\mathcal{M}$ , the amplitude of the density fluctuations is produced by a random succession of passing shocks. This produces a random distribution of multiplicative density enhancements, which become additive in the logarithm, and thus, by the central limit theorem, this produces a normal (Gaussian) distribution function in the logarithmic density, i.e., a lognormal function.

The corresponding  $\text{PDF}_N$  for an isothermal turbulent field, however, does not have a unique functional form (Vázquez-Semadeni and García, 2001). It transits from a Gaussian to the lognormal as the correlation length of the turbulence increases. The Gaussian is produced when the size of the cloud in the line of sight is large compared to the correlation length of the turbulence. In such case, by the central limit theorem again, the stochastic occurrence of density fluctuations in each line of sight produces a Gaussian distribution of column densities<sup>2</sup>. However, if the correlation length and the line of sight become comparable, this is no longer valid. In this case, the column density in each line of sight is representative of the mean density of the fluid in the line of sight, and thus, the  $\text{PDF}_N$  inherits the shape of the actual  $\text{PDF}_\rho$ , which, in the case of an isothermal turbulent fluid, is also lognormal, although certainly with a smaller width than the original distribution of the volume density because of the partial averaging performed in each line of sight.

We now turn to the observational  $\text{PDF}_N$  reported in the literature. An important warning has to be made first, however: as pointed out by Alves et al. (2017), any reported shape of the  $\text{PDF}_N$  from observations has to be made only for those contours that are closed in the map. The inclusion of data from non-closed column density contours when computing the  $\text{PDF}_N$  is necessarily incomplete, and thus, the  $\text{PDF}_N$  at those column densities is underestimated, causing a spurious drop in the PDF.

<sup>2</sup>It should be noticed that this result assumes that each line of sight is independent. This may not be the case in the case of strong magnetic fields, large scale gravitating structures, or a large correlation length of the turbulence.

In a similar way, some relationships between the physical properties and the shape of the PDFs of clouds in numerical simulations cannot be extrapolated to real life: in numerical simulations the PDF of volume and column density necessarily have a maximum at some intermediate value, and decrease towards lower densities due to the finite size and mass of the computational box. That is, the boundary of the simulation is in general equivalent to a non-closed density contour for the density statistics in the numerical box.

In summary, PDFs of interstellar gas do not necessarily have to decrease at low densities, and inferring physical properties of MCs by fitting the low-density regime of a PDF may be seriously wrong. In consequence, in what follows we will refer only to the upper-end column density of the PDF<sub>N</sub>s.

Observationally, PDF<sub>N</sub>s of MCs have been reported to be lognormal functions for clouds that do not exhibit substantial star formation, and power laws for actively-star forming clouds (Kainulainen et al., 2009). On the other hand, numerical simulations show that the PDF<sub>N</sub> from turbulent clouds is, typically, lognormal, and that they transit to a power-law as gravity takes over (Kritsuk et al., 2011; Ballesteros-Paredes et al., 2011b), which is indeed observed in low-star formation efficiency MCs in the Galactic Centre environment (Rathborne et al., 2014).

An interesting result arises from the observations quoted previously in this section: the ratio of active-to-non active clouds in the Solar Neighborhood is about  $\sim 10:1$  (Kainulainen et al., 2009). Assuming that the shape of the observed PDF<sub>N</sub>s reflects the internal physics that produce their structure, this result suggests, at face value, that only 10% of the clouds are dominated by homogeneous turbulence, which furthermore, is stirred from the large scales while the majority of MCs are dominated by gravity.

#### 4.3 The mass- and the density-size relations

The mass-size (or its equivalent, the mean density-size) relation has been used to analyse the internal structure (a single cloud at different column density thresholds) as well as a statistical relation between a set of clouds, of clumps, or of cores. Both cases provide different information about the properties of MCs, and thus, have to be discussed independently.

Before going into the details, two points need to be made. First the size of a projected cloud in the plane of the sky is typically computed as the radius of an equivalent circle that has the same area of the cloud. Thus, usually, the reported size is proportional to the square root of the area of the cloud. We notice that, for fractals, this is a mistake, since the estimate of the size of an object must be given by a quantity that is independent of the area or volume (e.g., its perimeter, see Falgarone et al., 1991; Stutzki, 1993). Therefore, if clouds have a fractal structure, the size calculation as the square root of the area is likely to introduce a spurious systematic bias. Second, the functional form of the PDF<sub>N</sub> has direct implications on the mass-size relation: given a PDF<sub>N</sub>, the area and the mass of the cloud above some column

density threshold  $N_{\text{thr}}$  can be computed from the  $\text{PDF}_N$  (see Lombardi et al., 2010) as:

$$S(N_{\text{thr}}) = S_{\text{tot}} \int_{N_{\text{thr}}}^{\infty} \text{PDF}_N dN \quad (13)$$

and

$$M(N_{\text{thr}}) = S_{\text{tot}} \mu m_H \int_{N_{\text{thr}}}^{\infty} N \text{PDF}_N dN \quad (14)$$

where  $S_{\text{tot}}$  is the total area of the cloud,  $\mu$  is the mean atomic weight and  $m_H$  is the mass of the hydrogen atom, and  $N$  is assumed to be in units of  $\text{cm}^{-2}$ . Note that eqs. (13) and (14) imply a definition of a cloud, as all the material that is above some column density threshold,  $N_{\text{thr}}$  in a given region. From these equations it is clear that the surface and the mass of a cloud are the zeroth and first moments of the  $\text{PDF}_N$ .

As a general result, it can be demonstrated that (i) the mass-size relation for the inner structure of a single cloud (i.e., for a molecular cloud seen at different thresholds) should be a power-law with slope smaller than 2, frequently modified at large radii by a curve with decreasing slope (Ballesteros-Paredes et al., 2012), as seen in observations (see, e.g., Kauffmann et al., 2010b; Lombardi et al., 2010). In contrast, (ii) the mass-size relation for an ensemble of objects should be a power-law with a slope of 2 (e.g., Beaumont et al., 2012; Ballesteros-Paredes et al., 2012), as observed by Lombardi et al. (2010).

Both results can be demonstrated from eqs. (13) and (14) in terms of the rapidly decreasing  $\text{PDF}_N$ s in MCs. For case (i) (the internal structure of a single cloud), if the  $\text{PDF}_N$  is a power law, i.e.,  $\text{PDF}_N dN \propto N^{-\beta} dN$ , it can be shown that the mass-size relationship necessarily has slopes smaller than 2 for  $\beta > 2$  (see Fig. 12 in Ballesteros-Paredes et al., 2012, where  $n$  is our  $\beta$ , and  $a$  is the exponent of the mass-size relation), a result observed in nearby MCs (Kainulainen et al., 2009; Kauffmann et al., 2010a,b; Lombardi et al., 2010). Also, following the formalism of Lombardi et al. (2010), it can be shown that the apparent flattening of the mass-size relation at large radii (see, e.g., Kauffmann et al., 2010b; Lombardi et al., 2010) is due to the departure of the  $\text{PDF}_N$  from the power-law behavior at low column densities, which has been shown to be due to incomplete sampling of clouds at low column density contours (Alves et al., 2017, see §4.2). It can be shown also that, if instead of a power-law, the  $\text{PDF}_N$  is assumed to be a lognormal, the increasing slope (in absolute value) of the  $\text{PDF}_N$  will produce a decreasing slope in the mass-size relation (Ballesteros-Paredes et al., 2012).

In case (ii) (the mass-size relation for an ensemble of clouds or cores defined by a single column density threshold), Ballesteros-Paredes et al. (2012) pointed out that, since the  $\text{PDF}_N$  is a rapidly decreasing function of  $N$ , with slopes typically steeper than  $-2$  (Kainulainen et al., 2009), averaging the column density above a threshold causes all clouds to exhibit the same mean column density, close to the threshold used. In fact, Ballesteros-Paredes and Mac Low (2002) noticed that if one were able to define clouds using volume thresholds, the resulting mass-size relation should be a powerlaw with exponent 3, since the mean volume density of clouds defined in such a way should be roughly constant if the  $\text{PDF}_\rho$  of MCs is a rapidly decaying distribution function. This fact has been circumstantially confirmed by Kainulainen et al. (2011),



who found a mass-size relation with slope close to 3 ( $\sim 2.7$ ), for a set of clumps defined in such a way that their volume density was roughly constant.

With these two basic results in mind, a crucial question is, then, whether exponents different from 2 of the mass-size relation for an ensemble of clouds or cores indicate intrinsically different physical properties, or whether such differences are the result of the procedure or definition used in the analysis. In fact, it is noteworthy that, while cloud surveys performed using dust extinction (e.g., Lombardi et al., 2010) give slopes very close to 2, CO observations typically show exponents larger than 2 (e.g., Bolatto et al., 2008; Roman-Duval et al., 2010; Miville-Deschênes et al., 2017). In all of these cases, the clouds are defined through intensity thresholds, which are essentially proportional to the column density. In view of the above discussion on the effect of selection, it is the excess over a slope of 2 that requires explanation. To do so, Ballesteros-Paredes et al. (2019) argued that, while surveys based on dust extinction are restricted to nearby clouds, CO surveys can reach up to very large distances, and the probability of random superposition of different clouds along the line of sight, due to non-circular motions in the Galaxy (Blitz and Shu, 1980; Gómez, 2006), increases with distance in any given velocity channel. In fact, superposing in the line of sight a random mass factor between  $10^{-4}$  and  $10^{-1}$  of the total mass of the cloud can account for mass-size relationships with slopes similar to those found in the observational surveys (Ballesteros-Paredes et al., 2019).

Finally, in the case of cores within a single cloud, different definitions and methods of core extraction may produce different slopes, and thus, there is no consensus on what is the slope of the mass-size relation for cores within a single cloud. For instance, using getsources (Men'shchikov et al., 2012) or wavelets (Román-Zúñiga et al., 2010), slopes between 2.2 and 2.7 are typically found (e.g., Lada et al., 2008; Román-Zúñiga et al., 2010; Könyves et al., 2015), although sometimes weak correlations are found (Bresnahan et al., 2018). In the case of Gaussclumps (Stutzki and Guesten, 1990), the mass-size relationships exhibit slopes that could be either larger than 2 (Mookerjee et al., 2004; Veltchev et al., 2018), as well as smaller (Zhang and Li, 2017).

#### 4.4 The velocity dispersion-size relation

Since the first detections of CO (e.g., Wilson et al., 1970), it is known that molecular clouds exhibit supersonic linewidths. Given the large Reynolds numbers in the interstellar medium,  $\mathcal{R} = v_l l / \nu \sim 10^5 - 10^8$  (Myers, 1983; Miesch et al., 1999; Elmegreen and Scalo, 2004), with  $v_l$  the characteristic velocity at the scale  $l$ , and  $\nu$  the kinematic viscosity of the fluid, molecular clouds are necessarily turbulent, and thus, naturally, the dynamical role of such turbulence on the evolution of MCs has been a matter of intense analysis and debate.

It should be recognised that in the astrophysical argot, the term turbulence has been somehow, synonymous of either supersonic turbulence, and/or support against gravity. Certainly, subsonic turbulence cannot account for support against self-gravity better than what thermal pressure does, but it should be noticed that there are regions in the interstellar medium, and within molecular clouds, where the linewidths become

sub- or trans-sonic, and that they could be very well subsonically turbulent, similarly to all natural terrestrial turbulent flows.

The velocity structure of MCs is substantially more difficult to determine than their mass structure: by considering spectroscopic data from molecular-line transitions we add a 3rd coordinate, and thus, the total emission has to be divided between different velocity channels, lowering the signal-to-noise ratio of the emission. In addition, different molecules frequently exhibit different spatial structure, either because of opacity or chemistry effects. As pointed out by, e.g., Traficante et al. (2018c), the volume from where the emission comes in one case or another may play a role in the determination of fundamental physical properties, such as the virial parameter. Nonetheless, assuming that the velocity structure measured with a particular tracer is representative of the volume it traces is approximately valid for most molecules, besides CO and its isotopes (Tafalla et al. 2020, in preparation).

One of the most frequent arguments in favour of supersonic turbulence as a universal dynamical ingredient in molecular clouds is the existence of a correlation between the velocity dispersion ( $\sigma_v$ ) and the size ( $R$ ) for ensembles of clouds, over 4 – 5 orders of magnitude in size (e.g., Falgarone et al., 2009). In his original work, Larson (1981) reported the correlation

$$\sigma_v \propto R^p, \quad (15)$$

with  $p \sim 0.38$ , over 3 orders of magnitude in size. Larson (1981) interpreted this correlation as incompressible turbulence in molecular clouds, since the exponent is close to that predicted by Kolmogorov (1941) for incompressible (i.e., subsonic) turbulence. However, this is mgt inconsistent with the fact that the velocity dispersion is typically supersonic in the Larson (1981) data.

The canonical exponent for the velocity dispersion-size relation has been taken as  $1/2$ , not only because, observationally, this value has been found in a variety of studies (e.g., Myers, 1983; Solomon et al., 1987; Ossenkopf and Mac Low, 2002; Heyer and Brunt, 2004, see also Falgarone et al. (2009) and references therein), but because, theoretically,  $p \sim 1/2$  is the expected value for a turbulent velocity field dominated by shocks (see, e.g., Passot et al., 1988; Vázquez-Semadeni, 1999; McKee and Ostriker, 2007, and references therein).

Although this result is apparently well settled (see e.g., Hennebelle and Falgarone, 2012; Klessen and Glover, 2016), the detailed slope of the velocity dispersion-size relation is far from being firmly established. There is still a large list of observational works where the exponent is typically smaller than  $1/2$  (e.g., Carr, 1987; Caselli and Myers, 1995; Loren, 1989; Plume et al., 1997; Shirley et al., 2003; Traficante et al., 2018a, to quote a few). In some cases,  $p$  has been found to be even negative (e.g., Wu et al., 2010), and in others,  $p > 1/2$ , not only for the Central Molecular Zone (Shetty et al., 2012; Kauffmann et al., 2017), but even for the ensemble of clouds in the whole galaxy, (Miville-Deschênes et al., 2017). Similarly, Ballesteros-Paredes et al. (2011a) showed that when massive-clumps are considered together with MCs, the relation is lost, and only a scatter plot remains. Fig. 4 shows the velocity dispersion-size diagram for a list of low-mass cores in regions of high-mass star formation, where there is no clear trend between the velocity dispersion and the size. Nevertheless, there is a trend to notice: high column density

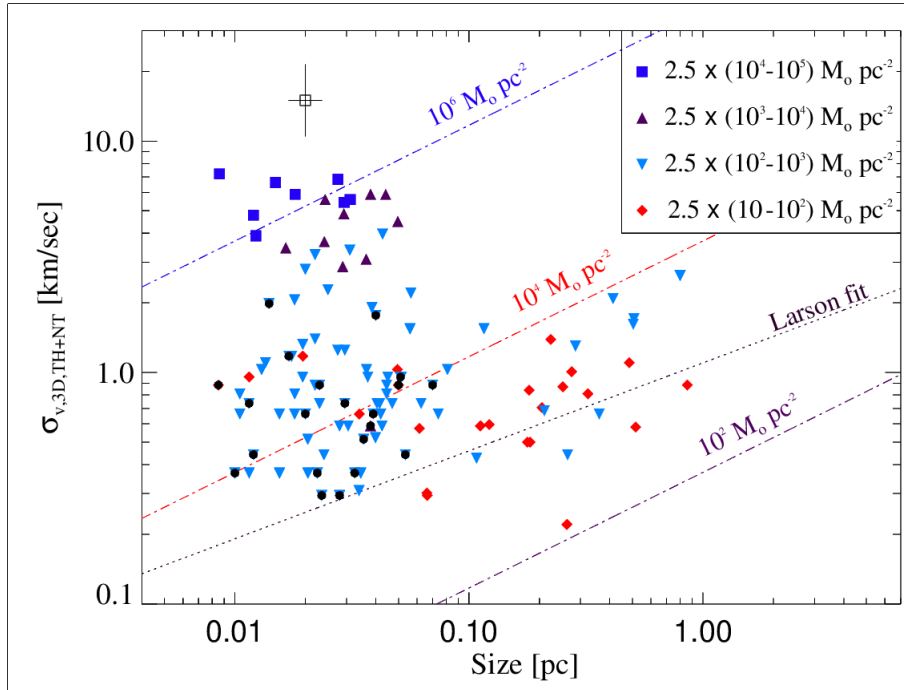


**Fig. 4** Velocity dispersion-size relation for cores in regions of massive star formation. Clearly, there is not a clear correlation between the size and the velocity dispersion. There is a tendency, with substantial scatter, of cores with large column densities to exhibit large velocity dispersion. Figure from (Ballesteros-Paredes et al., 2018).

cores exhibit larger velocity dispersions than low column density cores. This result is expected if either (a) cores are collapsing (see Sec. 4.5), or (b) localised feedback is present, since it could increase the velocity dispersion within the cores. However, the core selection was based on ammonia emission, which typically is destroyed if UV feedback is present. In addition, the cores shown in Fig. 4 were carefully selected to avoid morphological evidence of feedback (Palau et al., 2014). For these reasons, Ballesteros-Paredes et al. (2018) tend to favour the first option, that the larger velocity dispersion for larger column density cores is due to collapse. We will discuss this point in §4.5.

Another approach to the velocity dispersion-size relation in GMCs consists in measuring velocity differences within the GMC. There are two ways for approaching it: (i) measuring the structure function  $S_p(l)$  of the velocity field (Heyer and Brunt, 2004; Hily-Blant et al., 2008)

$$S_p(l) = \langle |v(r) - v(r+l)|^p \rangle, \quad (16)$$

(where  $l$  is the spatial displacement between two pixels in the map of the cloud, and  $p$  is the order of the structure function), and (ii) measuring the moments of the PDFs of the centroid velocity differences, as a function of the lag (Miesch and Scalo, 1995; Miesch et al., 1999). The results from these studies are in general consistent with the

clouds' dynamics being dominated by turbulence. However, it is important to notice that none of these approaches is equivalent to the velocity dispersion-size relation of clumps and cores within clouds: while the latter measures the motions exclusively in density enhancements (cores or clumps) of size  $\ell$ , the former two estimate the relative motions between points separated by a distance  $\ell$  for the whole field; i.e., regardless of whether there is a density enhancement or not at each point. For small scales, for instance, the structure function has more weight from the low-density regions than from the high density regions of the cloud, just because the filling factor of the latter is small. This difference in the sampled regions may introduce biases that must be taken into account when comparing results from the two methods.

At the smaller scales, however, there are velocity dispersion-size relations reported for single resolved cores. These are obtained, for example, by performing a succession of pointings at different distances from the core center and plotting the linewidth as a function of distance from the center (e.g., Pineda et al., 2010). While some of them exhibit power-laws consistent with  $p \sim 1/2$  (e.g., Rosolowsky et al., 2008), there is a class of cores for which velocity dispersion-size relation becomes flat at small scales, at essentially the speed of sound, implying a subsonic turbulent velocity dispersion (e.g., Barranco and Goodman, 1998; Goodman et al., 1998; Caselli et al., 2002; Tafalla et al., 2004; Pineda et al., 2010; Chen et al., 2019). These are the so-called (velocity) “coherent cores”. Three different physical interpretations for these cores have been made: some authors have interpreted the lack of velocity and density structure as an indication that these cores are “islands of calm” within a turbulent sea (Goodman et al., 1998; Pineda et al., 2010). Klessen et al. (2005), on the other hand, found that turbulent motions can produce coherent cores by shock compressions, so that a coherent core is the stagnation point of the velocity field behind the shock. Finally, Naranjo-Romero et al. (2015) have pointed out that the spherical collapse solution for cores in the protostellar stage contains a central region characterized by a flat density profile and an infall speed that decreases linearly with decreasing distance from the center. Therefore, if the nonthermal part of the linewidth in these regions is dominated by the infall speed, it should decrease toward the center, as observed.

In summary, it is not clear that there is a single value for the slope of the velocity dispersion-size relation; different kinds of objects can exhibit different slopes, depending on how the object selection is made.

#### 4.5 The Larson ratio-column density diagram

A breakthrough in the interpretation of Larson’s scaling relations was advanced by Heyer et al. (2009), who generalized them by noticing that the so-called Larson ratio<sup>3</sup>  $\mathcal{L} \equiv \sigma_v/R^{0.5}$ , for Galactic GMCs depends on the mass column density  $\Sigma = \mu m_H N$  as

$$\mathcal{L} \propto \Sigma^{0.5}, \quad (17)$$

<sup>3</sup>We call the Larson ratio the square root of the so-called velocity scaling,  $C \equiv \sigma_v^2/R$ , in the extragalactic literature.

instead of being constant, as would be required by Larson’s velocity dispersion-size relation and/or by strongly supersonic turbulence. This result has been confirmed by other authors, either for Galactic objects (e.g., Kruijssen and Longmore, 2013; Miville-Deschênes et al., 2017; Traficante et al., 2018b; Ballesteros-Paredes et al., 2018), as well for extragalactic (e.g., Leroy et al., 2015; Sun et al., 2018; Imara and Faesi, 2019), although with substantial scatter.

As pointed out by Heyer et al. (2009), this scaling is consistent with the clouds being in virial equilibrium, when the cloud sample is not restricted to a constant column density, as it follows directly from the condition  $2E_k = E_g$ , where  $E_k = M\sigma^2/2$ ,  $E_g = 3GM^2/5R$ , with  $\sigma$  being the one-dimensional velocity dispersion,  $M$  the cloud’s mass and  $R$  its radius, and defining the column density as  $\Sigma = M/\pi R^2$ . In addition, (Ballesteros-Paredes et al., 2011a) further pointed out that the scaling is also consistent with the clouds undergoing free-fall, in which case  $E_k = |E_g|$ . It is important to note that the free-fall condition in the  $\mathcal{L}$ - $\Sigma$  diagram coincides with what is often referred to as “marginal binding”, even though it corresponds to actually stronger binding than virial equilibrium. For practical purposes, the difference between free-fall and virial equilibrium in the  $\mathcal{L}$  vs.  $\Sigma$  diagram is within the typical uncertainty of the observations. Nevertheless, at face value, most of the clouds in the Heyer et al. (2009) sample appear slightly overvirial, and more consistent with free-fall. A similar result is seen in extragalactic GMC data as well as other Milky Way data (e.g., Sun et al., 2018).

Furthermore, Ballesteros-Paredes et al. (2011a) showed that the scaling given by eq. (17) holds not only for GMCs, but extends to massive dense cores, for which the Larson velocity dispersion-size relation does not hold. Thus, those authors suggested that the velocity dispersion in both GMCs and dense cores is driven by self-gravity, and specifically consists of infall motions, albeit highly chaotic, due to the presence of turbulence and of multiple collapse centers (see also Vázquez-Semadeni et al., 2019b). However, eq. (17) cannot be satisfied simultaneously with the standard Larson relation  $\sigma \propto R^{1/2}$  in objects of different column densities. Instead, clumps and cores of higher column density are expected to exhibit different loci in the  $\sigma$ - $R$  diagram, as observed (Caselli and Myers, 1995; Plume et al., 1997; Ballesteros-Paredes et al., 2011a, see also Fig. 4). Note, however, that an alternative interpretation to the different  $\sigma$ - $R$  scaling in dense cores is that their gravitational contraction is delayed by turbulent pressure (Murray and Chang, 2015; Xu and Lazarian, 2020).

Although the scaling (17) has been observed to hold for column densities from  $10$  to  $\gtrsim 10^4 M_\odot \text{pc}^{-2}$  (e.g., Leroy et al., 2015), significant systematic deviations from it are observed as well. Low-column density objects (the more diffuse clouds, with  $\Sigma \sim 10\text{--}100 M_\odot \text{pc}^{-2}$ ) often appear to be strongly over-virial, while high-column density clumps and cores, with  $\Sigma \gtrsim 10^3 M_\odot \text{pc}^{-2}$  often appear subvirial or super-virial. The standard interpretation of super-virial low-column density clouds is that they are confined by a large external pressure, since they are gravitationally unbound (Keto and Myers, 1986; Field et al., 2011). However, Camacho et al. (2016) found in numerical simulations of cloud formation that such objects are in general out of equilibrium, and are either dispersing or being assembled by externally-driven compressions. On the other hand, for dense cores that appear supervirial, Ballesteros-Paredes et al. (2018) showed that this may be simply an artifact of the fact that the

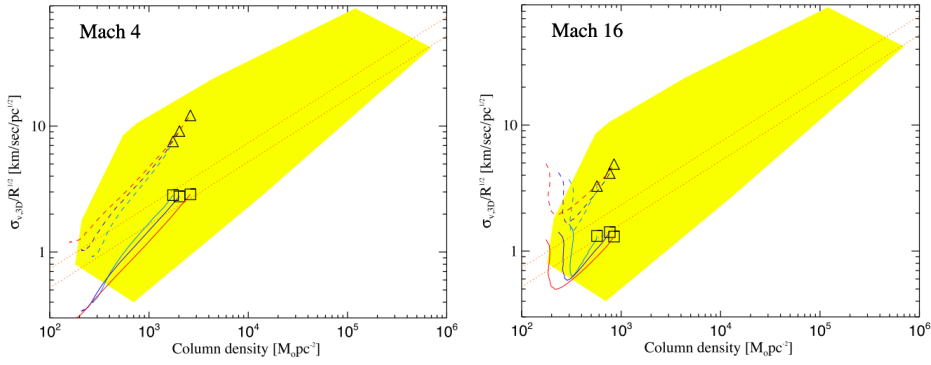


**Fig. 5** Evolution in the  $\mathcal{L} - \Sigma$  diagram of collapsing cores with initial velocity fluctuations. When the approximation  $|E_g| \sim 3GM/5R$  is used, cores frequently appear overvirial (dashed lines). When the correction to consider the actual gravitational energy is taken into account in the calculations, collapsing cores appear subvirial (solid lines). The yellow region denotes the locus occupied by observed cores in the sample studied by Ballesteros-Paredes et al. (2018). The dotted lines denote the locus where virial (below) and “free-fall” (above) cores should fall. (Figure from Ballesteros-Paredes et al., 2018).

actual gravitational energy of a structured core can be substantially larger (in absolute value) than the gravitational energy of an homogeneous sphere with the same mass, velocity dispersion, and size of the core (Ballesteros-Paredes et al., 2018). This occurs because the gravitational energy of clouds and cores is typically underestimated by using the approximation  $|E_g| \sim 3GM^2/5R$ , and thus, collapsing clouds/cores can appear to be unbound when they are not. In Fig. 5 we show the situation: collapsing cores exhibit overvirial values when the approximation to the gravitational energy is used (dashed lines), but sub-virial values evolving to virial after  $\sim$  one free-fall time when the actual gravitational potential is taken into account in the calculation. This result is consistent with observations by Cesaroni et al. (2019), who show collapsing line profiles in clouds with masses smaller than their virial mass.

Finally, Ballesteros-Paredes et al. (2018) also showed that, if a core is formed by an inertial externally-driven (i.e., not due to self-gravity) compression and it gradually transitions to collapse driven by its own self-gravity, its evolutionary track in the  $\mathcal{L} - \Sigma$  diagram starts out overvirial, then becomes subvirial, and finally approaches equipartition (a generic term for  $E_k \sim E_g$ ). This is because the core first starts with a kinetic energy (the external compression) larger than its gravitational energy. As the core becomes denser and smaller, its gravitational energy increases, and so the ratio  $\mathcal{L}$  decreases, and can in fact become subvirial, because the core may start with an infall speed smaller than the free-fall speed, since it starts infalling from a finite radius, not from infinity. Finally, as the core approaches the free-fall speed and the turbulent speed becomes negligible in comparison, it approaches equipartition. These trajectories are illustrated in Fig. 5.

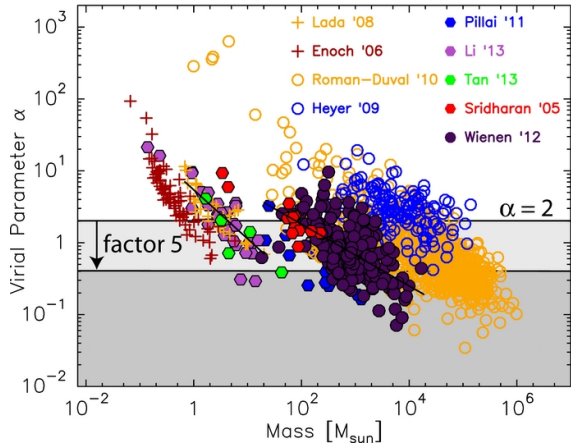


**Fig. 6** Virial parameter as a function of mass for different samples of cores and clouds in the literature. Figure from Kauffmann et al. (2013).

#### 4.6 The virial parameter

The relative importance between self gravity and kinetic energy has been studied since the work of Larson (1981), who showed that the so-called virial parameter  $\alpha_{\text{vir}}$  (see eq. [9]) of MCs has values around unity. Nevertheless, subsequent work showed a variety of virial ratios, as seen in Fig. 6 (from Kauffmann et al., 2013). This figure shows data from various studies, and that, for each one of them,  $\alpha_{\text{vir}} \propto M^{-\delta}$ , with  $0 \lesssim \delta \lesssim 1$  (e.g., Carr, 1987; Loren, 1989; Bertoldi and McKee, 1992; Miville-Deschênes et al., 2017; Traficante et al., 2018a). Assuming the standard values for the Larson relations,  $\sigma_v \propto R^{1/2}$ , and  $M \propto R^2$ , the virial parameter should be constant. In general, if  $M \propto R^q$ , and  $\sigma_v \propto R^p$ ,  $\delta = (2p + 1)/q - 1$ . However, uncertainties may play a crucial role in the determination of the slope of the relation  $\alpha_{\text{vir}} - M$ , as discussed by Kauffmann et al. (2013). For instance, Miville-Deschênes et al. (2017) found a strong  $M - R$  correlation, with  $q = 2.2$ , and a weaker correlation  $\sigma_v - R$  with  $p = 0.65$ . At face value,  $\delta \simeq 0$ , but in practice, these authors found  $\delta \sim -0.5$ . A better estimation of  $\delta$  is to assume that the  $\sigma - R$  correlation is weak enough to actually not contribute to the  $\alpha_{\text{vir}} - M$  correlation. Indeed, using the reported  $q = 2.2$ , and assuming  $p \sim 0$  because of the poor Pearson coefficient, one obtains  $\delta \sim -0.54$ , comparable to the value of  $-0.53$  reported by Miville-Deschênes et al. (2017).

Although values of  $\alpha_{\text{vir}} < 1$  are reported in a number of recent observations (e.g., Giannetti et al., 2014; Traficante et al., 2018c; Zhang et al., 2018; Russeil et al., 2019; Nguyen-Luong et al., 2020; Li et al., 2020), there is also a significant number of studies where  $\alpha_{\text{vir}}$  is reported to be systematically larger than 1–2 (e.g., Berné et al., 2014; Tsitali et al., 2015; Hernandez and Tan, 2015; Barnes et al., 2016; Storm et al., 2016; Kirk et al., 2017; Kerr et al., 2019; Colombo et al., 2019; Zhang et al., 2020). This fact has been interpreted as evidence that MCs are often unbound (e.g., Dobbs et al., 2011b), and thus require pressure confinement to remain coherent (e.g., Field et al., 2011; Leroy et al., 2015; Sun et al., 2018). There are, however, a few caveats that need to be taken into account on this respect. As commented above (see §3), not all the kinetic energy is available for support against collapse. Indeed, a purely-

collapsing cloud will exhibit values of  $\alpha_{\text{vir}} > 1$  after  $\sim$  one free-fall time just because the free-fall velocity is  $\sqrt{2}$  times larger than the virial velocity. In fact, it is easy to see that a Bonnor-Ebert core supported by microturbulence, rather than thermal pressure, has an  $\alpha_{\text{vir}} > 1$ . On the other hand, the velocity dispersion may be overestimated if the molecular lines are optically thick (Phillips et al., 1979; Goldsmith and Langer, 1999; Hacar et al., 2016a). For instance, in the L1517 region, part of the Taurus molecular cloud complex, Hacar et al. (2016a) estimate that the opacity broadening of the line is increasing the actual velocity dispersion by a factor of 4. Taking this result at face value, the 4-fold over estimation in the velocity dispersion will give an overestimation by a factor of  $\sim 16$  in the virial parameter.

There is another potential problem with the interpretation of the virial parameter:<sup>4</sup> the studies by Heyer et al. (2009) and Roman-Duval et al. (2010) shown in Fig. 6 are performed using the same observational dataset, but using different operational definition of clouds, with the result that each study produces substantially different values of  $\alpha_{\text{vir}}$ . In relation to this, Traficante et al. (2018a) argue that the volumes from which the dust emission and the line-emission come, if different, may also affect the estimation of  $\alpha_{\text{vir}}$ . Thus, cloud definition plays a relevant role in the estimation of the molecular cloud properties, in particular,  $\alpha_{\text{vir}}$  (see also Khoperskov et al., 2016).

#### 4.7 Magnetic fields

Diffuse, atomic and dense molecular clouds are partially ionized, and thus, both are subject to magnetic forces. Thus, they are relevant to understand the formation and evolution of MCs (see §2.2), as well as the formation of stars. However, evaluating the relative dynamical importance of magnetic fields compared to other physical ingredients is quite difficult, either because of the highly non-linear behavior of the magnetized ISM, as well as because the full information (intensity and direction) of magnetic fields is not available from observations.

In terms of the non-linear behavior of the fields, as a first approximation, one can expect that stronger the magnetic fields, the smaller the relative importance of gravity, such that collapse could be delayed (see e.g, Shu et al., 1987; Nakamura and Li, 2005; Hennebelle and Inutsuka, 2019). Although this is true in a static medium, the response of the magnetic field in the presence of other agents such as turbulence, rotation, or non-linear instabilities is not straightforward. For instance, a moderate magnetic field in a turbulent environment can have a stronger opposition to turbulent compressions than strong magnetic fields, mainly because of two reasons: on one hand, turbulence can entangle more efficiently the field, producing a larger and more isotropic magnetic pressure (Ballesteros-Paredes and Mac Low, 2002). By the same token, stronger fields can inhibit more efficiently the turbulence, resulting in higher rates of collapse (Zamora-Avilés et al., 2018). As a result, smaller density enhancements can be found in turbulent simulations with weaker fields, compared to simulations with stronger fields.

In a similar way, in rotating galactic disks, the Coriolis force can inhibit the formation of density enhancements when the magnetic fields are weak. However, an

<sup>4</sup>We thank the anonymous referee for pointing out this issue.



increase in the magnetic field intensity can counteract the Coriolis force, allowing for larger density enhancements, (and larger star formation rates, see, e.g., Passot et al., 1995; Kim and Ostriker, 2001; Kim et al., 2002). Thus, one has to be careful when relating the star formation properties with the magnetization of the field. In fact, Soler (2019) found no evidence of relationship between the magnetic fields and the star formation rate for a set of clouds in the Solar Neighborhood.

In terms of the observations, on the other hand, Zeeman effect can provide us information about the intensity of the magnetic field along the line of sight, but they are quite time intensive. On the other hand, polarization measurements are less time intensive, and can provide qualitative information about the morphology of the fields (and its relationship to the morphology of the clouds) as projected in the plane of the sky, but obtaining information about the intensity is only accurate to an order of magnitude. Nevertheless, even with those difficulties, we can infer valuable information about the relative importance of the magnetic fields in clouds and cores.

#### 4.8 Morphology of the magnetic field at the cloud scale

Measuring polarization of visible light dates  $\sim 70$  years back in time (Hiltner, 1949; Davis and Greenstein, 1951). The detailed mechanisms that produce polarization are summarized elsewhere (Heiles et al., 1993; Crutcher, 2012). One of the main successes of polarization measurements is that it provides us information about the relative orientation of the magnetic fields with respect to the cloud. Thus, having a qualitative idea on how the morphology of clouds and fields could be under different physical situations, the relative importance of magnetic fields in the region could be estimated. With this idea, Crutcher (2012) discussed how the relative morphology of the magnetic field and the cloud should be in the cases of strong and weak magnetic fields, as well as in the cases where gravity is or not relevant.

In the case of strong fields, Crutcher (2012) argues that (i) magnetic field lines should be smooth. (ii) If gravitationally unbound, density structures should be aligned along the field lines. (iii) If gravitationally bound, they should be perpendicular to the field lines. (iv) After collapse, the field should have hourglass morphology. In contrast, in the case of weak fields, (i) turbulence should make the field to appear substantially more tangled. (ii) If gravity is not important, column density should be aligned to magnetic fields, as in the previous case. (iii) If clouds are gravitationally bound, the field should be progressively more ordered, as collapse proceeds, (time-dependency). (iv) As in the previous case, after collapse the hourglass morphology should appear, but the pinch angles should be smaller in the strong-field case, due to the larger resistance of the field to be dragged.

With his in mind, Crutcher (2012) argues that the polarization maps quoted in the literature, which are quite smooth and show similar directions of the magnetic fields from large (MC) scales to small (core) scales, suggest that magnetic fields are strong enough to not be twisted by turbulence significantly.

The results discussed by Crutcher (2012) were settled in a more quantitative way using the histogram of relative orientations method (Soler et al., 2013; Soler and Hennebelle, 2017). Indeed, Soler (2019) analyzed Herschel and Planck observations

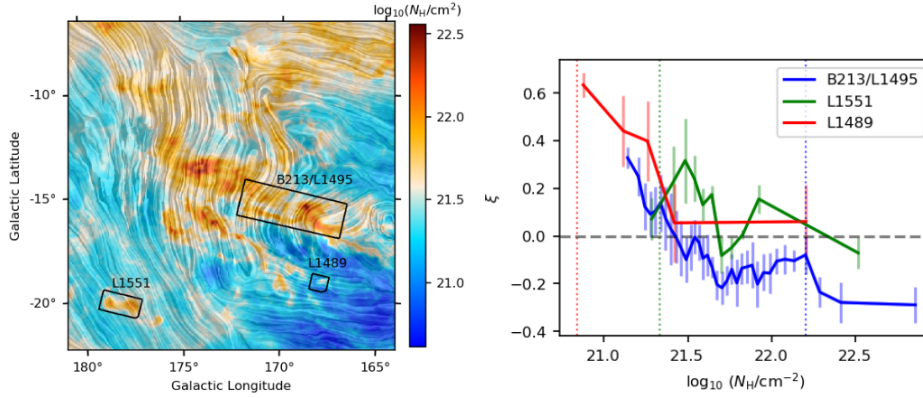


**Fig. 7** Left panel: plane of the sky magnetic field and column density measured by Planck toward the Taurus molecular cloud. Right panel: relative orientation parameter  $\xi$  between the magnetic field in the plane of the sky and the orientation of the filament, for 3 filaments in Taurus (from Soler, 2019).

of local clouds. He found that the relative orientation between the column density of MCs and the magnetic field in the plane of the sky transitions from nearly  $0^\circ$  at low column densities, to  $90^\circ$ , at large column densities (see left panel in Fig. 7). Furthermore, Soler (2019) found no correlation between the star formation rates in those clouds, and the relative orientation between the column density and the field. Such results suggest, then, that the magnetic fields could be relevant enough to shape the large-scale structure of MCs, but not strong enough to regulate star formation.

Such morphology has an interesting implication regarding the scaling of the magnetic field: compressions along the magnetic field lines increase the density, but not the magnetic field intensity. Thus, one can expect that in the magnetic field dominated regime, the field does not correlate with the density. In contrast, compressions perpendicular to the field lines will increase both the density and the magnetic field, and thus, one can expect the magnetic field to be related to the volume density. In general, the situation can be expected to be between these limits, and thus, it can be expected that the magnetic field and the density behave as

$$B = \begin{cases} B_0 n^\kappa, & \text{if } n \geq n_0. \\ B_0, & \text{if } n < n_0. \end{cases} \quad (18)$$

for a given volume density  $n_0$ , and with  $0 \leq \kappa \leq 1$ . Using Bayesian analysis for a set of clouds with magnetic field measurements, Crutcher et al. (2010) found that  $n_0 \sim 300 \text{ cm}^{-3}$ , and  $\kappa \sim 2/3$ . We will get back to this point in the next section, where this assumption is made as a proxy, in order to interpret the line-of sight intensity of the fields.

#### 4.9 Magnetic field intensity and collapse

There are two ways to estimate the intensity of magnetic fields. One is with the Chandrasekhar-Fermi method (Chandrasekhar and Fermi, 1953), the other through the Zeeman effect. Details on the methods can be found in Crutcher (2012) and references therein (e.g. Crutcher and Kemball, 2019). Here we just make few comments: in the first case, the method relies on two basic assumptions: (i) that the magnetic field is tangled by isotropic turbulence, and (ii) that there is equipartition between the kinetic and magnetic energy. In such case, the mean magnetic field becomes

$$\langle B \rangle^2 = 4\pi\rho \frac{\sigma_v^2}{\sigma_\phi^2} \quad (19)$$

where  $\sigma_v$  is the line-of-sight velocity dispersion, and  $\sigma_\phi$  is the dispersion of the orientation angles of the magnetic field. Although this method can give us order of magnitude estimates of the magnetic field, departures by a factor of two orders of magnitude can be found, specially in the weak fields case (Heitsch et al., 2001). Some modification of the original CF method are also proposed for more accurate estimate.

On the other hand, the Zeeman effect can give us direct measurements of the projection of the magnetic field along the line of sight. The problem with the Zeeman effect is that it is observationally expensive. Another difficulty is that there are only a few species showing observable level of the Zeeman shift, e.g., HI, OH, CN, and CCS. These species have large magnetic dipole moments which cause large frequency splitting. In addition, since we obtain only the intensity of the field along the line of sight, we obtain only a lower-limit estimate of the intensity of the field.

Once we have estimates of the magnetic field, as in the case of the kinetic energy, one could evaluate the relative importance of magnetic fields with respect to gravity through the magnetic-to-gravitational energies ratio. In this case, such ratio is proportional to the inverse of the so-called mass ( $M$ )-to-magnetic flux ( $\Phi_{\text{mag}} \sim B R^2$ ) ratio,

$$\frac{E_{\text{mag}}}{E_{\text{grav}}} \propto \left( \frac{\Phi_{\text{mag}}}{M} \right)^2 = \left( \frac{B}{N} \right)^2 \quad (20)$$

(see eqs. [10] and [11], where  $N \propto M/R^2$  is the column density). In ideal MHD, the magnetic flux is constant, since the magnetic field is frozen to the gas. Thus, there is a critical value for which the magnetic field cannot prevent collapse, and thus, it is common to define

$$\mu = \frac{(M/\Phi_{\text{mag}})}{(M/\Phi_{\text{mag}})_{\text{cr}}} \sim \frac{(N/B)}{(N/B)_{\text{cr}}} \quad (21)$$

such that clouds with  $\mu > 1$ , (usually called supercritical), will collapse, while clouds with  $\mu < 1$  (subcritical) will be supported by the magnetic field.

Recalling §3.2, in ideal MHD, the magnetic and gravitational energy of a cloud with fixed mass have the same dependency with size, implying that  $\mu$  is fixed. Mestel and Spitzer (1956) proposed ambipolar diffusion as a mechanism to increase the gravitational energy without increasing the magnetic energy at the same rate. In this process, while the ions are anchored to the field lines, the neutral particles can drift

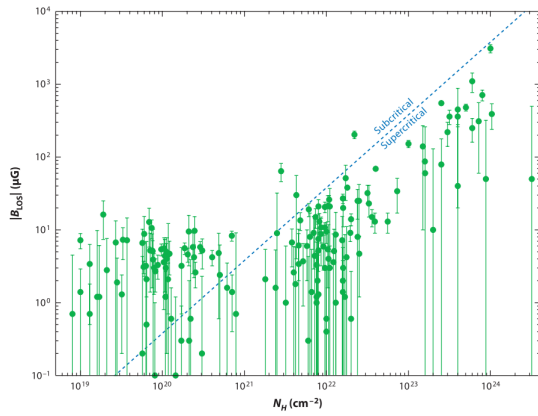


**Fig. 8** Estimated magnetic field intensities in the line of sight vs. column density of H I and molecular clouds (from Crutcher, 2012).

through them, falling into the gravitational potential well. This results in an increase of the mass-to-flux ratio, allowing magnetically subcritical clouds to eventually become supercritical and collapse.

Estimates of the magnetic field intensity in the line of sight and column densities from four different surveys (Crutcher et al., 2010; Heiles and Troland, 2005; Troland and Crutcher, 2008; Falgarone et al., 2008), and compiled by Crutcher (2012), are shown in Fig. 8. The dashed line shows the value of the critical ratio  $(N/B)_{\text{cr}}$ . Data points lying above it imply that these regions are subcritical, and supercritical if they lie below it. As can be seen from this figure, dense molecular cloud cores appear to be supercritical, and low-density H I clouds appear to be subcritical.

Crutcher et al. (2010) pointed out that such distribution of data points could be potentially interpreted as ambipolar diffusion regulated collapse: low column density clouds ( $N > 20^{21} \text{cm}^{-2}$ ) appear to be supported against gravity by magnetic fields, while large column density clouds have increased their mass-to-flux ratio due to ambipolar diffusion, appearing then supercritical. However, these authors caution that ambipolar diffusion cannot operate because low column density clouds are not self-gravitating, and thus, there is no potential well to which the neutrals will fall in. The results by Crutcher et al. (2010), along with the morphological results by Soler (2019), suggest that magnetic fields are relevant in diffuse clouds, but that dense molecular clouds in fact should be formed by compressions along the field lines, and that, once formed, they are mostly supercritical.

## 5 Cloud substructure: from filaments to cores

### 5.1 Universality of filamentary structures in MCs

While interstellar clouds have been known to be filamentary for a long time (e.g. Schneider and Elmegreen, 1979; Bally et al., 1987; Hartmann, 2002; Myers, 2009, and references therein), *Herschel* imaging surveys have established the ubiquity of filaments on almost all length scales ( $\sim 0.5 \text{pc}$  to  $\sim 100 \text{pc}$ ) in Galactic molecular

clouds and shown that this filamentary structure likely plays a key role in the star formation process (e.g. André et al., 2010; Henning et al., 2010; Molinari et al., 2010; Hill et al., 2011; Wang et al., 2015). In particular, filamentary structures appear to dominate the mass budget of MCs at high densities ( $\gtrsim 10^4 \text{ cm}^{-3}$ ) (Schisano et al., 2014; Könyves et al., 2015).

The interstellar filamentary structures detected with *Herschel* span broad ranges in length, central column density, and mass per unit length (e.g. Schisano et al., 2014; Arzoumanian et al., 2019). In contrast, detailed analysis of the radial column density profiles indicates that, at least in nearby molecular clouds, *Herschel* filaments are characterized by a narrow distribution of inner widths with a typical value of  $\sim 0.1$  pc and a dispersion of less than a factor of 2 when the data are averaged over the filament crests (Arzoumanian et al., 2011, 2019, see Fig. 9). Independent submillimeter continuum studies of filament widths in nearby clouds have generally confirmed this result (e.g. Alves de Oliveira et al., 2014; Koch and Rosolowsky, 2015; Salji et al., 2015; Rivera-Ingraham et al., 2016), even if factor of  $\gtrsim 2$ –4 variations around the mean inner width of  $\sim 0.1$  pc have been found along the main axis of a given filament (e.g. Juvela et al., 2012; Ysard et al., 2013). The distribution of local widths found by Arzoumanian et al. (2019) for 599 nearby molecular filaments prior to averaging along the filament crests is well described by a lognormal function centered at  $0.1 \pm 0.01$  pc with a standard deviation of  $0.33 \pm 0.03$  in  $\log_{10}(\text{width})$ , corresponding to a factor of  $\sim 2$  on either side of the median width (see Fig. 9b).

Measurements of filament widths obtained in molecular line tracers (e.g., Pineda et al., 2011; Fernández-López et al., 2014; Panopoulou et al., 2014; Hacar et al., 2018) have been less consistent with the *Herschel* dust continuum results, however. For instance, using  $^{13}\text{CO}$  emission, Panopoulou et al. (2014) found a broad distribution of widths in Taurus, with a peak of 0.4 pc. Hacar et al. (2018) found a median width of 0.035 pc for Orion “fibers” (see § 6.2, below) in the integral-shaped filament of Orion, combining  $\text{N}_2\text{H}^+$  ALMA and IRAM 30 m observations. These differences can be attributed to the lower dynamic range of densities sampled by observations in any given molecular line tracer compared to dust observations. More specifically,  $^{12}\text{CO}$  or  $^{13}\text{CO}$  data only trace low-density gas and cannot reliably measure the whole (column) density profile (hence the width) of a dense molecular filament. Likewise,  $\text{N}_2\text{H}^+$  or  $\text{NH}_3$  data only trace relatively high density gas (typically above the critical densities of the observed transitions) and cannot reliably measure the whole profile of a filament either. In contrast, submillimeter dust continuum images from space (with *Herschel*) achieve a significantly higher dynamic range and are sensitive to both the low density outer parts and the dense inner parts of filaments.

There has also been some controversy about the reliability of the *Herschel* result (Smith et al., 2014; Panopoulou et al., 2017). In particular, Panopoulou et al. (2017) pointed out an apparent contradiction between the existence of a characteristic filament width and the essentially scale-free nature of the power spectrum of interstellar cloud images (well described by a single power law from  $\sim 0.01$  pc to  $\sim 50$  pc – Miville-Deschênes et al., 2010, 2016). However, Roy et al. (2019) showed that there is no contradiction given the only modest area filling factors ( $\lesssim 10\%$ ) and column density contrasts ( $\leq 100\%$  in most cases) derived by Arzoumanian et al. (2019) for the filaments seen in *Herschel* images. This is because for realistic filament filling factors

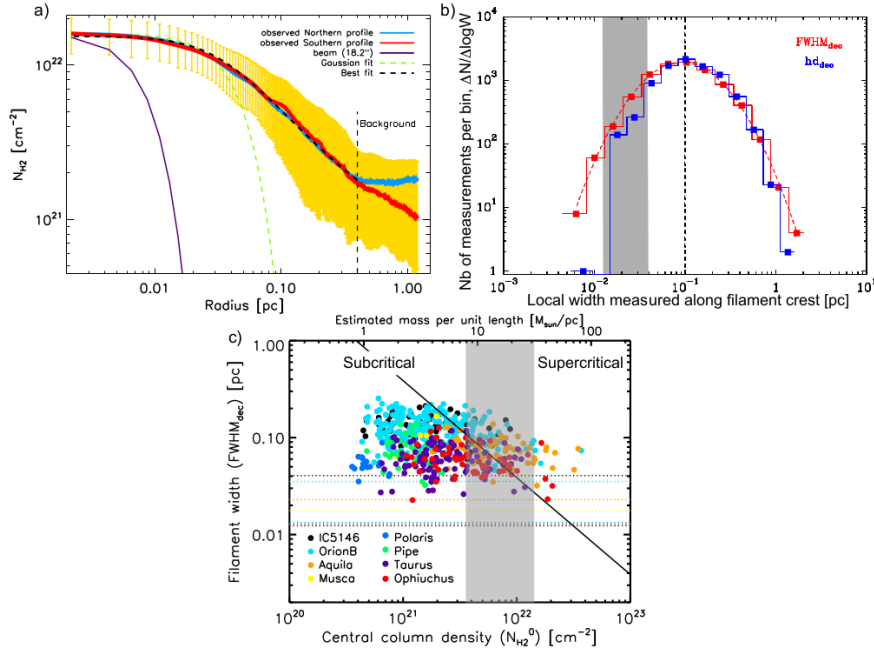


**Fig. 9** (a) Mean radial column density profile measured with *Herschel* perpendicular to the B213/B211 filament in Taurus for both the Northern (blue curve) and the Southern part (red curve) of the filament (Palmeirim et al., 2013). The yellow area shows the  $(\pm 1\sigma)$  dispersion of the distribution of radial profiles along the filament. The inner solid purple curve shows the effective  $18''$  resolution (0.012 pc at 140 pc) of the data. The dashed black curve is the best-fit Plummer-like model,  $N_p(r) = N_{\text{H}_2^0}^0 / [1 + (r/R_{\text{flat}})^2]^{p-1}$ , with a power-law index  $p=2.0\pm 0.4$  and a diameter  $2 \times R_{\text{flat}} = 0.07 \pm 0.01$  pc. (b) Distribution of local FWHM widths derived from nearly 9000 independent radial profile measurements along the crests of 599 *Herschel* filaments in 8 nearby molecular clouds (Arzoumanian et al., 2019). The red and blue histograms correspond to two methods of estimating the FWHM width (see Arzoumanian et al., 2019 for details). The dashed red curve is a lognormal fit to the red histogram. The vertical dashed line marks the peak value of the distribution at  $0.1 \pm 0.01$  pc. The grey band, between 0.012 pc and 0.041 pc, shows the range of resolutions achieved by *Herschel* in the 8 regions. (c) Deconvolved FWHM width (averaged along each filament) vs. central column density for the same 599 filaments as in panel b). The solid line shows the thermal Jeans length as a function of central column density. (Adapted from Arzoumanian et al., 2019.)

and column density contrasts, the filamentary structure contributes only a negligible fraction of the image power spectra. Another caveat pointed out by Panopoulou et al. (2017) is the presence of potential systematic biases in filament width measurements linked to somewhat arbitrary choices of measuring parameters. However, based on a number of tests on synthetic data, Arzoumanian et al. (2019) showed that their method of measuring filament profiles and widths was reliable and free of significant biases, at least when the contrast of the filaments over the local background exceeds  $\sim 50\%$ , which is the case for  $\sim 70\%$  of the *Herschel* filament population they measured and  $> 80\%$  of star-forming filaments. The median inner diameter of  $\sim 0.1$  pc measured with *Herschel* may thus reflect the presence of a true common scale in the filamentary structure of interstellar clouds. Further high-resolution submillimeter continuum studies would nevertheless be required to confirm that the same common

width applies to low-density, low-contrast ( $< 30\text{--}50\%$ ) filaments and to investigate whether it also holds beyond the Gould Belt (see André et al., 2016).

Many theoretical attempts to explain the common inner width of nearby *Herschel* filaments have been made (e.g. Fischera and Martin, 2012; Hennebelle and André, 2013; Auddy et al., 2016; Federrath, 2016; Ntormousi et al., 2016), and some of them are discussed in (Hennebelle and Inutsuka, 2019). However, none of the present explanations is fully convincing. We must admit that we are still missing something in our detailed physical description of filamentary molecular clouds.

Observationally, three families of molecular filaments may be distinguished according to the filament mass per unit length  $M_{\text{line}}$  compared to the thermal value of the critical mass per unit length (e.g. Ostriker, 1964),  $M_{\text{line,crit}} = 2c_s^2/G \sim 16M_{\odot}\text{pc}^{-1}$  for a sound speed  $c_s \sim 0.2\text{ km/s}$ , i.e., a typical gas temperature  $T \sim 10\text{ K}$ : *thermally supercritical* filaments with  $M_{\text{line}} \gtrsim 2M_{\text{line,crit}}$ , *transcritical* filaments with  $0.5M_{\text{line,crit}} \lesssim M_{\text{line}} \lesssim 2M_{\text{line,crit}}$ , and thermally *subcritical* filaments with  $M_{\text{line,crit}} \lesssim 0.5M_{\text{line,crit}}$  (cf. Arzoumanian et al., 2019). Again, it is remarkable that all three families of filaments appear to share approximately the same inner width  $\sim 0.1\text{ pc}$  (Arzoumanian et al., 2011, 2019, see Fig. 9b).

Using molecular line measurements with the IRAM 30m telescope for a sample of *Herschel* filaments (Arzoumanian et al., 2013) showed that thermally subcritical and transcritical filaments have “transonic” internal velocity dispersions  $\sigma_{\text{tot}}$  such that  $c_s \lesssim \sigma_{\text{tot}} < 2c_s$ . Only thermally supercritical filaments have internal velocity dispersions significantly in excess of the thermal sound speed  $c_s \sim 0.2\text{ km/s}$ . Furthermore, there is a positive correlation between the internal velocity dispersion and the column density (or mass per unit length) of thermally supercritical filaments, suggesting that these filaments are in approximate virial equipartition (but not necessarily virial equilibrium) with  $M_{\text{line}} \sim M_{\text{line,vir}} \equiv 2\sigma_{\text{tot}}^2/G$  (see Fig. 10a).

Most observed molecular filaments must be relatively long-lived structures. The fact that most prestellar cores are found to lie within transcritical or supercritical filaments (see § 5.5) implies that these filaments must live at least as long as prestellar cores, or at least  $\sim 1\text{ Myr}$  (André et al., 2014). A similar lifetime can be inferred for subcritical filaments from a typical sound crossing time  $\gtrsim 5 \times 10^5\text{ yr}$ , estimated using a nearly sonic internal velocity dispersion  $\sim 0.2\text{ km/s}$  and the typical filament width of  $\sim 0.1\text{ pc}$  measured with *Herschel*.

## 5.2 Striations and fibers

A striking feature of wide-field, high-dynamic-range images of molecular clouds in both CO lines from the ground (e.g. Goldsmith et al., 2008) and submillimeter dust continuum emission from space (*Herschel*) is the observation of common patterns in the organization of filamentary structures that tend to persist from cloud to cloud. A very common filamentary pattern observed with *Herschel* is that of a main filament surrounded by a population of fainter striations or “sub-filaments” approaching the main filament from the side and apparently connected to it (see Fig. 10b). Examples include the Musca filament (Cox et al., 2016), the B211/B213 filament in Taurus (Goldsmith et al., 2008; Palmeirim et al., 2013), the Serpens-South filament in Aquila

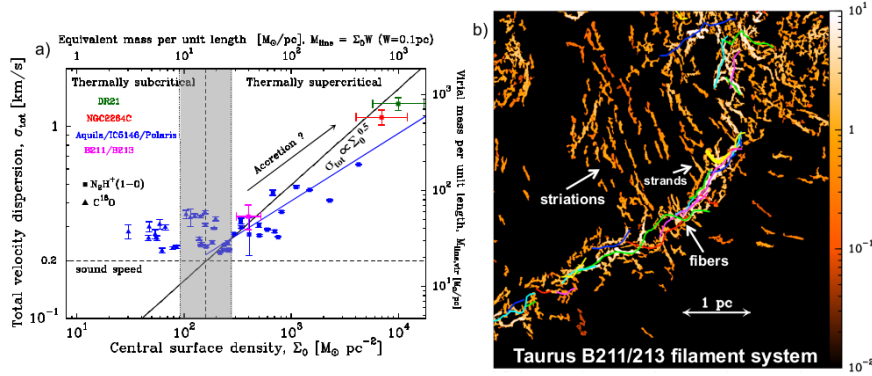


**Fig. 10** (a) Total velocity dispersion versus central surface density for a sample of nearby filaments (Arzoumanian et al., 2013). The horizontal dashed line marks the thermal sound speed  $\sim 0.2$  km/s for  $T = 10$  K. The vertical grey band marks the border zone between thermally subcritical and thermally supercritical filaments. The blue solid line shows the best power-law fit  $\sigma_{\text{tot}} \propto \Sigma_0^{0.36 \pm 0.14}$  to the data points corresponding to supercritical filaments. The latter are in approximate virial equipartition with  $M_{\text{line}} \sim M_{\text{line, vir}}$  and  $\sigma_{\text{tot}} \propto \Sigma_0^{0.5}$ . (b) Fine (column) density structure of the B211/B213 filament based on a filtered version of the *Herschel* 250  $\mu\text{m}$  image of Palmeirim et al. (2013) using the algorithm *getfilaments* (Men'shchikov, 2013). All transverse angular scales larger than  $72''$  (or  $\sim 0.05$  pc) were filtered out to enhance the contrast of small-scale structures. The color scale is in MJy/sr at 250  $\mu\text{m}$ . The colored curves display the velocity-coherent fibers identified by Hacar et al. (2013) using  $\text{N}_2\text{H}^+/\text{C}^{18}\text{O}$  observations.  $\perp$

(e.g. Kirk, H. et al., 2013), and the DR21 ridge in Cygnus X (Schneider et al., 2010; Hennemann et al., 2012). Interestingly, low-density striations and sub-filaments tend to be parallel to the local magnetic field, at least in projection on the plane of the sky (Chapman et al., 2011; Palmeirim et al., 2013; Planck int. res. XXXV, 2016). The morphology of these striations and sub-filaments is suggestive of accretion flows, possibly channeled by the local magnetic field, and feeding the main filaments with ambient cloud material. Low-density striations are remarkably ordered structures in an otherwise apparently chaotic turbulent medium and there is little doubt that magnetic fields are required to explain their properties (Heyer et al., 2016; Tritsis and Tassis, 2016; Chen et al., 2017).

Another seemingly common pattern is the presence of significant substructure within many dense molecular filaments, observed in the form of velocity-coherent features, called *fibers*. The presence of fibers was first reported by Hacar et al. (2013) in the Taurus B211/B213 filament ( $d \sim 140$  pc), for which a friends-of-friends algorithm in velocity (FIVE) was used to identify at least 20 velocity-coherent components in  $\text{N}_2\text{H}^+$  and  $\text{C}^{18}\text{O}$ . Subsequently, similar velocity-coherent components were also detected in  $\text{N}_2\text{H}^+$  in other regions, including the infrared dark cloud (IRDC) G035.39-00.33 (Henshaw et al., 2014), the NGC 1333 protocluster (Hacar et al., 2017), IRDC G034.43+00.24 (Barnes et al., 2018), the Orion A integral-shaped filament (Hacar et al., 2018), and the NGC 6334 main filament (Shimajiri et al., 2019a). The velocity-coherent substructures identified in NGC 1333 and Orion A are well separated in the plane of the sky, however, and may differ in nature from those observed in Taurus and NGC 6334 which are intertwined. Moreover, not all molecular filaments consist of multiple fiber-like substructures. The Musca filament, for in-



stance, appears to be a 6-pc-long velocity-coherent sonic filament with much less substructure than the Taurus B211/B213 filament and no evidence for multiple velocity-coherent fibers (Hacar et al., 2016b; Cox et al., 2016).

Interestingly, most of the line-identified fibers can also be detected in *Herschel* dust continuum maps when large-scale emission is filtered out, enhancing the contrast of small-scale structures in the data (cf. Fig. 10b). Moreover, the *Herschel* data are suggestive of a direct connection between striations and fibers. In Fig. 10b, for instance, hair-like strands or spur-like features, which appear to be the tips of larger-scale striations, are visible in the immediate vicinity of the Taurus B211/B213 filament, attached to its main body. This is consistent with the observed striations tracing accretion flows onto the Taurus main filament, possibly influencing its fiber-like substructure (see “accrete and fragment” scenario below).

The exact physical origin of genuine velocity-coherent fibers, i.e. intertwined filament substructures unaffected by line-of-sight confusion effects, is not well understood and remains highly debated (e.g. Zamora-Avilés et al., 2017; Clarke et al., 2017, 2018). In the “fray and fragment” scenario introduced by Tafalla and Hacar (2015) and supported by Clarke et al. (2017), a main filament forms first by collision of two supersonic turbulent gas flows. Then, the main filament fragments into an intertwined system of velocity-coherent fibers, due to a combination of vorticity in residual turbulent motions and self-gravity. Alternatively, in the “fray and gather” scenario (Smith et al., 2014, 2016), turbulent compression first generates short, velocity-coherent filamentary structures, which are then gathered by large-scale motions within the parent cloud, of either turbulent or gravitational origin. A variant of these two scenarios is the “accrete and fragment” picture, which explicitly links fibers to striations. In this picture, dense molecular filaments accrete ambient cloud material along field lines through a network of magnetically-dominated striations (see above). The accretion process supplies gravitational energy to the dense filament, which is then converted into turbulent kinetic energy in the form of MHD waves (Hennebelle and André, 2013). Radial accretion of gas from an inhomogeneous turbulent medium generates vorticity primarily in the direction of the filament axis, thus producing a system of velocity-coherent fibers in the main filament (cf. Clarke et al., 2017). Sterile fiber-like structures would correspond to portions of the accretion flow onto the central filament (see Clarke et al., 2018), while fertile fibers would be the direct imprint of accretion-driven MHD waves and vorticity within the main filament system.

### 5.3 The characteristic line mass of molecular filaments

To understand the dynamics of filamentary molecular clouds we have to understand the critical mass per unit length above which a cylindrical cloud cannot be in equilibrium with the isothermal equation of state, as explained below. This critical line mass for an isothermal cylindrical cloud does not depend on the density or radius of the cloud and depends only on temperature. As the gas temperature in nearby molecular clouds is always on the order of 10 K, the critical line mass is almost a constant value in the solar neighborhood. Using observations from the *Herschel* space observatory, (André et al., 2010) found a remarkable threshold for star formation process, which

can be summarized as follows: stars are formed in molecular filaments whose line mass is comparable to or larger than the critical line mass. Therefore, the line mass of filaments plays an important role in the evolution of molecular clouds. Let us first discuss this basic property of cylindrical geometry.

Early papers on filament structure such as the classic solution for a self-gravitating isothermal filament (Stodólkiewicz, 1963; Ostriker, 1964), assumed that filaments are in cylindrical hydrostatic equilibrium. Poisson's equation for self-gravity in a cylinder of infinite length is

$$\nabla^2 \Phi = \frac{1}{r} \frac{d}{dr} r \frac{d\Phi}{dr} = 4\pi G \rho. \quad (22)$$

If we multiply by  $r$  on both sides and integrate from the center to the outermost radius  $r = R$ , we obtain

$$R \left. \frac{d\Phi}{dr} \right|_{r=R} = 2G \int_0^R 2\pi r \rho dr \equiv 2GM_{\text{line}}, \quad (23)$$

where we define the mass per unit length (i.e., the line mass) as  $M_{\text{line}} = \int_0^R 2\pi r \rho dr$ . This line mass remains constant in a change of the cylinder radius where  $\rho \propto R^{-2}$ . Thus, the self-gravitational force  $F_{\text{g,cyl}}$  is

$$F_{\text{g,cyl}} = \left. \frac{d\Phi}{dr} \right|_{r=R} = 2 \frac{GM_{\text{line}}}{R} \propto \frac{1}{R}. \quad (24)$$

On the other hand, if we denote the relation between gas pressure  $P$  and density  $\rho$  as  $P = K\rho^{\gamma_{\text{eff}}}$ , the pressure gradient force  $F_{\text{p}}$  scales as

$$F_{\text{p}} = \frac{1}{\rho} \frac{\partial P}{\partial r} \propto R^{1-2\gamma_{\text{eff}}}. \quad (25)$$

Therefore, we have

$$\frac{F_{\text{p}}}{F_{\text{g,cyl}}} \propto R^{2-2\gamma_{\text{eff}}}. \quad (26)$$

This means that, if  $\gamma_{\text{eff}} > 1$ , the pressure gradient force will dominate self-gravity for a sufficiently small radius  $R$ . On the contrary, if  $\gamma_{\text{eff}} \leq 1$ , the radial collapse will continue indefinitely, once self-gravity dominates over the pressure force. Therefore, we can define the critical ratio of specific heats for the radial stability of a self-gravitating cylinder as  $\gamma_{\text{crit,cyl}} = 1$ . In the case of  $\gamma_{\text{eff}} = 1$  a cylinder (under sufficiently small ambient pressure) will be in hydrostatic equilibrium only when its line mass has the special value for which  $F_{\text{p}} = F_{\text{g,cylinder}}$ . This is the reason why we can define a critical line mass for an isothermal cylinder:

$$M_{\text{line,crit}} \equiv \int_0^\infty 2\pi \rho(r) r dr = \frac{2c_s^2}{G}. \quad (27)$$

Using similar arguments, we can define the critical  $\gamma_{\text{eff}}$  for a sphere,  $\gamma_{\text{crit,sphere}} = 4/3$ , and for a sheet,  $\gamma_{\text{crit,sheet}} = 0$ . The thermodynamical property of molecular clouds corresponds to  $\gamma_{\text{eff}} \approx 1$ . Therefore, the significance of filamentary geometry can be understood in terms of ISM thermodynamics. Importantly, filaments differ from both

sheets and spheroids in their global gravitational instability properties. For a sheet-like cloud, there is always an equilibrium configuration since the internal pressure gradient can always become strong enough to halt the gravitational collapse of the sheet independently of the initial state (e.g. Miyama et al., 1987; Inutsuka and Miyama, 1997). In contrast, the radial collapse of an isothermal cylindrical cloud cannot be halted and no equilibrium is possible when the line mass exceeds the critical mass per unit length  $M_{\text{line,crit}}$ . Conversely, if the line mass of a filamentary cloud is less than  $M_{\text{line,crit}}$ , gravity can never be made to dominate by increasing the external pressure, so that the collapse is always halted at some finite cylindrical radius. Thus, filaments differ markedly from isothermal spherical clouds which can always be induced to collapse by a sufficient increase in external pressure (e.g. Bonnor, 1956; Shu, 1977).

A major feature of equilibrium filament models is a critical condition for stability; the mass per unit length of the filament. For isothermal systems, this is simply  $M_{\text{line,crit}} = 2c_s^2/G$  (where  $c_s$  is the isothermal sound speed). This quantity plays an analogous role to the virial mass  $M_{\text{vir}} = 5Rc_s^2/G$  for spherical clouds and equilibria. Filaments become gravitationally unstable when the critical line mass is exceeded.

The peculiar behavior of filamentary geometry in isothermal collapse is due to the fact that the isothermal equation of state ( $\gamma = 1$ ) is a critical case for the collapse of a filament (e.g. Larson, 2005): For a polytropic equation of state ( $P \propto \rho^\gamma$ ) with  $\gamma < 1$ , an unstable cylinder can collapse indefinitely toward its axis, while if  $\gamma > 1$  the pressure gradient increases faster than gravity during contraction and the collapse is always halted at a finite radius. For comparison, the critical value is  $\gamma = 0$  for sheets and  $\gamma = 4/3$  for spheres. Indefinite, global gravitational collapse of a structure can occur when  $\gamma$  is smaller than the critical value and is suppressed when  $\gamma$  is larger than the critical value. Gravitational fragmentation thus tends to be favored over global collapse when  $\gamma$  is close to or larger than the critical value.

The critical mass per unit length  $M_{\text{line,crit}} \approx 16M_\odot/\text{pc} \times (T_{\text{gas}}/10\text{K})$  as originally derived, depends only on gas temperature  $T_{\text{gas}}$ . This expression can be readily generalized to include the fact that filaments have non-thermal internal velocity dispersions (see §5.1 and Fig. 10). In the presence of non-thermal gas motions, the critical mass per unit length becomes  $M_{\text{line,vir}} = 2\sigma_{\text{tot}}^2/G$ , also called the virial mass per unit length, where  $\sigma_{\text{tot}} = \sqrt{c_s^2 + \sigma_{\text{NT}}^2}$  is the total one-dimensional velocity dispersion including both thermal and non-thermal components (Fiege and Pudritz, 2000). Clearly, both the equation of state of the gas and filament turbulence play a role in deciding the actual critical line mass.

#### 5.4 Nature of MC filaments: equilibrium structures vs. funnel flows

The mere existence of thermally supercritical filaments with  $M_{\text{line}} \gg M_{\text{line,crit}}$  poses a problem, since such filaments would be expected to collapse radially to spindles in only about one free-fall time (or  $< 10^5$  yr for dense systems such as the NGC 6334 filament – André et al., 2016), without significant fragmentation along their axis according to non-magnetized models for the evolution of isolated self-gravitating cylinders (Inutsuka and Miyama, 1992, 1997, see § 5.3 above). In contrast, *Herschel*

observations have revealed the presence of numerous  $\sim 0.1$ -pc-wide supercritical filaments with widespread fragmentation into prestellar cores and an estimated lifetime of  $\gtrsim 1$  Myr (e.g. Arzoumanian et al., 2019; Könyves et al., 2015; André et al., 2014, 2019).

Two extreme views for the dynamical state of molecular filaments have been proposed to explain this paradox. First, thermally supercritical filaments may be close to virial and/or magneto-hydrostatic equilibrium, with support against self-gravity provided by a combination of internal MHD turbulence and magnetic fields. Indeed, supercritical filaments are known to be virialized accreting systems with  $M_{\text{line}} \sim M_{\text{line, vir}}$  (see above, Fiege and Pudritz, 2000, and Arzoumanian et al., 2013). While this does not necessarily imply virial *equilibrium*, accretion-driven MHD waves can possibly maintain an effective virial equilibrium (cf. Hennebelle and André, 2013). Assuming rough equipartition between magnetic and kinetic energy, thermally supercritical filaments may also be close to magneto-hydrostatic equilibrium since the magnetic critical line mass  $M_{\text{line, crit}}^{\text{mag}} \approx 1.66 c_s^2 / G + 0.24 \Phi_{\text{cl}} / G^{1/2}$  largely exceeds  $M_{\text{line, crit}}$  when the magnetic flux per unit length  $\Phi_{\text{cl}}$  is large (Tomisaka, 2014).

A second, alternative picture posits that most dense molecular filaments are far from equilibrium and represent dynamical accretion flows onto denser cluster-forming clumps or hubs (e.g. Gómez and Vázquez-Semadeni, 2014). In this picture, filaments form from gravitational amplification of initial anisotropies as part of the “global hierarchical collapse” of strongly Jeans-unstable molecular clouds, and constitute the collapse flow itself from the larger scales to the small-scale dense hubs (Vázquez-Semadeni et al., 2019a). Magnetic fields are present but essentially passive. Large-scale collapse occurs first along the shortest axis creating sheets and subsequently filaments. Gas from sheet-like cloud structures flows onto the filaments roughly perpendicular to them, and is then diverted to flow *along* the filaments onto the hubs. Thus, dense molecular filaments are like rivers and can approach a quasi-stationary state without being in equilibrium.

In practice, real molecular filaments may consist of a mix of quasi-equilibrium and non-equilibrium structures, and observational constraints on the velocity field and (geometry of) the magnetic field may be used to discriminate between the two types of filamentary structures. In the quasi-equilibrium view, significant longitudinal velocity gradients are not expected and the magnetic field lines should be only slightly distorted, due to local protostellar collapse at the positions of dense cores along each filament. In contrast, in the funnel flow hypothesis, supersonic longitudinal velocity gradients are expected, owing to gravitational acceleration of gas toward the central hub, and the magnetic field lines should be dragged by the longitudinal gas flow, adopting a “V-shape” within the filament (Gómez et al., 2018).

Observationally, there is little doubt that gravity is the main player shaping strongly self-gravitating “hub-filament” systems, where a cluster-forming hub is observed at the center of a converging network of filaments (Myers, 2009). Such systems are particularly prominent in massive star-forming regions (e.g. MonR2: Didelon et al., 2015; Pokhrel et al., 2016; SDC335: Peretto et al., 2013), but also exist in clouds forming mostly (or only) low- to intermediate-mass stars (e.g. B59: Peretto et al., 2012; L1688: Ladjelate et al., 2020). Good candidates for longitudinally collapsing filaments have also been identified, such as the SDC13 system of infrared dark fila-

ments (Peretto et al., 2014). While the magnetic field *inside* dense filaments is poorly constrained by current dust polarization observations, it may well be parallel to the filament axis in some cases (cf. the G9.62 massive clump – Dall’Olio et al., 2019), as in the hierarchical collapse picture described above or the “inertial-inflow” model of (Padoan et al., 2019).

In most cases, however, transverse velocity gradients *across* dense molecular filaments, suggestive of accretion *onto* rather than along the filaments, appear to dominate over longitudinal velocity gradients (Kirk, H. et al., 2013; Fernández-López et al., 2014; Dhabal et al., 2018; Shimajiri et al., 2019b). Some examples of subsonic longitudinal motions, possibly core-forming, have also been found (Hacar and Tafalla, 2011). Moreover, chains of dense cores with quasi-periodic spacings have been observed toward some of these transcritical or supercritical filament systems (Tafalla and Hacar, 2015; Bracco et al., 2017; Shimajiri et al., 2019a, Zhang et al. 2020). Such quasi-periodic features are expected in quasi-equilibrium filaments because they have a preferred fragmentation lengthscale (cf. Inutsuka and Miyama, 1992), even in the presence of geometrical bends (Gritschneder et al., 2017) or accretion from a weakly turbulent medium (Clarke et al., 2016). Filaments formed by large-scale gravitational collapse accrete from inhomogeneous parent structures which are themselves collapsing on larger scales and therefore highly “turbulent” (Vázquez-Semadeni et al., 2019a). They are thus less likely to develop quasi-periodic chains of dense cores (cf. Clarke et al., 2017). While current observations suggest that quasi-equilibrium configurations may dominate, more work would be needed to draw definitive conclusions on the relative importance of the two modes (i.e., equilibrium vs. flow structures).

### 5.5 The filament-core connection

The collapse and fragmentation properties of filaments under the assumption of cylindrical symmetry were extensively studied theoretically a few decades ago (e.g. Nagasawa, 1987) but have received renewed attention with the *Herschel* results. The gravitational instability of nearly isothermal filaments is primarily controlled by the value of their mass per unit length  $M_{\text{line}} \equiv M/L$ . Above the critical value  $M_{\text{line,crit}} = 2c_s^2/G$  (where  $c_s$  is the isothermal sound speed) cylindrical filaments are expected to be globally unstable to both radial collapse and fragmentation along their lengths (e.g. Inutsuka and Miyama, 1992, 1997), while below  $M_{\text{line,crit}}$  filaments are gravitationally unbound and thus expected to expand into the surrounding medium unless they are confined by some external pressure (e.g. Fischera and Martin, 2012).

The fragmentation properties of filaments and sheets differ from those of spheroidal clouds in that there is a preferred scale for gravitational fragmentation which directly scales with the scale height of the filamentary or sheet-like medium (e.g. Larson, 1985). In the spherical case, the largest possible scale or mode (i.e., overall collapse of the medium) has the fastest growth rate so that global collapse tends to overwhelm the local collapse of finite-sized density perturbations, and fragmentation is generally suppressed in the absence of sufficiently large initial density enhancements (e.g. Tohline, 1982). It also well known that spherical collapse quickly becomes strongly

centrally concentrated (Larson, 1969; Shu, 1977), which tends to produce a single central density peak as opposed to several condensations (e.g. Whitworth et al., 1996). In contrast, sheets have a natural tendency to fragment into filaments (e.g. Miyama et al., 1987) and filaments with line masses close to  $M_{\text{line,crit}}$  have a natural tendency to fragment into spheroidal cores (e.g. Inutsuka and Miyama, 1997).

The filamentary geometry is thus the most beneficial configuration in molecular clouds for small-scale perturbations to collapse locally and grow significantly before global collapse overwhelms them (Pon et al., 2011, 2012; Toalá et al., 2012). This is because the isothermal equation of state represents a critical case for filaments, possibly halting or slowing down radial collapse (e.g. Larson, 2005, see also § 5.3 above), and the longitudinal collapse timescale of a filament increases almost linearly with the filament length or aspect ratio (e.g. Clarke and Whitworth, 2015), thus greatly exceeding the local free-fall timescale.

Indeed, *Herschel* studies of nearby molecular clouds have found that most (> 75%) prestellar dense cores and young protostars lie in thermally transcritical or supercritical filaments (André et al., 2010; Könyves et al., 2015; Marsh et al., 2016, see also § 3.2 in Chap. 8). Adopting the typical  $\sim 0.1$  pc inner width measured with *Herschel* for molecular filaments, the critical mass per unit length is equivalent to a critical threshold or transition at  $\sim 160 M_{\odot}/\text{pc}^2$  in gas surface density ( $A_V \sim 8$ ) or  $n_{\text{H}_2} \sim 2 \times 10^4 \text{ cm}^{-3}$  in volume density. A similar surface density threshold for the formation of prestellar cores (at  $A_V \sim 5\text{--}10$ ) had been suggested earlier based on ground-based millimeter and submillimeter studies (e.g. Onishi et al., 1998; Johnstone et al., 2004; Kirk et al., 2006), but without any clear connection to filaments. Interestingly, a comparable threshold in extinction (at  $A_V \sim 8$ ) has also been observed in the spatial distribution of young stellar objects (YSOs) with *Spitzer* (e.g. Heiderman et al., 2010; Lada et al., 2010; Evans et al., 2014).

We refer the reader to § 3 in Chap. 8 for more observational details on the filament–core connection and a summary of dense core properties.

## 5.6 Towards the IMF

As already mentioned in § 4.1, the mass function of GMCs and CO clumps within GMCs is known to be rather shallow,  $\Delta N/\Delta \log M \propto M^{-0.6 \pm 0.2}$  (e.g. Solomon et al., 1987; Blitz, 1993), implying that most of the molecular gas mass in the Galaxy resides in the *most massive* GMCs, and within the GMCs themselves in the most massive CO clumps.

More recently, a good estimate of the filament mass function (FMF) and filament line mass function (FLMF) in nearby molecular clouds has been derived using a comprehensive study of filament properties from *Herschel* Gould Belt survey observations (Arzoumanian et al., 2019; André et al., 2019). The FLMF is well fit by a power-law distribution in the supercritical mass per unit length regime (above  $16 M_{\odot}/\text{pc}$ ),  $\Delta N/\Delta \log M_{\text{line}} \propto M_{\text{line}}^{-1.6 \pm 0.1}$  (see Fig. 11a). The FMF is very similar in shape to the FLMF and also follows a power-law distribution at the high-mass end (for  $M_{\text{tot}} > 15 M_{\odot}$ ),  $\Delta N/\Delta \log M_{\text{tot}} \propto M_{\text{tot}}^{-1.4 \pm 0.1}$ , which is significantly steeper than the GMC mass function. Both the FLMF and the FMF are roughly consistent with the

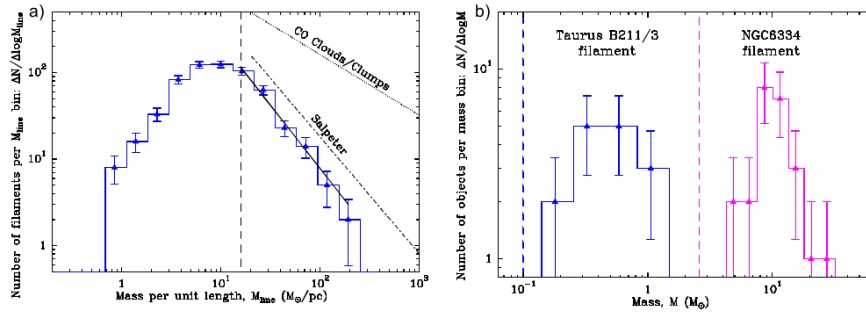


**Fig. 11** (a) Filament line mass function (FLMF) derived for 599 *Herschel* filaments in eight nearby clouds (from André et al., 2019; Arzoumanian et al., 2019). Above the critical line mass  $M_{\text{line,crit}} \sim 16 M_{\odot}/\text{pc}$  (vertical dashed line), the filament sample is more than 90% complete and the FLMF is well fitted by a Salpeter-like power law  $\Delta N/\Delta \log M_{\text{line}} \propto M_{\text{line}}^{-1.6 \pm 0.1}$  (solid line segment). (b) Comparison of the prestellar core mass function (CMF) observed with *Herschel* in the low-mass ( $M_{\text{line}} \sim 50 M_{\odot}/\text{pc}$ ) B211/B213 filament in Taurus (blue histogram – cf. Marsh et al., 2016) with the CMF derived from ALMA data in the high-density ( $M_{\text{line}} \sim 500\text{--}1000 M_{\odot}/\text{pc}$ ) NGC 6334 filament (magenta histogram – Shimajiri et al., 2019a). The vertical dashed lines mark the  $\sim 90\%$  core completeness levels achieved in the two filaments. (From Palmeirim et al., in prep.)

Salpeter power-law IMF (Salpeter, 1955), which scales as  $dN/d\log M_{\star} \propto M_{\star}^{-1.35}$  in the same format. Thus, molecular filaments may represent the key evolutionary step in the hierarchy of cloud structures at which a steep Salpeter-like mass distribution is established. Note that the filament mass function differs in a fundamental way from the GMC mass function in that most of the filament mass lies in *low-mass* filaments. In particular, this result implies that most of the mass of star-forming filaments lies in thermally transcritical with masses per unit length within a factor 2 of the critical value  $M_{\text{line,crit}} = 2c_s^2/G \sim 16 M_{\odot} \text{pc}^{-1}$ .

As most prestellar cores are born in transcritical or supercritical filaments (cf. § 5.5) and the prestellar core formation efficiency is typically  $\sim 15\%$ – $25\%$  in such filaments (e.g. Könyves et al., 2015, 2020, – see also Fig. 3a in Chap. 8), the form of the FLMF has direct implications for the prestellar core mass function (CMF) and, by extension, the stellar initial mass function (IMF) itself (cf. André et al., 2019). Indeed, one expects that there should be a characteristic prestellar core mass corresponding to the local Jeans or critical Bonnor-Ebert mass (e.g. Bonnor, 1956) in transcritical filaments. For a critical  $\sim 0.1$ -pc-wide filament of molecular gas at  $\sim 10$  K with  $M_{\text{line}} \approx M_{\text{line,crit}} \sim 16 M_{\odot} \text{pc}^{-1}$  and surface density  $\Sigma_{\text{fil}} \approx \Sigma_{\text{gas}}^{\text{crit}} \sim 160 M_{\odot} \text{pc}^{-2}$ , the critical Bonnor-Ebert mass is:

$$M_{\text{BE,th}} \sim 1.3 \frac{c_s^4}{G^2 \Sigma_{\text{fil}}} \sim 0.5 M_{\odot} \times \left( \frac{T}{10 \text{ K}} \right)^2 \times \left( \frac{\Sigma_{\text{fil}}}{160 M_{\odot} \text{pc}^{-2}} \right)^{-1}. \quad (28)$$

Thus, one may expect a peak in the prestellar CMF at  $\approx 0.5 M_{\odot}$ . This value matches very well with the observed peak of the prestellar CMFs at  $\sim 0.3\text{--}0.7 M_{\odot}$  derived from *Herschel* data in nearby molecular clouds (Könyves et al., 2015, 2020; Marsh et al., 2016, Ladjelate et al. 2020; Di Francesco et al. 2020; Pezzuto et al. 2020; see also § 3.3 and Fig. 3b in Chap. 8). Moreover, the shape of the prestellar

CMF at the high-mass end is consistent with a Salpeter-like power law (see § 4.1 above) and thus resembles the FMF, suggesting that it may be directly inherited from the latter.

The close link between the FMF (or FLMF) and the prestellar CMF may be understood if we recall that the thermally supercritical filaments observed with *Herschel* in nearby clouds have a typical inner width  $W_{\text{fil}} \sim 0.1$  pc (see § 5.1) and are virialized with  $M_{\text{line}} \sim \Sigma_{\text{fil}} \times W_{\text{fil}} \sim M_{\text{line,vir}} \equiv 2 \sigma_{\text{tot}}^2 / G$ , where  $\sigma_{\text{tot}}$  is equivalent to the effective sound speed (see § 5.4). This implies that the effective Bonnor-Ebert mass  $M_{\text{BE,eff}} \sim 1.3 \sigma_{\text{tot}}^4 / (G^2 \Sigma_{\text{fil}})$  scales roughly as  $\Sigma_{\text{fil}}$  or  $M_{\text{line}}$  in supercritical filaments. Thus, higher-mass cores may form in higher  $M_{\text{line}}$  filaments, as indeed suggested by observations (Shimajiri et al., 2019a, see Fig. 11b). If the CMF produced by a single supercritical filament were a narrow  $\delta$  function peaked at  $M_{\text{BE,eff}}$ , then there would be a direct correspondence between the FMF and the prestellar CMF (cf. André et al., 2014). In reality, the prestellar CMF generated by a single filament is expected to be broader than a  $\delta$  function (cf. Inutsuka, 2001) and observationally appears to broaden as  $M_{\text{line}}$  increases (Könyves et al., 2020), although for statistical reasons, this is difficult to constrain precisely. The global prestellar CMF therefore results from the “convolution” of the FMF with the CMFs produced by individual filaments (Lee et al., 2017). It can be shown, however, that the high-mass end of the global CMF is primarily driven by the power-law shape of the FMF and depends only weakly on the widths of the individual CMFs (cf. Appendix B of André et al., 2019).

The global prestellar CMF is itself apparently closely linked to the stellar IMF, or more precisely the stellar system IMF (cf. Chabrier, 2005), with to first order only a systematic shift between the two, corresponding to a core-to-star formation efficiency  $\epsilon_{\text{core}} \sim 0.4_{-0.1}^{+0.2}$  (Könyves et al., 2015; see also Alves et al., 2007 and § 3.3 of Chap. 8). This is suggestive of a one-to-one mapping between prestellar core mass and stellar system mass,  $M_{\text{sys}} = \epsilon_{\text{core}} M_{\text{core}}$ , at least for core masses  $\sim 0.1$ – $10 M_{\odot}$ . The existence of a direct *physical* connection between the prestellar CMF and the stellar IMF remains uncertain and debated, however (see, e.g., Chap. 8). Clearly, mechanisms controlling the core-to-star formation efficiency  $\epsilon_{\text{core}}$ , such as feedback from protostellar outflows and rotationally-driven subfragmentation of cores into binary/multiple systems, also play important roles in the origin of the IMF.

## 6 Summary

Molecular clouds are the structures through which galaxies funnel their diffuse, warm gas into stars. In the present work we have reviewed the current knowledge of the mechanisms that control the formation and evolution of molecular clouds in their way to form stars.

We started reviewing how MCs are formed. Chemically, the  $\text{H}_2$  molecule is formed in the present-day Universe mainly on the surfaces of dust grains. This molecule is highly sensitive to the UV radiation, and thus, extinctions of the order of  $A_V \gtrsim 1$  are required to allow the formation of molecular hydrogen. In terms of the physical processes, MCs are formed from the convergence of diffuse, warm atomic flows, which may contain some pre-existing molecular gas mixed in. There is a variety of



possibilities on the origin of such flows, namely the passage of a spiral arm, large-scale gravitational instabilities in the disk, the agglomeration of smaller clouds, the expansion of a SN remnant, stellar winds from clusters, etc. In all of these processes, the convergence of flows itself allows the density to increase. Since the warm H I is thermally unstable, the compressed region cools down rapidly, further increasing the density, and allowing gravity to take over. This results in contraction in all directions, producing an even faster growth of the column density, and thus, a rapid formation of molecules.

The physical state of MCs is frequently described by means of the virial theorem, as well as by its statistical properties. The virial theorem, which arises from the momentum equation, describes the generation of kinetic energy in the cloud and the change in its internal mass distribution due to the work done on the cloud by the various forces acting on it, resulting in a relationship between the energies involved on the cloud, which can be estimated observationally. However, such estimations may have important caveats that could lead to misinterpretations about the dynamical state of MCs. Two of the more important caveats are: (a) the assumption that the cloud can be considered to be a homogeneous, isolated sphere, and (b) to interpret the equality  $2E_{\text{kin}} = E_{\text{grav}}$  as implying equilibrium, when the actual equilibrium (force balance) is instead that  $\dot{I}/2 = 2E_{\text{kin}}$ .

In terms of the statistical properties of MCs, a wide set of properties have been studied. The mass distribution of MCs appears to be flatter than the mass distribution of protostellar cores, the last one having similar slopes to that of the stellar initial mass function (IMF), a result that suggests a link between the physics involved in defining the mass of prestellar cores and that of the stars. The column-density probability distribution functions of clouds, on the other hand, is generally agreed to have either of two main shapes at large column densities: lognormal or power-law. The first one has been interpreted in terms of turbulence dominating the dynamics of MCs at the beginning of the formation of MCs. The last one, as a consequence of gravity producing centres of collapse within the cloud. The fact that the PDFs of the density of MCs decrease rapidly implies that most of their volume and mass are in the low-density regime.

Another property of ensembles of MCs is that they have a mass-size relation that is also a power law. The exponent is typically around 2, which implies that the ensemble has a roughly constant column density. This has been interpreted as a consequence of clouds typically being defined by column density thresholds. Moreover, since most of the mass is at low column densities, the clouds in an ensemble defined by means of a column density threshold will all have the approximately same mean column density, regardless of their size, mass or star formation activity.

In terms of their velocity structure, larger MCs exhibit larger values of the velocity dispersion, although with substantial scatter. Typically, a power-law of the form  $\sigma \propto R^\eta$ , with  $\eta \sim 1/2$  is thought to be valid in general, although the exponents found in observational studies range between 0 and 1, depending on the performed survey and methodology. This correlation is frequently considered to be evidence that MCs are dominated by supersonic turbulence. However, a generalization of the velocity dispersion-size correlation has been recently suggested, as surveys have allowed to reach a broader dynamical range in column density. In this case, the so called Larson

ratio  $\mathcal{L} \equiv \sigma_v/R^{1/2}$  is not constant, but rather increases with column density as  $\Sigma^{1/2}$ , thus following a virial relation. This correlation also has substantial scatter, and the global trend has been interpreted in terms of gravity driving chaotic infall motions in MCs, which combine with truly random turbulent motions in different proportions in the clouds as they evolve.

The magnetic fields of MCs, at scales of the clouds themselves, are found to be preferentially perpendicular to their filamentary structure. In terms of support against gravity, it has been found that dense cores are in general not supported by magnetic fields.

MCs are also found to be highly filamentary. In the Solar Neighborhood, *Herschel*-identified filaments appear to exhibit similar widths. No theoretical explanation has yet been found for this result. These filaments also exhibit striations and fibers. The former are low column density features protruding out of the filaments, mostly aligned with the magnetic field, and thus, perpendicular to the high-column density cloud. The latter are velocity-coherent subfilaments that appear in position-position-velocity cubes from emission line observations. Whether such sub-filamentary structure is real, or the result of superposition structure in the line of sight, is currently matter of debate.

Finally, in terms of the dynamics of the filaments, there is a critical linear mass density, above which filaments in hydrostatic equilibrium should collapse radially. It is also matter of debate whether filaments are structures in equilibrium, or flows of gas from the low-density regions of MCs through dense, star-forming cores. In any event, filaments are not homogeneous, and their denser regions are the so-called molecular cloud cores, the sites where stars are formed. Most of the prestellar dense cores are formed by fragmentation of filaments that have a mass line density larger than the critical.

**Acknowledgements** The authors acknowledge the hospitality of the International Space Science Institute during the "Workshop on Star Formation", held in Bern, Switzerland, May 2019. JBP acknowledges UNAM-DGAPA-PAPIIT support through grant number IN-111-219. PhA acknowledges support from the French national programs of CNRS/INSU on stellar and ISM physics (PNPS and PCMI) and from the European Research Council via the ERC Advanced Grant ORISTARS (Grant Agreement no. 291294). RSK acknowledges financial support from the German Research Foundation (DFG) via the collaborative research center (SFB 881, project-id 138713538) The Milky Way System (subprojects A1, B1, B2, and B8). He also thanks for funding from the Heidelberg Cluster of Excellence STRUCTURES in the framework of Germany's Excellence Strategy (grant EXC-2181/1 - 390900948) and for funding from the European Research Council via the ERC Synergy Grant ECOGAL (grant 855130) and the ERC Advanced Grant STARLIGHT (grant 339177). M.C. and J.M.D.K. gratefully acknowledge funding from the German Research Foundation (DFG) in the form of an Emmy Noether Research Group (grant number KR4801/1-1) and a DFG Sachbeihilfe Grant (grant number KR4801/2-1). J.M.D.K. gratefully acknowledges funding from the European Research Council (ERC) under the European Union's Horizon 2020 research and innovation programme via the ERC Starting Grant MUSTANG (grant agreement number 714907), and from Sonderforschungsbereich SFB 881 "The Milky Way System" (subproject B2) of the DFG. A.A. acknowledges the support of the Swedish Research Council, Vetenskapsrådet, and the Swedish National Space Agency (SNSA).

## References

Adamo A, Kruijssen JMD, Bastian N, et al. (2015) Probing the role of the galac-

- tic environment in the formation of stellar clusters, using M83 as a test bench. *MNRAS*452:246–260
- Agertz O, Kravtsov AV, Leitner SN, et al. (2013) Toward a Complete Accounting of Energy and Momentum from Stellar Feedback in Galaxy Formation Simulations. *ApJ*770(1):25
- Alves J, Lombardi M, and Lada CJ (2007) The mass function of dense molecular cores and the origin of the IMF. *A&A*462(1):L17–L21
- Alves J, Lombardi M, and Lada CJ (2017) The shapes of column density PDFs. The importance of the last closed contour. *A&A*606:L2
- Alves de Oliveira C, Schneider N, Merín B, et al. (2014) Herschel view of the large-scale structure in the  $\rho$ ASTROBJ $\rho$ Chamaeleon/ $\rho$ ASTROBJ $\rho$  dark clouds. *A&A*568:A98
- André P, Men'shchikov A, Bontemps S, et al. (2010) From filamentary clouds to prestellar cores to the stellar IMF: Initial highlights from the Herschel Gould Belt Survey. *A&A* 518:L102
- André P, Di Francesco J, Ward-Thompson D, et al. (2014) From Filamentary Networks to Dense Cores in Molecular Clouds: Toward a New Paradigm for Star Formation. in *Protostars and Planets VI*, ed H Beuther et al pp 27–51
- André P, Revéret V, Könyves V, et al. (2016) Characterizing filaments in regions of high-mass star formation: High-resolution submillimeter imaging of the massive star-forming complex NGC 6334 with ArTéMiS. *A&A* 592:A54
- André P, Arzoumanian D, Könyves V, et al. (2019) The role of molecular filaments in the origin of the prestellar core mass function and stellar initial mass function. *A&A* 629:L4
- Arzoumanian D, André P, Didelon P, et al. (2011) Characterizing interstellar filaments with Herschel in IC 5146. *A&A* 529:L6
- Arzoumanian D, André P, Peretto N, et al. (2013) Formation and evolution of interstellar filaments. Hints from velocity dispersion measurements. *A&A* 553:A119
- Arzoumanian D, André P, Könyves V, et al. (2019) Characterizing the properties of nearby molecular filaments observed with Herschel. *A&A* 621:A42
- Auddy S, Basu S, and Kudoh T (2016) A Magnetic Ribbon Model for Star-forming Filaments. *ApJ*831:46
- Audit E and Hennebelle P (2005) Thermal condensation in a turbulent atomic hydrogen flow. *A&A* 433:1–13
- Audit E and Hennebelle P (2010) On the structure of the turbulent interstellar clouds . Influence of the equation of state on the dynamics of 3D compressible flows. *A&A* 511:A76
- Ballesteros-Paredes J (2006) Six myths on the virial theorem for interstellar clouds. *MNRAS*372(1):443–449
- Ballesteros-Paredes J and Hartmann L (2007) Remarks on Rapid vs. Slow Star Formation. *Rev. Mex. Astron. Astrofis.*43:123–136
- Ballesteros-Paredes J and Mac Low MM (2002) Physical versus Observational Properties of Clouds in Turbulent Molecular Cloud Models. *ApJ*570:734–748
- Ballesteros-Paredes J and Vázquez-Semadeni E (1997) Virial balance in turbulent MHD two dimensional numerical simulations of the ISM. In: Holt SS and Mundy LG (eds) *American Institute of Physics Conference Series*, American Institute of

- Physics Conference Series, vol 393, pp 81–84
- Ballesteros-Paredes J, Hartmann L, and Vázquez-Semadeni E (1999a) Turbulent Flow-driven Molecular Cloud Formation: A Solution to the Post-T Tauri Problem? *ApJ*527(1):285–297
- Ballesteros-Paredes J, Vázquez-Semadeni E, and Scalo J (1999b) Clouds as Turbulent Density Fluctuations: Implications for Pressure Confinement and Spectral Line Data Interpretation. *ApJ*515(1):286–303
- Ballesteros-Paredes J, Gazol A, Kim J, et al. (2006) The Mass Spectra of Cores in Turbulent Molecular Clouds and Implications for the Initial Mass Function. *ApJ*637(1):384–391
- Ballesteros-Paredes J, Gómez GC, Loinard L, et al. (2009a) Tidal forces as a regulator of star formation in Taurus. *MNRAS*395(1):L81–L84
- Ballesteros-Paredes J, Gómez GC, Pichardo B, et al. (2009b) On the gravitational content of molecular clouds and their cores. *MNRAS*393(4):1563–1572
- Ballesteros-Paredes J, Hartmann LW, Vázquez-Semadeni E, et al. (2011a) Gravity or turbulence? Velocity dispersion-size relation. *MNRAS*411(1):65–70
- Ballesteros-Paredes J, Vázquez-Semadeni E, Gazol A, et al. (2011b) Gravity or turbulence? - II. Evolving column density probability distribution functions in molecular clouds. *MNRAS*416(2):1436–1442
- Ballesteros-Paredes J, D’Alessio P, and Hartmann L (2012) On the structure of molecular clouds. *MNRAS*427:2562–2571
- Ballesteros-Paredes J, Hartmann LW, Pérez-Goytia N, et al. (2015) Bondi-Hoyle-Littleton accretion and the upper-mass stellar initial mass function. *MNRAS*452(1):566–574
- Ballesteros-Paredes J, Vázquez-Semadeni E, Palau A, et al. (2018) Gravity or turbulence? - IV. Collapsing cores in out-of-virial disguise. *MNRAS*479(2):2112–2125
- Ballesteros-Paredes J, Román-Zúñiga C, Salomé Q, et al. (2019) What is the physics behind the Larson mass-size relation? *MNRAS*490(2):2648–2655
- Bally J, Langer WD, Stark AA, et al. (1987) Filamentary structure in the Orion molecular cloud. *ApJL*312:L45–L49
- Banerjee R, Vázquez-Semadeni E, Hennebelle P, et al. (2009) Clump morphology and evolution in MHD simulations of molecular cloud formation. *MNRAS*398:1082–1092
- Barnes AT, Longmore SN, Battersby C, et al. (2017) Star formation rates and efficiencies in the Galactic Centre. *MNRAS*469:2263–2285
- Barnes AT, Henshaw JD, Caselli P, et al. (2018) Similar complex kinematics within two massive, filamentary infrared dark clouds. *MNRAS*475(4):5268–5289
- Barnes PJ, Hernandez AK, O’Dougherty SN, et al. (2016) The Galactic Census of High- and Medium-mass Protostars. III.  $^{12}\text{CO}$  Maps and Physical Properties of Dense Clump Envelopes and Their Embedding GMCs. *ApJ*831(1):67
- Barranco JA and Goodman AA (1998) Coherent Dense Cores. I.  $\text{NH}_3$  Observations. *ApJ*504(1):207–222
- Baumont CN, Goodman AA, Alves JF, et al. (2012) A simple perspective on the mass-area relationship in molecular clouds. *MNRAS*423(3):2579–2586
- Bergin EA, Hartmann LW, Raymond JC, et al. (2004) Molecular Cloud Formation behind Shock Waves. *ApJ*612(2):921–939

- Berné O, Marcelino N, and Cernicharo J (2014) IRAM 30 m Large Scale Survey of  $^{12}\text{CO}(2-1)$  and  $^{13}\text{CO}(2-1)$  Emission in the Orion Molecular Cloud. *ApJ*795(1):13
- Bertoldi F and McKee CF (1992) Pressure-confined Clumps in Magnetized Molecular Clouds. *ApJ*395:140
- Beuther H and Schilke P (2004) Fragmentation in Massive Star Formation. *Science* 303(5661):1167–1169
- Bigiel F, Leroy A, Walter F, et al. (2008) the Star Formation Law in Nearby Galaxies on Sub-Kpc Scales. *AJ*136(6):2846–2871
- Blitz L (1993) Giant molecular clouds. In: Levy E and Lunine J (eds) *Protostars and Planets III*, pp 125–161
- Blitz L and Shu FH (1980) The origin and lifetime of giant molecular cloud complexes. *ApJ*238:148–157
- Blitz L, Fukui Y, Kawamura A, et al. (2007) Giant Molecular Clouds in Local Group Galaxies. In: Reipurth B, Jewitt D, and Keil K (eds) *Protostars and Planets V*, University of Arizona Press, Tucson, p 81
- Bolatto AD, Leroy AK, Rosolowsky E, et al. (2008) The Resolved Properties of Extragalactic Giant Molecular Clouds. *ApJ*686(2):948–965
- Bonnell IA and Bate MR (2006) Star formation through gravitational collapse and competitive accretion. *MNRAS*370(1):488–494
- Bonnor W (1956) Boyle's Law and gravitational instability. *MNRAS*116:351–+
- Bracco A, Palmeirim P, André P, et al. (2017) Probing changes of dust properties along a chain of solar-type prestellar and protostellar cores in Taurus with NIKA. *A&A*604:A52
- Bresnahan D, Ward-Thompson D, Kirk JM, et al. (2018) The dense cores and filamentary structure of the molecular cloud in Corona Australis: Herschel SPIRE and PACS observations from the Herschel Gould Belt Survey. *A&A*615:A125
- Briceno C, Hartmann LW, Stauffer JR, et al. (1997) X-Rays Surveys and the Post-T Tauri Problem. *AJ*113:740–752
- Camacho V, Vázquez-Semadeni E, Ballesteros-Paredes J, et al. (2016) Energy Budget of Forming Clumps in Numerical Simulations of Collapsing Clouds. *ApJ*833:113
- Carr JS (1987) A Study of Clumping in the Cepheus OB 3 Molecular Cloud. *ApJ*323:170
- Caselli P and Myers PC (1995) The Line Width–Size Relation in Massive Cloud Cores. *ApJ*446:665
- Caselli P, Benson PJ, Myers PC, et al. (2002) Dense Cores in Dark Clouds. XIV.  $\text{N}_2\text{H}^+$  (1-0) Maps of Dense Cloud Cores. *ApJ*572(1):238–263
- Cesaroni R, Beuther H, Ahmadi A, et al. (2019) IRAS 23385+6053: an embedded massive cluster in the making. *A&A*627:A68
- Chabrier G (2005) The Initial Mass Function: from Salpeter 1955 to 2005. In: E Corbelli, F Palla, & H Zinnecker (ed) *The Initial Mass Function 50 Years Later*, Astrophysics and Space Science Library, vol 327, pp 41–+
- Chandrasekhar S and Fermi E (1953) Magnetic Fields in Spiral Arms. *ApJ*118:113
- Chapman NL, Goldsmith PF, Pineda JL, et al. (2011) The Magnetic Field in Taurus Probed by Infrared Polarization. *ApJ*741:21
- Chen CY, Li ZY, King PK, et al. (2017) Fantastic Striations and Where to Find Them: The Origin of Magnetically Aligned Striations in Interstellar Clouds. *ApJ*847:140

- Chen HHH, Pineda JE, Goodman AA, et al. (2019) Droplets. I. Pressure-dominated Coherent Structures in L1688 and B18. *ApJ*877(2):93
- Cheng Y, Tan JC, Liu M, et al. (2018) The Core Mass Function in the Massive Procluster G286.21+0.17 Revealed by ALMA. *ApJ*853(2):160
- Chevance M, Madden SC, Lebouteiller V, et al. (2016) A milestone toward understanding PDR properties in the extreme environment of LMC-30 Doradus. *A&A*590:A36
- Chevance M, Kruijssen JMD, Hygate APS, et al. (2020a) The lifecycle of molecular clouds in nearby star-forming disc galaxies. *MNRAS*493(2):2872–2909
- Chevance M, Kruijssen JMD, Vazquez-Semadeni E, et al. (2020b) The Molecular Cloud Lifecycle. *Space Science Reviews*216(4):50
- Clark PC, Glover SCO, Klessen RS, et al. (2012) How long does it take to form a molecular cloud? *MNRAS*424:2599–2613
- Clarke SD and Whitworth AP (2015) Investigating the global collapse of filaments using smoothed particle hydrodynamics. *MNRAS*449(2):1819–1825
- Clarke SD, Whitworth AP, and Hubber DA (2016) Perturbation growth in accreting filaments. *MNRAS*458:319–324
- Clarke SD, Whitworth AP, Duarte-Cabral A, et al. (2017) Filamentary fragmentation in a turbulent medium. *MNRAS*468:2489–2505
- Clarke SD, Whitworth AP, Spowage RL, et al. (2018) Synthetic C<sup>18</sup>O observations of fibrous filaments: the problems of mapping from PPV to PPP. *MNRAS*479(2):1722–1746
- Colombo D, Rosolowsky E, Duarte-Cabral A, et al. (2019) The integrated properties of the molecular clouds from the JCMT CO(3-2) High-Resolution Survey. *MNRAS*483(4):4291–4340
- Corbelli E, Braine J, Bandiera R, et al. (2017) From molecules to young stellar clusters: the star formation cycle across the disk of M 33. *A&A*601:A146
- Cottaar M, Meyer MR, Andersen M, et al. (2012) Is the massive young cluster West-erlund I bound? *A&A*539:A5
- Cox NLJ, Arzoumanian D, André P, et al. (2016) Filamentary structure and magnetic field orientation in Musca. *A&A*590:A110
- Crutcher RM (2012) Magnetic Fields in Molecular Clouds. *ARA&A*50:29–63
- Crutcher RM and Kembell AJ (2019) Review of Zeeman Effect Observations of Regions of Star Formation K Zeeman Effect, Magnetic Fields, Star formation, Masers, Molecular clouds. *Frontiers in Astronomy and Space Sciences* 6:66
- Crutcher RM, Wandelt B, Heiles C, et al. (2010) Magnetic Fields in Interstellar Clouds from Zeeman Observations: Inference of Total Field Strengths by Bayesian Analysis. *ApJ*725(1):466–479
- Dale JE, Ngoumou J, Ercolano B, et al. (2014) Before the first supernova: combined effects of H II regions and winds on molecular clouds. *MNRAS*442(1):694–712
- Dall’Olio D, Vlemmings WHT, Persson MV, et al. (2019) ALMA reveals the magnetic field evolution in the high-mass star forming complex G9.62+0.19. *A&A*626:A36
- Davis J Leverett and Greenstein JL (1951) The Polarization of Starlight by Aligned Dust Grains. *ApJ*114:206

- de Avillez MA and Breitschwerdt D (2005) Global dynamical evolution of the ISM in star forming galaxies. I. High resolution 3D simulations: Effect of the magnetic field. *A&A* 436(2):585–600
- Dhabal A, Mundy LG, Rizzo MJ, et al. (2018) Morphology and Kinematics of Filaments in the Serpens and Perseus Molecular Clouds. *ApJ* 853(2):169
- Didelon P, Motte F, Tremblin P, et al. (2015) From forced collapse to H ii region expansion in Mon R2: Envelope density structure and age determination with Herschel. *A&A* 584:A4
- Dobbs CL (2008) GMC formation by agglomeration and self gravity. *MNRAS* 391(2):844–858
- Dobbs CL, Burkert A, and Pringle JE (2011a) The properties of the interstellar medium in disc galaxies with stellar feedback. *MNRAS* 417(2):1318–1334
- Dobbs CL, Burkert A, and Pringle JE (2011b) Why are most molecular clouds not gravitationally bound? *MNRAS* 413(4):2935–2942
- Dobbs CL, Krumholz MR, Ballesteros-Paredes J, et al. (2014) Formation of Molecular Clouds and Global Conditions for Star Formation. In: Beuther H, Klessen RS, Dullemond CP, et al. (eds) *Protostars and Planets VI*, p 3
- Dobbs CL, Pringle JE, and Duarte-Cabral A (2015) The frequency and nature of ‘cloud-cloud collisions’ in galaxies. *MNRAS* 446(4):3608–3620
- Draine BT (2011) *Physics of the Interstellar and Intergalactic Medium*. Princeton University Press
- Draine BT and Bertoldi F (1996) Structure of Stationary Photodissociation Fronts. *ApJ* 468:269
- Elmegreen BG (1987) Supercloud formation by nonaxisymmetric gravitational instabilities in sheared magnetic galaxy disks. *ApJ* 312:626–639
- Elmegreen BG (1993) Disk instabilities and star formation. In: Franco J, Ferrini F, and Tenorio-Tagle G (eds) *Star Formation, Galaxies and the Interstellar Medium*, p 337
- Elmegreen BG (1997) Theory of Starbursts in Nuclear Rings. In: Franco J, Terlevich R, and Serrano A (eds) *Revista Mexicana de Astronomia y Astrofisica Conference Series, Revista Mexicana de Astronomia y Astrofisica*, vol. 27, vol 6, p 165
- Elmegreen BG (2000) Star Formation in a Crossing Time. *ApJ* 530(1):277–281
- Elmegreen BG (2008) Variations in Stellar Clustering with Environment: Dispersed Star Formation and the Origin of Faint Fuzzies. *ApJ* 672:1006–1012
- Elmegreen BG and Scalo J (2004) Interstellar Turbulence I: Observations and Processes. *ARA&A* 42(1):211–273
- Engargiola G, Plambeck R, Rosolowsky E, et al. (2003) Giant Molecular Clouds in M33 - I. BIMA All Disk Survey. *ApJS* 149(2):343–363
- Evans NJ II, Heiderman A, and Vutisalchavakul N (2014) Star Formation Relations in Nearby Molecular Clouds. *ApJ* 782:114
- Falgarone E, Phillips TG, and Walker CK (1991) The Edges of Molecular Clouds: Fractal Boundaries and Density Structure. *The Astrophysical Journal* 378:186
- Falgarone E, Troland TH, Crutcher RM, et al. (2008) CN Zeeman measurements in star formation regions. *A&A* 487(1):247–252
- Falgarone E, Pety J, and Hily-Blant P (2009) Intermittency of interstellar turbulence: extreme velocity-shears and CO emission on milliparsec scale. *Astronomy and*

- Astrophysics 507(1):355–368
- Federrath C (2015) Inefficient star formation through turbulence, magnetic fields and feedback. *MNRAS*450:4035–4042
- Federrath C (2016) On the universality of interstellar filaments: theory meets simulations and observations. *MNRAS*457:375–388
- Federrath C and Klessen RS (2012) The Star Formation Rate of Turbulent Magnetized Clouds: Comparing Theory, Simulations, and Observations. *ApJ*761:156
- Federrath C, Klessen RS, and Schmidt W (2008) The Density Probability Distribution in Compressible Isothermal Turbulence: Solenoidal versus Compressive Forcing. *ApJL*688(2):L79
- Federrath C, Roman-Duval J, Klessen RS, et al. (2010) Comparing the statistics of interstellar turbulence in simulations and observations. Solenoidal versus compressive turbulence forcing. *A&A*512:A81
- Feldmann R, Gnedin NY, and Kravtsov AV (2011) How Universal is the  $\Sigma_{SFR} - \Sigma_{H_2}$  Relation? *ApJ*732:115
- Fernández-López M, Arce HG, Looney L, et al. (2014) CARMA Large Area Star Formation Survey: Observational Analysis of Filaments in the Serpens South Molecular Cloud. *ApJL*790:L19
- Ferrière KM (2001) The interstellar environment of our galaxy. *Reviews of Modern Physics* 73:1031–1066
- Fiege JD and Pudritz RE (2000) Polarized Submillimeter Emission from Filamentary Molecular Clouds. *ApJ*544:830–837
- Field GB (1965) Thermal Instability. *ApJ*142:531
- Field GB and Saslaw WC (1965) A Statistical Model of the Formation of Stars and Interstellar Clouds. *ApJ*142:568
- Field GB, Goldsmith DW, and Habing HJ (1969) Cosmic-Ray Heating of the Interstellar Gas. *ApJL*155:L149
- Field GB, Blackman EG, and Keto ER (2011) Does external pressure explain recent results for molecular clouds? *MNRAS*416(1):710–714
- Fischera J and Martin PG (2012) Physical properties of interstellar filaments. *A&A*542:A77
- Franco J and Cox DP (1986) Molecular clouds in galaxies with different Z: fragmentation of diffuse clouds driven by opacity. *PASP*98:1076–1079
- Gazol A, Vázquez-Semadeni E, Sánchez-Salcedo FJ, et al. (2001) The Temperature Distribution in Turbulent Interstellar Gas. *ApJL*557(2):L121–L124
- Giannetti A, Wyrowski F, Brand J, et al. (2014) ATLASGAL-selected massive clumps in the inner Galaxy. I. CO depletion and isotopic ratios. *A&A*570:A65
- Girichidis et al J (2020) Physical processes in star formation. *Space Science Reviews*
- Glover SCO and Clark PC (2012a) Approximations for modelling CO chemistry in giant molecular clouds: a comparison of approaches. *MNRAS*421(1):116–131
- Glover SCO and Clark PC (2012b) Is molecular gas necessary for star formation? *MNRAS*421(1):9–19
- Glover SCO and Mac Low MM (2007) Simulating the Formation of Molecular Clouds. II. Rapid Formation from Turbulent Initial Conditions. *ApJ*659(2):1317–1337



- Goldreich P and Lynden-Bell D (1965) I. Gravitational stability of uniformly rotating disks. *MNRAS*130:97
- Goldsmith PF and Langer WD (1999) Population Diagram Analysis of Molecular Line Emission. *ApJ*517(1):209–225
- Goldsmith PF, Heyer M, Narayanan G, et al. (2008) Large-Scale Structure of the Molecular Gas in Taurus Revealed by High Linear Dynamic Range Spectral Line Mapping. *ApJ*680:428–445
- Gómez GC (2006) Errors in Kinematic Distances and Our Image of the Milky Way Galaxy. *AJ*132(6):2376–2382
- Gómez GC and Vázquez-Semadeni E (2014) Filaments in Simulations of Molecular Cloud Formation. *ApJ*791:124
- Gómez GC, Vázquez-Semadeni E, and Zamora-Avilés M (2018) The magnetic field structure in molecular cloud filaments. *MNRAS*480:2939–2944
- Gong M, Ostriker EC, and Kim CG (2018) The  $X_{CO}$  Conversion Factor from Galactic Multiphase ISM Simulations. *ApJ*858(1):16
- Goodman AA, Barranco JA, Wilner DJ, et al. (1998) Coherence in Dense Cores. II. The Transition to Coherence. *ApJ*504:223–246
- Gritschneider M, Naab T, Walch S, et al. (2009) Driving Turbulence and Triggering Star Formation by Ionizing Radiation. *ApJL*694(1):L26–L30
- Gritschneider M, Heigl S, and Burkert A (2017) Oscillating Filaments. I. Oscillation and Geometrical Fragmentation. *ApJ*834:202
- Grudić, MY, Hopkins PF, et al. (2019) On the nature of variations in the measured star formation efficiency of molecular clouds. *MNRAS*488(2):1501–1518
- Gutermuth RA, Pipher JL, Megeath ST, et al. (2011) A Correlation between Surface Densities of Young Stellar Objects and Gas in Eight Nearby Molecular Clouds. *ApJ*739:84
- Habing HJ (1968) The interstellar radiation density between 912 Å and 2400 Å. *Bull. Astron. Inst. Netherlands*19:421
- Hacar A and Tafalla M (2011) Dense core formation by fragmentation of velocity-coherent filaments in L1517. *A& A*533:A34
- Hacar A, Tafalla M, Kauffmann J, et al. (2013) Cores, filaments, and bundles: hierarchical core formation in the L1495/B213 Taurus region. *A& A*554:A55
- Hacar A, Alves J, Burkert A, et al. (2016a) Opacity broadening and interpretation of suprathermal CO linewidths: Macroscopic turbulence and tangled molecular clouds. *A& A*591:A104
- Hacar A, Kainulainen J, Tafalla M, et al. (2016b) The Musca cloud: A 6 pc-long velocity-coherent, sonic filament. *A& A*587:A97
- Hacar A, Tafalla M, and Alves J (2017) Fibers in the NGC 1333 proto-cluster. *A& A*606:A123
- Hacar A, Tafalla M, Forbrich J, et al. (2018) An ALMA study of the Orion Integral Filament. I. Evidence for narrow fibers in a massive cloud. *A& A*610:A77
- Hartmann L (2002) Flows, Fragmentation, and Star Formation. I. Low-Mass Stars in Taurus. *ApJ*578:914–924
- Hartmann L, Ballesteros-Paredes J, and Bergin EA (2001) Rapid Formation of Molecular Clouds and Stars in the Solar Neighborhood. *ApJ*562(2):852–868

- Hartmann L, Ballesteros-Paredes J, and Heitsch F (2012) Rapid star formation and global gravitational collapse. *MNRAS*420(2):1457–1461
- Hausman MA (1982) Theoretical models of the mass spectrum of interstellar clouds. *ApJ*261:532–542
- Heiderman A, Evans NJ II, Allen LE, et al. (2010) The Star Formation Rate and Gas Surface Density Relation in the Milky Way: Implications for Extragalactic Studies. *ApJ*723:1019–1037
- Heiles C (1979) H I shells and supershells. *ApJ*229:533–537
- Heiles C (1984) HI shells, supershells, shell-like objects, and “worms”. *ApJS*55:585–595
- Heiles C and Troland TH (2005) The Millennium Arecibo 21 Centimeter Absorption-Line Survey. IV. Statistics of Magnetic Field, Column Density, and Turbulence. *ApJ*624(2):773–793
- Heiles C, Goodman AA, McKee CF, et al. (1993) Magnetic Fields in Star-Forming Regions - Observations. In: Levy EH and Lunine JI (eds) *Protostars and Planets III*, p 279
- Heithausen A, Bensch F, Stutzki J, et al. (1998) The IRAM key project: small-scale structure of pre-star forming regions. Combined mass spectra and scaling laws. *A&A*331:L65–L68
- Heitsch F, Zweibel EG, Mac Low MM, et al. (2001) Magnetic Field Diagnostics Based on Far-Infrared Polarimetry: Tests Using Numerical Simulations. *ApJ*561(2):800–814
- Heitsch F, Slyz AD, Devriendt JEG, et al. (2006) The Birth of Molecular Clouds: Formation of Atomic Precursors in Colliding Flows. *ApJ*648:1052–1065
- Heitsch F, Hartmann LW, and Burkert A (2008) Fragmentation of Shocked Flows: Gravity, Turbulence, and Cooling. *ApJ*683(2):786–795
- Heitsch F, Ballesteros-Paredes J, and Hartmann L (2009a) Gravitational Collapse and Filament Formation: Comparison with the Pipe Nebula. *ApJ*704(2):1735–1742
- Heitsch F, Stone JM, and Hartmann LW (2009b) Effects of Magnetic Field Strength and Orientation on Molecular Cloud Formation. *ApJ*695(1):248–258
- Hennebelle P and André P (2013) Ion-neutral friction and accretion-driven turbulence in self-gravitating filaments. *A&A*560:A68
- Hennebelle P and Falgarone E (2012) Turbulent molecular clouds. *Astron. & Astrophys. Rev.*20:55
- Hennebelle P and Inutsuka Si (2019) The role of magnetic field in molecular cloud formation and evolution. *Frontiers in Astronomy and Space Sciences* 6:5
- Hennebelle P and Pérault M (1999) Dynamical condensation in a thermally bistable flow. Application to interstellar cirrus. *A&A*351:309–322
- Hennebelle P, Banerjee R, Vázquez-Semadeni E, et al. (2008) From the warm magnetized atomic medium to molecular clouds. *A&A*486:L43–L46
- Hennebelle P, Lee YN, and Chabrier G (2019) How First Hydrostatic Cores, Tidal Forces, and Gravoturbulent Fluctuations Set the Characteristic Mass of Stars. *ApJ*883(2):140
- Hennemann M, Motte F, Schneider N, et al. (2012) The spine of the swan: a Herschel study of the DR21 ridge and filaments in Cygnus X. *A&A*543:L3

- Henning T, Linz H, Krause O, et al. (2010) The seeds of star formation in the filamentary infrared-dark cloud G011.11-0.12. *A&A* 518:L95
- Henshaw JD, Caselli P, Fontani F, et al. (2014) The dynamical properties of dense filaments in the infrared dark cloud G035.39-00.33. *MNRAS* 440:2860–2881
- Henshaw JD, Longmore SN, Kruijssen JMD, et al. (2016) Molecular gas kinematics within the central 250 pc of the Milky Way. *MNRAS* 457:2675–2702
- Herbig GH (1978) Can Post-T Tauri Stars Be Found? In: Mirzoyan LV (ed) *Problems of Physics and Evolution of the Universe.*, Publishing House of the Armenian Academy of Sciences, p 171
- Hernandez AK and Tan JC (2015) The Giant Molecular Cloud Environments of Infrared Dark Clouds. *ApJ* 809(2):154
- Heyer M and Dame TM (2015) Molecular Clouds in the Milky Way. *ARA&A* 53:583–629
- Heyer M, Krawczyk C, Duval J, et al. (2009) Re-Examining Larson’s Scaling Relationships in Galactic Molecular Clouds. *ApJ* 699(2):1092–1103
- Heyer M, Goldsmith PF, Yıldız UA, et al. (2016) Striations in the Taurus molecular cloud: Kelvin-Helmholtz instability or MHD waves? *MNRAS* 461:3918–3926
- Heyer MH and Brunt CM (2004) The Universality of Turbulence in Galactic Molecular Clouds. *ApJL* 615(1):L45–L48
- Heyer MH and Terebey S (1998) The Anatomy of the Perseus Spiral Arm:  $^{12}\text{CO}$  and IRAS Imaging Observations of the W3-W4-W5 Cloud Complex. *ApJ* 502(1):265–277
- Heyer MH, Brunt C, Snell RL, et al. (1998) The Five College Radio Astronomy Observatory CO Survey of the Outer Galaxy. *ApJS* 115:241
- Heyer MH, Carpenter JM, and Snell RL (2001) The Equilibrium State of Molecular Regions in the Outer Galaxy. *ApJ* 551(2):852–866
- Hill T, Motte F, Didelon P, et al. (2011) Filaments and ridges in Vela C revealed by Herschel: from low-mass to high-mass star-forming sites. *A&A* 533:A94
- Hiltner WA (1949) Polarization of Light from Distant Stars by Interstellar Medium. *Science* 109(2825):165
- Hily-Blant P, Falgarone E, and Pety J (2008) Dissipative structures of diffuse molecular gas. III. Small-scale intermittency of intense velocity-shears. *A&A* 481(2):367–380
- Hopkins PF, Wetzel A, Kereš D, et al. (2018) FIRE-2 simulations: physics versus numerics in galaxy formation. *MNRAS* 480(1):800–863
- Hughes A, Meidt SE, Colombo D, et al. (2013) A Comparative Study of Giant Molecular Clouds in M51, M33, and the Large Magellanic Cloud. *ApJ* 779(1):46
- Hygate APS, Kruijssen JMD, Chevance M, et al. (2019) The cloud-scale physics of star-formation and feedback in M33. *MNRAS* submitted
- Ibáñez-Mejía JC, Mac Low MM, Klessen RS, et al. (2016) Gravitational Contraction versus Supernova Driving and the Origin of the Velocity Dispersion-Size Relation in Molecular Clouds. *ApJ* 824(1):41
- Iffrig O and Hennebelle P (2017) Structure distribution and turbulence in self-consistently supernova-driven ISM of multiphase magnetized galactic discs. *A&A* 604:A70

- Imara N and Faesi CM (2019) ALMA Observations of Giant Molecular Clouds in the Starburst Dwarf Galaxy Henize 2-10. *ApJ*876(2):141
- Inoue T and Inutsuka Si (2008) Two-Fluid Magnetohydrodynamic Simulations of Converging H I Flows in the Interstellar Medium. I. Methodology and Basic Results. *ApJ*687:303–310
- Inoue T and Inutsuka Si (2009) Two-Fluid Magnetohydrodynamics Simulations of Converging H I Flows in the Interstellar Medium. II. Are Molecular Clouds Generated Directly from a Warm Neutral Medium? *ApJ*704:161–169
- Inoue T and Inutsuka Si (2012) Formation of Turbulent and Magnetized Molecular Clouds via Accretion Flows of H I Clouds. *ApJ*759:35
- Inutsuka Si (2001) The Mass Function of Molecular Cloud Cores. *ApJL*559:L149–L152
- Inutsuka Si and Miyama SM (1992) Self-similar solutions and the stability of collapsing isothermal filaments. *ApJ*388:392–399
- Inutsuka Si and Miyama SM (1997) A Production Mechanism for Clusters of Dense Cores. *ApJ*480:681
- Inutsuka Si, Inoue T, Iwasaki K, et al. (2015) The formation and destruction of molecular clouds and galactic star formation. An origin for the cloud mass function and star formation efficiency. *A&A*580:A49
- Iwasaki K, Tomida K, Inoue T, et al. (2018) The Early Stage of Molecular Cloud Formation by Compression of Two-phase Atomic Gases. *arXiv e-prints*
- Jeffreson SMR and Kruijssen JMD (2018) A general theory for the lifetimes of giant molecular clouds under the influence of galactic dynamics. *MNRAS*476:3688–3715
- Jeffreson SMR, Kruijssen JMD, Krumholz MR, et al. (2018) On the physical mechanisms governing the cloud lifecycle in the Central Molecular Zone of the Milky Way. *MNRAS*478:3380–3385
- Johnstone D, Wilson CD, Moriarty-Schieven G, et al. (2000) Large-Area Mapping at 850 Microns. I. Optimum Image Reconstruction from Chop Measurements. *ApJS*131(2):505–518
- Johnstone D, Fich M, Mitchell GF, et al. (2001) Large Area Mapping at 850 Microns. III. Analysis of the Clump Distribution in the Orion B Molecular Cloud. *ApJ*559(1):307–317
- Johnstone D, Di Francesco J, and Kirk H (2004) An Extinction Threshold for Protostellar Cores in Ophiuchus. *ApJL*611:L45–L48
- Jura M (1975) Interstellar clouds containing optically thin H<sub>2</sub>. *ApJ*197:575–580
- Juvela M, Ristorcelli I, Pagani L, et al. (2012) Galactic cold cores. III. General cloud properties. *A&A*541:A12
- Kainulainen J, Beuther H, Henning T, et al. (2009) Probing the evolution of molecular cloud structure. From quiescence to birth. *A&A*508:L35–L38
- Kainulainen J, Beuther H, Banerjee R, et al. (2011) Probing the evolution of molecular cloud structure. II. From chaos to confinement. *A&A*530:A64
- Kalberla PMW and Kerp J (2009) The Hi Distribution of the Milky Way. *ARA&A*47(1):27–61
- Kauffmann J, Pillai T, Shetty R, et al. (2010a) The Mass-Size Relation from Clouds to Cores. I. A New Probe of Structure in Molecular Clouds. *ApJ*712(2):1137–1146

- Kauffmann J, Pillai T, Shetty R, et al. (2010b) The Mass-size Relation from Clouds to Cores. II. Solar Neighborhood Clouds. *ApJ*716(1):433–445
- Kauffmann J, Pillai T, and Goldsmith PF (2013) Low Virial Parameters in Molecular Clouds: Implications for High-mass Star Formation and Magnetic Fields. *ApJ*779(2):185
- Kauffmann J, Pillai T, Zhang Q, et al. (2017) The Galactic Center Molecular Cloud Survey. I. A steep linewidth-size relation and suppression of star formation. *A&A*603:A89
- Kawamura A, Mizuno Y, Minamidani T, et al. (2009) the Second Survey of the Molecular Clouds in the Large Magellanic Cloud By Nanten. II. Star Formation. *ApJS*184(1):1–17
- Kennicutt J Robert C (1998) The Global Schmidt Law in Star-forming Galaxies. *The Astrophysical Journal* 498(2):541–552
- Kennicutt RC and Evans NJ (2012) Star Formation in the Milky Way and Nearby Galaxies. *ARA&A*50:531–608
- Kerr R, Kirk H, Di Francesco J, et al. (2019) The Green Bank Ammonia Survey: A Virial Analysis of Gould Belt Clouds in Data Release 1. *ApJ*874(2):147
- Keto ER and Myers PC (1986) CO Observations of Southern High-Latitude Clouds. *ApJ*304:466
- Khoperskov SA, Vasiliev EO, Ladeyschikov DA, et al. (2016) Giant molecular cloud scaling relations: the role of the cloud definition. *MNRAS*455(2):1782–1795
- Kim JG, Kim WT, and Ostriker EC (2018) Modeling UV Radiation Feedback from Massive Stars. II. Dispersal of Star-forming Giant Molecular Clouds by Photoionization and Radiation Pressure. *ApJ*859(1):68
- Kim WT and Ostriker EC (2001) Amplification, Saturation, and Q Thresholds for Runaway: Growth of Self-Gravitating Structures in Models of Magnetized Galactic Gas Disks. *ApJ*559(1):70–95
- Kim WT and Ostriker EC (2002) Formation and Fragmentation of Gaseous Spurs in Spiral Galaxies. *ApJ*570(1):132–151
- Kim WT and Ostriker EC (2007) Gravitational Runaway and Turbulence Driving in Star-Gas Galactic Disks. *ApJ*660(2):1232–1245
- Kim WT, Ostriker EC, and Stone JM (2002) Three-dimensional Simulations of Parker, Magneto-Jeans, and Swing Instabilities in Shearing Galactic Gas Disks. *ApJ*581(2):1080–1100
- Kim WT, Ostriker EC, and Stone JM (2003) Magnetorotationally Driven Galactic Turbulence and the Formation of Giant Molecular Clouds. *ApJ*599(2):1157–1172
- Kirk H, Johnstone D, and Di Francesco J (2006) The Large- and Small-Scale Structures of Dust in the Star-forming Perseus Molecular Cloud. *ApJ*646:1009–1023
- Kirk H, Friesen RK, Pineda JE, et al. (2017) The Green Bank Ammonia Survey: Dense Cores under Pressure in Orion A. *ApJ*846(2):144
- Kirk, H, Myers PC, Bourke TL, et al. (2013) Filamentary Accretion Flows in the Embedded Serpens South Protocluster. *ApJ*766:115
- Klessen RS and Glover SCO (2016) Physical Processes in the Interstellar Medium. *Saas-Fee Advanced Course* 43:85
- Klessen RS and Hennebelle P (2010) Accretion-driven turbulence as universal process: galaxies, molecular clouds, and protostellar disks. *A&A*520:A17

- Klessen RS, Ballesteros-Paredes J, Vázquez-Semadeni E, et al. (2005) Quiescent and Coherent Cores from Gravoturbulent Fragmentation. *ApJ*620(2):786–794
- Koch EW and Rosolowsky EW (2015) Filament identification through mathematical morphology. *MNRAS*452:3435–3450
- Koda J, Scoville N, Sawada T, et al. (2009) DYNAMICALLY DRIVEN EVOLUTION OF THE INTERSTELLAR MEDIUM IN M51. *ApJ*700(2):L132–L136
- Koda J, Scoville N, and Heyer M (2016) Evolution of Molecular and Atomic Gas Phases in the Milky Way. *ApJ*823(2):76
- Kolmogorov A (1941) The Local Structure of Turbulence in Incompressible Viscous Fluid for Very Large Reynolds' Numbers. *Akademiia Nauk SSSR Doklady* 30:301–305
- Könyves V, André P, Men'shchikov A, et al. (2015) A census of dense cores in the Aquila cloud complex: SPIRE/PACS observations from the Herschel Gould Belt survey. *A&A*584:A91
- Könyves V, André P, Arzoumanian D, et al. (2020) Properties of the dense core population in Orion B as seen by the Herschel Gould Belt survey. *A&A*635:A34
- Körtgen B and Banerjee R (2015) Impact of magnetic fields on molecular cloud formation and evolution. *MNRAS*451:3340–3353
- Koyama H and Inutsuka Si (2000) Molecular Cloud Formation in Shock-compressed Layers. *ApJ*532:980–993
- Koyama H and Inutsuka Si (2002) An Origin of Supersonic Motions in Interstellar Clouds. *ApJL*564:L97–L100
- Kramer C, Stutzki J, Rohrig R, et al. (1998) Clump mass spectra of molecular clouds. *A&A*329:249–264
- Kreckel K, Faesi C, Kruijssen JMD, et al. (2018) A 50 pc Scale View of Star Formation Efficiency across NGC 628. *ApJL*863:L21
- Kreckel K, Ho IT, Blanc GA, et al. (2019) Mapping Metallicity Variations across Nearby Galaxy Disks. *ApJ*887(1):80
- Kritsuk AG, Norman ML, and Wagner R (2011) On the Density Distribution in Star-forming Interstellar Clouds. *ApJ*727(1):L20
- Kruijssen JMD (2012) On the fraction of star formation occurring in bound stellar clusters. *MNRAS*426:3008–3040
- Kruijssen JMD and Longmore SN (2013) Comparing molecular gas across cosmic time-scales: the Milky Way as both a typical spiral galaxy and a high-redshift galaxy analogue. *MNRAS*435:2598–2603
- Kruijssen JMD and Longmore SN (2014) An uncertainty principle for star formation - I. why galactic star formation relations break down below a certain spatial scale. *MNRAS*439(4):3239–3252
- Kruijssen JMD, Dale JE, and Longmore SN (2015) The dynamical evolution of molecular clouds near the Galactic Centre - I. Orbital structure and evolutionary timeline. *MNRAS*447:1059–1079
- Kruijssen JMD, Schruba A, Hygate APS, et al. (2018) An uncertainty principle for star formation - II. A new method for characterizing the cloud-scale physics of star formation and feedback across cosmic history. *MNRAS*479:1866–1952
- Kruijssen JMD, Dale JE, Longmore SN, et al. (2019a) The dynamical evolution of molecular clouds near the Galactic Centre - II. Spatial structure and kinematics of

- simulated clouds. *MNRAS*484(4):5734–5754
- Kruijssen JMD, Schrubba A, Chevance M, et al. (2019b) Fast and inefficient star formation due to short-lived molecular clouds and rapid feedback. *Nature*569(7757):519–522
- Krumholz MR and McKee CF (2005) A General Theory of Turbulence-regulated Star Formation, from Spirals to Ultraluminous Infrared Galaxies. *ApJ*630:250–268
- Krumholz MR, McKee CF, and Bland-Hawthorn J (2019) Star Clusters Across Cosmic Time. *ARA&A*57:227–303
- Kuznetsova A, Hartmann L, and Ballesteros-Paredes J (2015) Signatures of Star Cluster Formation by Cold Collapse. *ApJ*815(1):27
- Kuznetsova A, Hartmann L, and Ballesteros-Paredes J (2018) Kinematics and structure of star-forming regions: insights from cold collapse models. *MNRAS*473(2):2372–2377
- Kwan J (1979) The mass spectrum of interstellar clouds. *ApJ*229:567–577
- Kwan J and Valdes F (1983) Spiral gravitational potentials and the mass growth of molecular clouds. *ApJ*271:604–610
- Kwan J and Valdes F (1987) The Spatial and Mass Distributions of Molecular Clouds and Spiral Structures. *ApJ*315:92
- Lada CJ, Muench AA, Rathborne J, et al. (2008) The Nature of the Dense Core Population in the Pipe Nebula: Thermal Cores Under Pressure. *ApJ*672(1):410–422
- Lada CJ, Lombardi M, and Alves JF (2010) On the Star Formation Rates in Molecular Clouds. *ApJ* 724:687–693
- Lada CJ, Lombardi M, Roman-Zuniga C, et al. (2013) Schmidt’s Conjecture and Star Formation in Molecular Clouds. *ApJ*778(2):133
- Ladjelate B, André P, Könyves V, et al. (2020) The Herschel view of the dense core population in the Ophiuchus molecular cloud. *A&A*, in press (arXiv:200111036)
- Larson RB (1969) Numerical calculations of the dynamics of collapsing proto-star. *MNRAS*145:271
- Larson RB (1981) Turbulence and star formation in molecular clouds. *Mon Not R Astron Soc* 194:809–826
- Larson RB (1985) Cloud fragmentation and stellar masses. *MNRAS*214:379–398
- Larson RB (2005) Thermal physics, cloud geometry and the stellar initial mass function. *MNRAS*359:211–222
- Lee YN and Hennebelle P (2018) Stellar mass spectrum within massive collapsing clumps. II. Thermodynamics and tidal forces of the first Larson core. A robust mechanism for the peak of the IMF. *A&A*611:A89
- Lee YN, Hennebelle P, and Chabrier G (2017) Analytical Core Mass Function (CMF) from Filaments: Under Which Circumstances Can Filament Fragmentation Reproduce the CMF? *ApJ*847(2):114
- Leisawitz D, Bash FN, and Thaddeus P (1989) A CO Survey of Regions around 34 Open Clusters. *ApJS*70:731
- Leroy AK, Walter F, Sandstrom K, et al. (2013) Molecular Gas and Star Formation in Nearby Disk Galaxies. *AJ*146(2):19
- Leroy AK, Bolatto AD, Ostriker EC, et al. (2015) ALMA Reveals the Molecular Medium Fueling the Nearest Nuclear Starburst. *ApJ*801(1):25

- Leroy AK, Schinnerer E, Hughes A, et al. (2017) Cloud-scale ISM Structure and Star Formation in M51. *ApJ*846:71
- Levrier F, Le Petit F, Hennebelle P, et al. (2012) UV-driven chemistry in simulations of the interstellar medium. I. Post-processed chemistry with the Meudon PDR code. *A&A*544:A22
- Li S, Zhang Q, Liu HB, et al. (2020) ALMA observations of NGC 6334S – I: Forming massive stars and cluster in subsonic and transonic filamentary clouds. *arXiv e-prints arXiv:2003.13534*
- Li Y, Mac Low MM, and Klessen RS (2005) Control of Star Formation in Galaxies by Gravitational Instability. *ApJ*L620(1):L19–L22
- Lombardi M, Alves JF, and Lada CJ (2010) Larson’s third law and the universality of molecular cloud structure. *Astron Astrophys* 519:L7
- Longmore SN, Kruijssen JMD, Bastian N, et al. (2014) The Formation and Early Evolution of Young Massive Clusters. *Protostars and Planets VI* pp 291–314
- Lopez LA, Krumholz MR, Bolatto AD, et al. (2011) What Drives the Expansion of Giant H II Regions?: A Study of Stellar Feedback in 30 Doradus. *ApJ*731:91
- Lopez LA, Krumholz MR, Bolatto AD, et al. (2014) The Role of Stellar Feedback in the Dynamics of H II Regions. *ApJ*795:121
- Loren RB (1989) The Cobwebs of Ophiuchus. II. 13CO Filament Kinematics. *ApJ*338:925
- Marsh KA, Kirk JM, André P, et al. (2016) A census of dense cores in the Taurus L1495 cloud from the Herschel. *MNRAS*459:342–356
- Maschberger T, Bonnell IA, Clarke CJ, et al. (2014) The relation between accretion rates and the initial mass function in hydrodynamical simulations of star formation. *MNRAS*439(1):234–246
- McKee CF and Ostriker EC (2007) Theory of Star Formation. *ARA&A*45(1):565–687
- McKee CF and Ostriker JP (1977) A theory of the interstellar medium - Three components regulated by supernova explosions in an inhomogeneous substrate. *ApJ*218:148–169
- McKee CF and Zweibel EG (1992) On the Virial Theorem for Turbulent Molecular Clouds. *ApJ*399:551
- McLeod AF, Dale JE, Evans CJ, et al. (2019a) Feedback from massive stars at low metallicities: MUSE observations of N44 and N180 in the Large Magellanic Cloud. *MNRAS*486(4):5263–5288
- McLeod AF, Kruijssen JMD, Weisz DR, et al. (2019b) Stellar Feedback and Resolved Stellar IFU Spectroscopy in the nearby Spiral Galaxy NGC 300. *ApJ*in press *arXiv:1910.11270*
- Meidt SE, Schinnerer E, García-Burillo S, et al. (2013) Gas Kinematics on Giant Molecular Cloud Scales in M51 with PAWS: Cloud Stabilization through Dynamical Pressure. *ApJ*779(1):45
- Meidt SE, Hughes A, Dobbs CL, et al. (2015) Short GMC lifetimes: an observational estimate with the PdBI Arcsecond Whirlpool Survey (PAWS). *ApJ*806(1):72
- Meidt SE, Leroy AK, Rosolowsky E, et al. (2018) A Model for the Onset of Self-gravitation and Star Formation in Molecular Gas Governed by Galactic Forces. I. Cloud-scale Gas Motions. *ApJ*854(2):100



- Meidt SE, Glover S, Kruijssen JMD, et al. (2019) A model for the onset of self-gravitation and star formation in molecular gas governed by galactic forces: II. a bottleneck set by cloud-environment decoupling. *ApJ* submitted
- Men'shchikov A (2013) A multi-scale filament extraction method: getfilaments. *A&A* 560:A63
- Men'shchikov A, André P, Didelon P, et al. (2012) A multi-scale, multi-wavelength source extraction method: getsources. *A&A* 542:A81
- Mestel L and Spitzer J L (1956) Star formation in magnetic dust clouds. *MNRAS* 116:503
- Miesch MS and Scalo JM (1995) Exponential Tails in the Centroid Velocity Distributions of Star-Forming Regions. *ApJL* 450:L27
- Miesch MS, Scalo J, and Bally J (1999) Velocity Field Statistics in Star-forming Regions. I. Centroid Velocity Observations. *ApJ* 524(2):895–922
- Miura RE, Kohno K, Tosaki T, et al. (2012) Giant Molecular Cloud Evolutions in the Nearby Spiral Galaxy M33. *ApJ* 761(1):37
- Miville-Deschênes MA, Martin PG, Abergel A, et al. (2010) Herschel-SPIRE observations of the Polaris flare: Structure of the diffuse interstellar medium at the sub-parsec scale. *A&A* 518:L104
- Miville-Deschênes MA, Duc PA, Marleau F, et al. (2016) Probing interstellar turbulence in cirrus with deep optical imaging: no sign of energy dissipation at 0.01 pc scale. *A&A* 593:A4
- Miville-Deschênes MA, Murray N, and Lee EJ (2017) Physical properties of molecular clouds for the entire Milky Way disk. *Astrophys J* 834(1):1–31
- Miyama SM, Narita S, and Hayashi C (1987) Fragmentation of Isothermal Sheet-Like Clouds. II —Full Nonlinear Numerical Simulations—. *Progress of Theoretical Physics* 78(6):1273–1287
- Molinari S, Swinyard B, Bally J, et al. (2010) Clouds, filaments, and protostars: The Herschel Hi-GAL Milky Way. *A&A* 518:L100
- Molinari S, Bally J, Noriega-Crespo A, et al. (2011) A 100 pc Elliptical and Twisted Ring of Cold and Dense Molecular Clouds Revealed by Herschel Around the Galactic Center. *ApJL* 735(2):L33
- Mookerjee B, Kramer C, Nielbock M, et al. (2004) The Giant Molecular Cloud associated with RCW 106. A 1.2 mm continuum mapping study. *A&A* 426:119–129
- Motte F, André P, and Neri R (1998) The initial conditions of star formation in the rho Ophiuchi main cloud: wide-field millimeter continuum mapping. *A&A* 336:150–172
- Motte F, André P, Ward-Thompson D, et al. (2001) A SCUBA survey of the NGC 2068/2071 protoclusters. *A&A* 372:L41–L44
- Motte F, Nony T, Louvet F, et al. (2018) The unexpectedly large proportion of high-mass star-forming cores in a Galactic mini-starburst. *Nature Astronomy* 2:478–482
- Murray N and Chang P (2015) Star Formation in Self-gravitating Turbulent Fluids. *ApJ* 804(1):44
- Myers P (2009) Filamentary Structure of Star-forming Complexes. *ApJ* 700:1609–1625
- Myers PC (1983) Dense cores in dark clouds. III. Subsonic turbulence. *ApJ* 270:105–118

- Nagasawa M (1987) Gravitational Instability of the Isothermal Gas Cylinder with an Axial magnetic Field. *Progress of Theoretical Physics* 77(3):635–652
- Nakamura F and Li ZY (2005) Quiescent Cores and the Efficiency of Turbulence-accelerated, Magnetically Regulated Star Formation. *ApJ*631(1):411–428
- Naranjo-Romero R, Vázquez-Semadeni E, and Loughnane RM (2015) Hierarchical Gravitational Fragmentation. I. Collapsing Cores within Collapsing Clouds. *ApJ*814(1):48
- Nguyen-Luong Q, Nakamura F, Sugitani K, et al. (2020) Large-scale Molecular Gas Distribution in the M17 Cloud Complex: Dense Gas Conditions of Massive Star Formation? *ApJ*891(1):66
- Ntormousi E, Hennebelle P, André P, et al. (2016) The effect of ambipolar diffusion on low-density molecular ISM filaments. *A&A*589:A24
- Offner SSR and Liu Y (2018) Turbulent action at a distance due to stellar feedback in magnetized clouds. *Nature Astronomy* 2:896–900
- Ohashi S, Sanhueza P, Chen HRV, et al. (2016) Dense Core Properties in the Infrared Dark Cloud G14.225-0.506 Revealed by ALMA. *ApJ*833(2):209
- Onishi T, Mizuno A, Kawamura A, et al. (1998) A  $C^{18}O$  Survey of Dense Cloud Cores in Taurus: Star Formation. *ApJ*502:296–314
- Oort JH (1954) Outline of a theory on the origin and acceleration of interstellar clouds and O associations. *Bull. Astron. Inst. Netherlands*12:177
- Ossenkopf V and Mac Low MM (2002) Turbulent velocity structure in molecular clouds. *A&A*390:307–326
- Ostriker J (1964) The Equilibrium of Polytropic and Isothermal Cylinders. *ApJ*140:1056
- Padoan P and Nordlund Å (2011) The Star Formation Rate of Supersonic Magneto-hydrodynamic Turbulence. *ApJ*730:40
- Padoan P, Pan L, Haugbølle T, et al. (2016) Supernova Driving. I. The Origin of Molecular Cloud Turbulence. *ApJ*822(1):11
- Padoan P, Pan L, Juvela M, et al. (2019) The Origin of Massive Stars: The Inertial-Inflow Model. arXiv e-prints arXiv:1911.04465
- Palau A, Estalella R, Girart JM, et al. (2014) Fragmentation of Massive Dense Cores Down to  $\sim 1000$  AU: Relation between Fragmentation and Density Structure. *ApJ*785(1):42
- Palmeirim P, André P, Kirk J, et al. (2013) Herschel view of the Taurus B211/3 filament and striations: evidence of filamentary growth? *A&A*550:A38
- Pan HA, Fujimoto Y, Tasker EJ, et al. (2016) Effects of galactic disc inclination and resolution on observed GMC properties and Larson’s scaling relations. *MNRAS*458(3):2443–2453
- Pan L, Padoan P, and Nordlund Å (2019) The Probability Distribution of Density Fluctuations in Supersonic Turbulence. *ApJ*881:155
- Panopoulou GV, Tassis K, Goldsmith PF, et al. (2014)  $^{13}CO$  filaments in the Taurus molecular cloud. *MNRAS*444:2507–2524
- Panopoulou GV, Psaradaki I, Skalidis R, et al. (2017) A closer look at the ‘characteristic’ width of molecular cloud filaments. *MNRAS*466:2529–2541
- Parker EN (1979) *Cosmical magnetic fields. Their origin and their activity.* Oxford University Press

- Passot T and Vázquez-Semadeni E (1998) Density probability distribution in one-dimensional polytropic gas dynamics. *Phys. Rev. E* 58(4):4501–4510
- Passot T, Pouquet A, and Woodward P (1988) The plausibility of Kolmogorov-type spectra in molecular clouds. *A&A* 197(1-2):228–234
- Passot T, Vázquez-Semadeni E, and Pouquet A (1995) A Turbulent Model for the Interstellar Medium. II. Magnetic Fields and Rotation. *ApJ* 455:536
- Peretto N, André P, Könyves V, et al. (2012) The Pipe Nebula as seen with Herschel: formation of filamentary structures by large-scale compression? *A&A* 541:A63
- Peretto N, Fuller GA, Duarte-Cabral A, et al. (2013) Global collapse of molecular clouds as a formation mechanism for the most massive stars. *A&A* 555:A112
- Peretto N, Fuller GA, André P, et al. (2014) SDC13 infrared dark clouds: Longitudinally collapsing filaments? *A&A* 561:A83
- Phillips TG, Huggins PJ, Wannier PG, et al. (1979) Observations of CO( $J = 2-1$ ) emission from molecular clouds. *ApJ* 231:720–731
- Pineda JE, Goodman AA, Arce HG, et al. (2010) Direct Observation of a Sharp Transition to Coherence in Dense Cores. *ApJL* 712(1):L116–L121
- Pineda JE, Goodman AA, Arce HG, et al. (2011) Expanded Very Large Array Observations of the Barnard 5 Star-forming Core: Embedded Filaments Revealed. *ApJL* 739:L2
- Pineda JL, Langer WD, Velusamy T, et al. (2013) A Herschel [C ii] Galactic plane survey. I. The global distribution of ISM gas components. *A&A* 554:A103
- Planck int res XXXV (2016) *Planck* intermediate results. XXXV. Probing the role of the magnetic field in the formation of structure in molecular clouds. *A&A* 586:A138
- Plume R, Jaffe DT, Evans I Neal J, et al. (1997) Dense Gas and Star Formation: Characteristics of Cloud Cores Associated with Water Masers. *ApJ* 476(2):730–749
- Pokhrel R, Gutermuth R, Ali B, et al. (2016) A Herschel-SPIRE survey of the Mon R2 giant molecular cloud: analysis of the gas column density probability density function. *MNRAS* 461:22–35
- Pon A, Johnstone D, and Heitsch F (2011) Modes of Star Formation in Finite Molecular Clouds. *ApJ* 740(2):88
- Pon A, Toalá JA, Johnstone D, et al. (2012) Aspect Ratio Dependence of the Free-fall Time for Non-spherical Symmetries. *ApJ* 756(2):145
- Rathborne JM, Longmore SN, Jackson JM, et al. (2014) Turbulence Sets the Initial Conditions for Star Formation in High-pressure Environments. *ApJL* 795:L25
- Reid MA and Wilson CD (2005) High-Mass Star Formation. I. The Mass Distribution of Submillimeter Clumps in NGC 7538. *ApJ* 625(2):891–905
- Reid MA and Wilson CD (2006a) High-Mass Star Formation. II. The Mass Function of Submillimeter Clumps in M17. *ApJ* 644(2):990–1005
- Reid MA and Wilson CD (2006b) High-Mass Star Formation. III. The Functional Form of the Submillimeter Clump Mass Function. *ApJ* 650(2):970–984
- Reina-Campos M and Kruijssen JMD (2017) A unified model for the maximum mass scales of molecular clouds, stellar clusters and high-redshift clumps. *MNRAS* 469:1282–1298

- Rivera-Ingraham A, Ristorcelli I, Juvela M, et al. (2016) Galactic cold cores. VII. Filament formation and evolution: Methods and observational constraints. *A&A* 591:A90
- Roman-Duval J, Jackson JM, Heyer M, et al. (2010) Physical Properties and Galactic Distribution of Molecular Clouds Identified in the Galactic Ring Survey. *Astrophys J* 723(1):492–507
- Roman-Duval J, Heyer M, Brunt CM, et al. (2016) Distribution and Mass of Diffuse and Dense CO Gas in the Milky Way. *ApJ* 818(2):144
- Román-Zúñiga CG, Alves JF, Lada CJ, et al. (2010) Deep Near-infrared Survey of the Pipe Nebula. II. Data, Methods, and Dust Extinction Maps. *ApJ* 725(2):2232–2250
- Rosolowsky E, Dunham MK, Ginsburg A, et al. (2010) The Bolocam Galactic Plane Survey. II. Catalog of the Image Data. *ApJS* 188(1):123–138
- Rosolowsky EW, Pineda JE, Kauffmann J, et al. (2008) Structural Analysis of Molecular Clouds: Dendrograms. *ApJ* 679(2):1338–1351
- Rowles J and Froebrich D (2009) The structure of molecular clouds - I. All-sky near-infrared extinction maps. *MNRAS* 395(3):1640–1648
- Roy A, André P, Arzoumanian D, et al. (2019) How the power spectrum of dust continuum images may hide the presence of a characteristic filament width. *A&A* 626:A76
- Russeil D, Figueira M, Zavagno A, et al. (2019) Herschel-HOBYS study of the earliest phases of high-mass star formation in NGC 6357. *A&A* 625:A134
- Salji CJ, Richer JS, Buckle JV, et al. (2015) The JCMT Gould Belt Survey: properties of star-forming filaments in Orion A North. *MNRAS* 449:1782–1796
- Salpeter EE (1955) The Luminosity Function and Stellar Evolution. *ApJ* 121:161
- Sanders DB, Scoville NZ, and Solomon PM (1985) Giant molecular clouds in the galaxy. II. Characteristics of discrete features. *ApJ* 289:373–387
- Scalo J (1990) Perception of interstellar structure - Facing complexity. In: Capuzzo-Dolcetta R, Chiosi C, and di Fazio A (eds) *Physical Processes in Fragmentation and Star Formation*, Astrophysics and Space Science Library, vol 162, pp 151–176
- Schisano E, Rygl KLJ, Molinari S, et al. (2014) The Identification of Filaments on Far-infrared and Submillimeter Images: Morphology, Physical Conditions and Relation with Star Formation of Filamentary Structure. *ApJ* 791:27
- Schneider N, Csengeri T, Bontemps S, et al. (2010) Dynamic star formation in the massive DR21 filament. *A&A* 520:A49
- Schneider S and Elmegreen BG (1979) A catalog of dark globular filaments. *ApJs* 41:87–95
- Schruba A, Leroy AK, Walter F, et al. (2010) the Scale Dependence of the Molecular Gas Depletion Time in M33. *ApJ* 722(2):1699–1706
- Schruba A, Kruijssen JMD, and Leroy AK (2019) How Galactic Environment Affects the Dynamical State of Molecular Clouds and Their Star Formation Efficiency. *ApJ* 883(1):2
- Scoville NZ and Hersh K (1979) Collisional growth of Giant Molecular Clouds. *ApJ* 229:578–582
- Scoville NZ and Wilson CD (2004) Molecular Gas forming Massive Star Clusters and Starbursts. In: Lamers HJGLM, Smith LJ, and Nota A (eds) *The Formation and Evolution of Massive Young Star Clusters*, Astronomical Society of the Pacific

- Conference Series, vol 322, p 245
- Seifried D, Schmidt W, and Niemeyer JC (2011) Forced turbulence in thermally bistable gas: a parameter study. *A&A* 526:A14
- Seifried D, Walch S, Haid S, et al. (2018) Is Molecular Cloud Turbulence Driven by External Supernova Explosions? *ApJ* 855(2):81
- Shetty R and Ostriker EC (2008) Cloud and Star Formation in Disk Galaxy Models with Feedback. *ApJ* 684(2):978–995
- Shetty R, Glover SC, Dullemond CP, et al. (2011) Modelling CO emission - I. CO as a column density tracer and the X factor in molecular clouds. *MNRAS* 412(3):1686–1700
- Shetty R, Beaumont CN, Burton MG, et al. (2012) The linewidth-size relationship in the dense interstellar medium of the Central Molecular Zone. *MNRAS* 425(1):720–729
- Shimajiri Y, André P, Ntormousi E, et al. (2019a) Probing fragmentation and velocity sub-structure in the massive NGC 6334 filament with ALMA. *A&A* 632:A83
- Shimajiri Y, André P, Palmeirim P, et al. (2019b) Probing accretion of ambient cloud material into the Taurus B211/B213 filament. *A&A* 623:A16
- Shirley YL, Evans I Neal J, Young KE, et al. (2003) A CS J=5–&4 Mapping Survey Toward High-Mass Star-forming Cores Associated with Water Masers. *ApJS* 149(2):375–403
- Shu FH (1977) Self-similar collapse of isothermal spheres and star formation. *ApJ* 214:488–497
- Shu FH, Adams FC, and Lizano S (1987) Star formation in molecular clouds: observation and theory. *ARA&A* 25:23–81
- Silk J (1997) Feedback, Disk Self-Regulation, and Galaxy Formation. *ApJ* 481(2):703–709
- Smith RJ, Glover SCO, and Klessen RS (2014) On the nature of star-forming filaments - I. Filament morphologies. *MNRAS* 445(3):2900–2917
- Smith RJ, Glover SCO, Klessen RS, et al. (2016) On the nature of star-forming filaments - II. Subfilaments and velocities. *MNRAS* 455(4):3640–3655
- Soler JD (2019) Using Herschel and Planck observations to delineate the role of magnetic fields in molecular cloud structure. *A&A* 629:A96
- Soler JD and Hennebelle P (2017) What are we learning from the relative orientation between density structures and the magnetic field in molecular clouds? *A&A* 607:A2
- Soler JD, Hennebelle P, Martin PG, et al. (2013) An Imprint of Molecular Cloud Magnetization in the Morphology of the Dust Polarized Emission. *ApJ* 774(2):128
- Solomon PM, Rivolo AR, Barrett J, et al. (1987) Mass, Luminosity, and Line Width Relations of Galactic Molecular Clouds. *ApJ* 319:730
- Stahler SW and Palla F (2005) *The Formation of Stars*. Wiley-VCH
- Stanke T, Smith MD, Gredel R, et al. (2006) An unbiased search for the signatures of protostars in the  $\rho$  Ophiuchi molecular cloud . II. Millimetre continuum observations. *A&A* 447(2):609–622
- Stodólkiewicz JS (1963) On the Gravitational Instability of Some Magneto-Hydrodynamical Systems of Astrophysical Interest. Part III. *Acta Astron* 13:30–54

- Storm S, Mundy LG, Lee KI, et al. (2016) CARMA Large Area Star Formation Survey: Dense Gas in the Young L1451 Region of Perseus. *ApJ*830(2):127
- Stutzki J and Guesten R (1990) High Spatial Resolution Isotopic CO and CS Observations of M17 SW: The Clumpy Structure of the Molecular Cloud Core. *ApJ*356:513
- Stutzki R (1993) The Small Scale Structure of Molecular Clouds. *Reviews in Modern Astronomy* 6:209–232
- Sun J, Leroy AK, Schruba A, et al. (2018) Cloud-scale Molecular Gas Properties in 15 Nearby Galaxies. *ApJ*860(2):172
- Sun J, Leroy AK, Ostriker EC, et al. (2020) Dynamical Equilibrium in the Molecular ISM in 28 Nearby Star-Forming Galaxies. *ApJ* in press
- Tafalla M and Hacar A (2015) Chains of dense cores in the Taurus L1495/B213 complex. *A&A*574:A104
- Tafalla M, Myers PC, Caselli P, et al. (2004) On the internal structure of starless cores. I. Physical conditions and the distribution of CO, CS,  $N_2H^+$ , and  $NH_3$  in L1498 and L1517B. *A&A*416:191–212
- Taff LG and Savedoff MP (1973) The mass distribution of objects under-going collisions with applications to interstellar HI clouds. *MNRAS*164:357
- Tasker EJ and Tan JC (2009) Star Formation in Disk Galaxies. I. Formation and Evolution of Giant Molecular Clouds via Gravitational Instability and Cloud Collisions. *ApJ*700(1):358–375
- Tassis K, Christie DA, Urban A, et al. (2010) Do lognormal column-density distributions in molecular clouds imply supersonic turbulence? *MNRAS*408(2):1089–1094
- Tenorio-Tagle G and Bodenheimer P (1988) Large-scale expanding superstructures in galaxies. *ARA&A*26:145–197
- Testi L and Sargent AI (1998) Star Formation in Clusters: A Survey of Compact Millimeter-Wave Sources in the Serpens Core. *ApJL*508(1):L91–L94
- Tielens AGGM (2010) *The Physics and Chemistry of the Interstellar Medium*. Cambridge University Press
- Toalá JA, Vázquez-Semadeni E, and Gómez GC (2012) The Free-fall Time of Finite Sheets and Filaments. *ApJ*744(2):190
- Tohline JE (1982) Hydrodynamic Collapse. *Fundamentals of Cosmic Physics* 8:1–82
- Tomisaka K (1984) Coagulation of interstellar clouds in spiral gravitational potential and formation of giant molecular clouds. *PASJ*36(3):457–475
- Tomisaka K (2014) Magnetohydrostatic Equilibrium Structure and Mass of Filamentary Isothermal Cloud Threaded by Lateral Magnetic Field. *ApJ*785:24
- Traficante A, Duarte-Cabral A, Elia D, et al. (2018a) Testing the Larson relations in massive clumps. *MNRAS*477(2):2220–2242
- Traficante A, Fuller GA, Smith RJ, et al. (2018b) Massive  $70 \mu\text{m}$  quiet clumps - II. Non-thermal motions driven by gravity in massive star formation? *MNRAS*473(4):4975–4985
- Traficante A, Lee YN, Hennebelle P, et al. (2018c) A possible observational bias in the estimation of the virial parameter in virialized clumps. *A&A*619:L7
- Tritsis A and Tassis K (2016) Striations in molecular clouds: streamers or MHD waves? *MNRAS*462:3602–3615

- Troland TH and Crutcher RM (2008) Magnetic Fields in Dark Cloud Cores: Arecibo OH Zeeman Observations. *ApJ*680(1):457–465
- Tsitali AE, Belloche A, Garrod RT, et al. (2015) Star formation in Chamaeleon I and III: a molecular line study of the starless core population. *A&A*575:A27
- Utomo D, Sun J, Leroy AK, et al. (2018) Star Formation Efficiency per Free-fall Time in nearby Galaxies. *ApJL*861(2):L18
- Valdivia V, Hennebelle P, Génin M, et al. (2016) H<sub>2</sub> distribution during the formation of multiphase molecular clouds. *A&A*587:A76
- Valdivia V, Godard B, Hennebelle P, et al. (2017) Origin of CH<sup>+</sup> in diffuse molecular clouds. Warm H<sub>2</sub> and ion-neutral drift. *A&A*600:A114
- Vázquez-Semadeni E (1994) Hierarchical Structure in Nearly Pressureless Flows as a Consequence of Self-similar Statistics. *ApJ*423:681
- Vázquez-Semadeni E (1999) Turbulence in Molecular Clouds. In: Wall WF, Carramiñana A, and Carrasco L (eds) *Millimeter-Wave Astronomy: Molecular Chemistry & Physics in Space*, Proceedings of the 1996 INAOE Summer School of Millimeter-Wave Astronomy held at INAOE, Tonantzintla, Puebla, Mexico, 15-31 July 1996. Edited by W. F. Wall, A. Carramiñana, and L. Carrasco. Kluwer Academic Publishers, 1999., p.161, *Astrophysics and Space Science Library*, vol 241, p 161
- Vázquez-Semadeni E and García N (2001) The Probability Distribution Function of Column Density in Molecular Clouds. *ApJ*557(2):727–735
- Vázquez-Semadeni E, Passot T, and Pouquet A (1995) A Turbulent Model for the Interstellar Medium. I. Threshold Star Formation and Self-Gravity. *ApJ*441:702
- Vázquez-Semadeni E, Ryu D, Passot T, et al. (2006) Molecular Cloud Evolution. I. Molecular Cloud and Thin Cold Neutral Medium Sheet Formation. *ApJ*643:245–259
- Vázquez-Semadeni E, Gómez GC, Jappsen AK, et al. (2007) Molecular Cloud Evolution. II. From Cloud Formation to the Early Stages of Star Formation in Decaying Conditions. *ApJ*657(2):870–883
- Vázquez-Semadeni E, González-Samaniego A, and Colín P (2017) Hierarchical star cluster assembly in globally collapsing molecular clouds. *MNRAS*467:1313–1328
- Vázquez-Semadeni E, Zamora-Avilés M, Galván-Madrid R, et al. (2018) Molecular cloud evolution - VI. Measuring cloud ages. *MNRAS*479(3):3254–3263
- Vázquez-Semadeni E, Palau A, Ballesteros-Paredes J, et al. (2019a) Global Hierarchical Collapse In Molecular Clouds. Towards a Comprehensive Scenario. *MNRASp* 2348
- Vázquez-Semadeni E, Palau A, Ballesteros-Paredes J, et al. (2019b) Global hierarchical collapse in molecular clouds. Towards a comprehensive scenario. *MNRAS*490(3):3061–3097
- Veltchev TV, Ossenkopf-Okada V, Stanchev O, et al. (2018) Spatially associated clump populations in Rosette from CO and dust maps. *MNRAS*475:2215–2235
- Walch S and Naab T (2015) The energy and momentum input of supernova explosions in structured and ionized molecular clouds. *MNRAS*451:2757–2771
- Wang K, Testi L, Ginsburg A, et al. (2015) Large-scale filaments associated with Milky Way spiral arms. *MNRAS*450:4043–4049

- Ward JL, Chevance M, Kruijssen JMD, et al. (2019) Towards a multi-tracer timeline of star formation in the lmc i: Deriving the lifetimes of h I clouds. MNRAS submitted
- Whitworth AP, Bhattal AS, Francis N, et al. (1996) Star formation and the singular isothermal sphere. MNRAS283(3):1061–1070
- Williams JP, de Geus EJ, and Blitz L (1994) Determining structure in molecular clouds. ApJ428:693–712
- Wilson RW, Jefferts KB, and Penzias AA (1970) Carbon Monoxide in the Orion Nebula. ApJL161:L43
- Wolfire MG, McKee CF, Hollenbach D, et al. (2003) Neutral Atomic Phases of the Interstellar Medium in the Galaxy. ApJ587:278–311
- Wu J, Evans I Neal J, Shirley YL, et al. (2010) The Properties of Massive, Dense Clumps: Mapping Surveys of HCN and CS. ApJS188(2):313–357
- Xu S and Lazarian A (2020) Turbulence in a Self-gravitating Molecular Cloud Core. ApJ890(2):157
- Ysard N, Abergel A, Ristorcelli I, et al. (2013) Variation in dust properties in a dense filament of the Taurus molecular complex (L1506). A& A559:A133
- Zamora-Avilés M, Vázquez-Semadeni E, and Colín P (2012) An Evolutionary Model for Collapsing Molecular Clouds and Their Star Formation Activity. ApJ751(1):77
- Zamora-Avilés M, Ballesteros-Paredes J, and Hartmann LW (2017) Are fibres in molecular cloud filaments real objects? MNRAS472(1):647–656
- Zamora-Avilés M, Vázquez-Semadeni E, Körtgen B, et al. (2018) Magnetic suppression of turbulence and the star formation activity of molecular clouds. MNRAS474(4):4824–4836
- Zhang CP and Li GX (2017) Mass-size scaling  $M \propto r^{1.67}$  of massive star-forming clumps - evidences of turbulence-regulated gravitational collapse. MNRAS469(2):2286–2291
- Zhang GY, Xu JL, Vasyunin AI, et al. (2018) Physical properties and chemical composition of the cores in the California molecular cloud. A& A620:A163
- Zhang S, Zavagno A, Yuan J, et al. (2020) HII regions and high-mass starless clump candidates I: Catalogs and properties. arXiv e-prints arXiv:2003.11433